

SANDIA REPORT

NUREG/CR-4855

SAND87-8203

R3

Printed July 1987

Development and Application of a Computer Model for Large-Scale Flame Acceleration Experiments

K. D. Marx

Prepared by
Sandia National Laboratories
Albuquerque, New Mexico 87185 and Livermore, California 94550
for the United States Department of Energy
under Contract DE-AC04-76DP00789



Prepared for
U.S. NUCLEAR REGULATORY COMMISSION

Issued by Sandia National Laboratories, operated for the United States Department of Energy by Sandia Corporation.

NOTICE: This report was prepared as an account of work sponsored by an agency of the United States Government. Neither the United States Government nor any agency thereof, nor any of their employees, nor any of the contractors, subcontractors, or their employees, makes any warranty, express or implied, or assumes any legal liability or responsibility for the accuracy, completeness, or usefulness of any information, apparatus, product, or process disclosed, or represents that its use would not infringe privately owned rights. Reference herein to any specific commercial product, process, or service by trade name, trademark, manufacturer, or otherwise, does not necessarily constitute or imply its endorsement, recommendation, or favoring by the United States Government, any agency thereof or any of their contractors or subcontractors. The views and opinions expressed herein do not necessarily state or reflect those of the United States Government, any agency thereof or any of their contractors or subcontractors.

Available from
Superintendent of Documents
U.S. Government Printing Office
Post Office Box 37082
Washington, D.C. 20013-7982
and
National Technical Information Service
Springfield, VA 22161

NUREG/CR-4855
SAND87-8203
R3

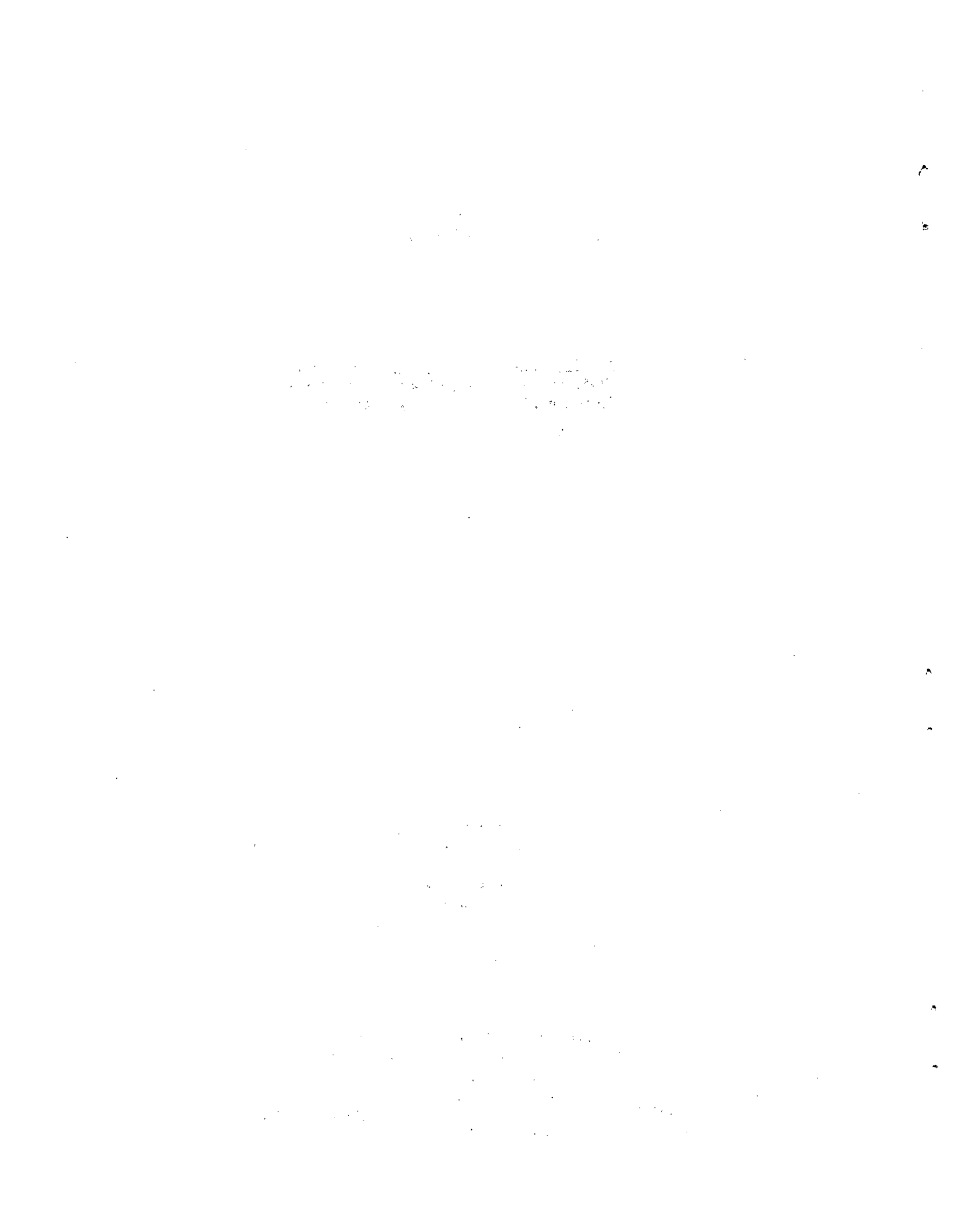
**DEVELOPMENT AND APPLICATION OF
A COMPUTER MODEL FOR LARGE-SCALE
FLAME ACCELERATION EXPERIMENTS**

K. D. Marx

July 1987

Sandia National Laboratories
Livermore, CA 94550
Operated by
Sandia Corporation
for the
U. S. Department of Energy

Prepared for
Division of Reactor Accident Analysis
Office of Nuclear Regulatory Research
U. S. Nuclear Regulatory Commission
Washington, DC 20555
Under Memorandum of Understanding DOE 40-550-75
NRC FIN No. A1246



**DEVELOPMENT AND APPLICATION OF
A COMPUTER MODEL FOR LARGE-SCALE
FLAME ACCELERATION EXPERIMENTS***

K. D. Marx
Thermofluids Division
Sandia National Laboratories
Livermore, CA 94550

ABSTRACT

A new computational model for large-scale premixed flames is developed and applied to the simulation of flame acceleration experiments. The primary objective is to circumvent the necessity for resolving turbulent flame fronts; this is imperative because of the relatively coarse computational grids which must be used in engineering calculations. The essence of the model is to artificially thicken the flame by increasing the appropriate diffusivities and decreasing the combustion rate, but to do this in such a way that the burn velocity varies with pressure, temperature, and turbulence intensity according to prespecified phenomenological characteristics. The model is particularly aimed at implementation in computer codes which simulate compressible flows. To this end, it is applied to the two-dimensional simulation of hydrogen-air flame acceleration experiments in which the flame speeds and gas flow velocities attain or exceed the speed of sound in the gas. It is shown that many of the features of the flame trajectories and pressure histories in the experiments are simulated quite well by the model. Using the comparison of experimental and computational results as a guide, some insight is developed into the processes which occur in such experiments.

* This work was performed at the Combustion Research Facility and supported by the U. S. Nuclear Regulatory Commission.

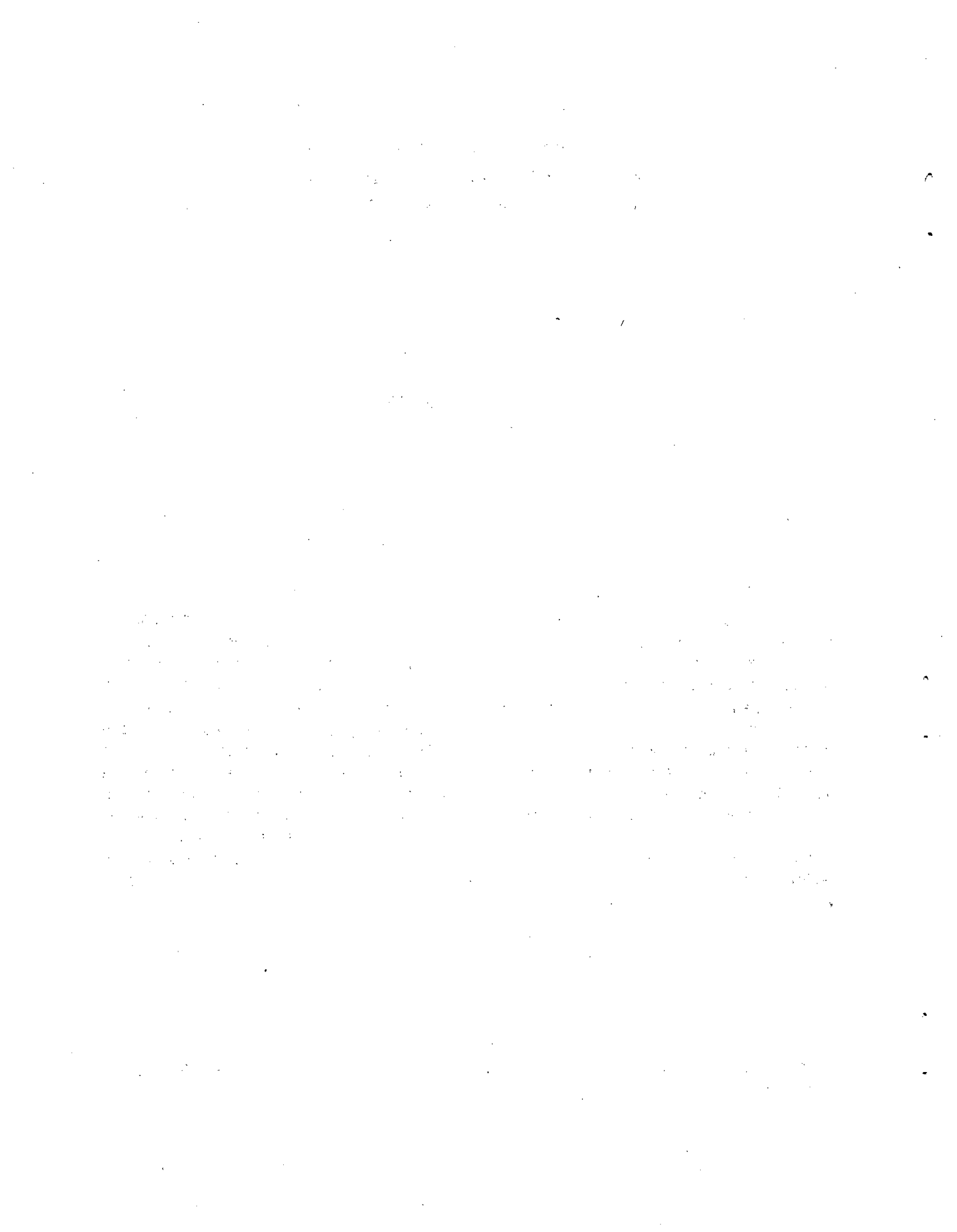


Table of Contents

	<u>Page</u>
Acknowledgements	xv
Executive Summary	xvii
I. Introduction	1
II. Computer Code and Turbulence Model	5
Flow Variables and Chemistry	5
The k - ϵ Turbulence Model	7
III. The Combustion Model	10
Properties of Turbulent Flames and Numerical Flames	10
Development of a Model With Appropriate Properties	13
Dependence on Pressure and Pre flame Temperature	15
Summary of the Model	17
IV. Comparison of Computational Results With Experiment	20
Experimental Considerations	20
Comparison of Flame Trajectories and Pressure Histories	22
Further Discussion of the Computational Results	35
Results of Variations in the Computational Parameters	40
V. Concluding Remarks	45
Appendix A. Integration of Production-Dissipation Terms	51
Appendix B. Difference Formula for ϵ at Walls	54
References	55



List of Illustrations

		<u>Page</u>
1	Sketch of the FLAME Facility	2
2	Schematic of the FLAME Facility with obstacles installed	3
3	Problem domain and finite-difference grid	8
4	Length scales in the flame	11
5	Turbulent burn velocity vs turbulence intensity	16
6	Arrival time data for Experiment F-22	23
7	Flame front profiles for Experiment F-22	24
8	Arrival time data for Experiment F-23	25
9	Flame front profiles for Experiment F-23	26
10	Computed and experimental flame trajectories (Experiment F-23)	29
11	Computed and experimental pressure histories at 14.6 m (Experiment F-23, transducer PKU4)	30
12	Computed and experimental pressure histories at 18.6 m (Experiment F-23, transducers PKU5 and PKU10)	31
13	Computed and experimental pressure histories at 21.5m (Experiment F-23, transducers PKU6 and PKU9)	32
14	Computed and experimental pressure histories at 25.6 m (Experiment F-23, transducers PKU7 and PKU8)	33
15	Three-dimensional plots of computed pressure (baseline parameters)	36
16	Three-dimensional plots of computed temperature (baseline parameters)	37
17	Three-dimensional plots of computed turbulent kinetic energy (baseline parameters)	38
18	Three-dimensional plots of computed combustion rate (baseline parameters)	39
19	Flow pattern in two chambers at $t = 310$ ms	41
20	Flame trajectories, including computation on fine grid	42
21	Pressure histories, including computation on fine grid	43
22	Three-dimensional plots of pressure computed on fine grid	44
23	Flame trajectories, including computation with altered model	46
24	Pressure histories, including computation with altered model	47
25	Pressure histories, including computation with $n = 2$	48



List of Tables

	<u>Page</u>
I. Results of Tests of the Combustion Model	19
II. Summary of FLAME Tests With Obstacles	21
III. Summary of Experimental and Numerical Parameters	27
IV. Location of Pressure Transducers in Experiment F-23	34

10
11
12
13
14

The following information is provided for the purpose of illustrating the use of the system. It is not intended to be a substitute for the actual data provided in the report.

List of Symbols

Roman:

A	Coefficient in burn velocity formula
A_c	Combustion coefficient
B	Coefficient in burn velocity formula
c_p	Specific heat at constant pressure
c_{po}	Constant in approximation for specific heat
c'_p	Slope in approximation for specific heat
C	Progress variable
$C_{1\epsilon}$	Coefficient in production of ϵ
$C_{2\epsilon}$	Coefficient in dissipation of ϵ
C_μ	Coefficient in eddy viscosity formula
D	Diffusion coefficient
E (App. A only)	$\rho\epsilon$
$f(T)$	Special burn rate function
$f_p(\underline{u}, k, \epsilon)$ (App. A only)	$\sigma : \nabla \underline{u} / \mu$
$h(p, T_u)$	Special burn rate function
h_i	Specific Enthalpy of i^{th} species
I	Specific energy
k	Turbulent kinetic energy
k_e	Effective turbulent kinetic energy
k_m	Threshold turbulent kinetic energy
k_T	Thermal conductivity
L	Turbulent length scale
L_e	Effective turbulent length scale
L_m	Threshold turbulent length scale
m	Pressure exponent in burn velocity formula
m_i	Molecular weight of i^{th} species
n	Temperature exponent in burn velocity formula
p	Pressure
P (App. A only)	$\sigma : \nabla \underline{u}$
Pr	Prandtl number
P' (App. A only)	$C_\mu f_p$
Q (App. A only)	ρk
Q_i^c	Rate of energy release due to chemistry
r	Thermal expansion ratio
R_T	Turbulent Reynolds number
Sc	Schmidt number
S_L	Laminar burn velocity
S_T	Turbulent burn velocity
S_{Ti}	Initial turbulent burn velocity
S_T^e (Table I only)	Expected turbulent burn velocity
S_T'	$dS_T / d\sqrt{k}$

t	Time
t_t	Typical transit time
t_T	Turbulence time scale
T	Temperature
T_a	Adiabatic flame temperature
T_o	Initial gas temperature
T_u	Unburned gas temperature
t_χ	Thermal diffusion time
u	Gas velocity
u_*	Wall shear velocity
u'	Turbulence intensity
v_{fo}	Initial flame speed
v_T	Turbulent flame speed
w	Channel width
x	Spanwise coordinate
y	Vertical coordinate
y (App. B only)	Coordinate measuring distance from wall
Y_i	Mass fraction of the i^{th} species
Y_p^∞	Mass fraction of product species for completed burn
z	Lengthwise coordinate

Greek:

β	Refers to β -transformation
δ	Unit tensor
δ_c	Computational flame thickness
δ_c^e (Table I only)	Expected computational flame thickness
δ_L	Laminar flame thickness
δ_T	Turbulent flame thickness
Δt	Time step
Δx	Grid spacing
Δy (App. B only)	Grid spacing
ϵ	Turbulence dissipation rate
κ	Von Kármán constant
μ	Total viscosity
μ_L	Laminar viscosity
μ_T	Eddy viscosity
ν_i	Stoichiometric coefficient of i^{th} species
ξ (App. A only)	Q/E
ρ	Total density
ρ_i	Density of i^{th} species

ρ_f	Rate of consumption of fuel
$\dot{\rho}_i^c$	Rate of change of density of i^{th} species due to reactions
σ	Stress tensor
σ_ϵ	Coefficient in diffusion of ϵ
τ	Wall shear stress
χ	Thermal diffusivity

Subscripts:

e	Effective values
f	Fuel
i	Species
i (App. B only)	Grid index
L	Laminar
p	Product species
T	Turbulent
ϵ	Refers to turbulent dissipation rate

Superscripts:

$base$ (Table I only)	Refers to baseline calculation
c	Chemistry
e (Table I only)	Expected values
T	Transpose of tensor
prime ($'$) (on c_p, S_T)	Differentiation
prime ($'$) (on μ, t_T, μ_T)	Values of quantities in final form of combustion model

Abbreviations:

CJ	Chapman-Jouguet
DDT	Deflagration-to-detonation transition
FLAME	Flame Acceleration Measurements and Experiments facility

1. The first part of the document discusses the importance of maintaining accurate records of all transactions. This is essential for ensuring the integrity of the financial statements and for providing a clear audit trail. The records should be kept up-to-date and should be easily accessible to all relevant parties.

2. The second part of the document outlines the various methods used to collect and analyze data. These methods include interviews, surveys, and focus groups. Each method has its own strengths and weaknesses, and it is important to choose the most appropriate method for the specific research objectives. The data collected should be analyzed carefully to identify any trends or patterns.

3. The third part of the document describes the results of the research. The findings indicate that there is a significant correlation between the variables studied. This suggests that the factors being investigated are closely related and may have a direct impact on the outcomes. The results should be interpreted in the context of the existing literature and should be used to inform future research and practice.

4. The final part of the document provides a conclusion and a list of recommendations. The conclusion summarizes the key findings and highlights the implications of the research. The recommendations are based on the findings and provide practical advice for how the results can be applied in the real world.

Acknowledgements

Many thanks are due M. P. Sherman, S. R. Tieszen, J. T. Hitchcock, J. E. Shepherd, J. H. S. Lee, W. B. Benedick, P. K. Barr, and A. R. Kerstein for valuable discussions of this project. I would also like to thank P. Worthington, C. Tinkler, M. Berman, and B. R. Sanders for their continued advice and support.

Executive Summary

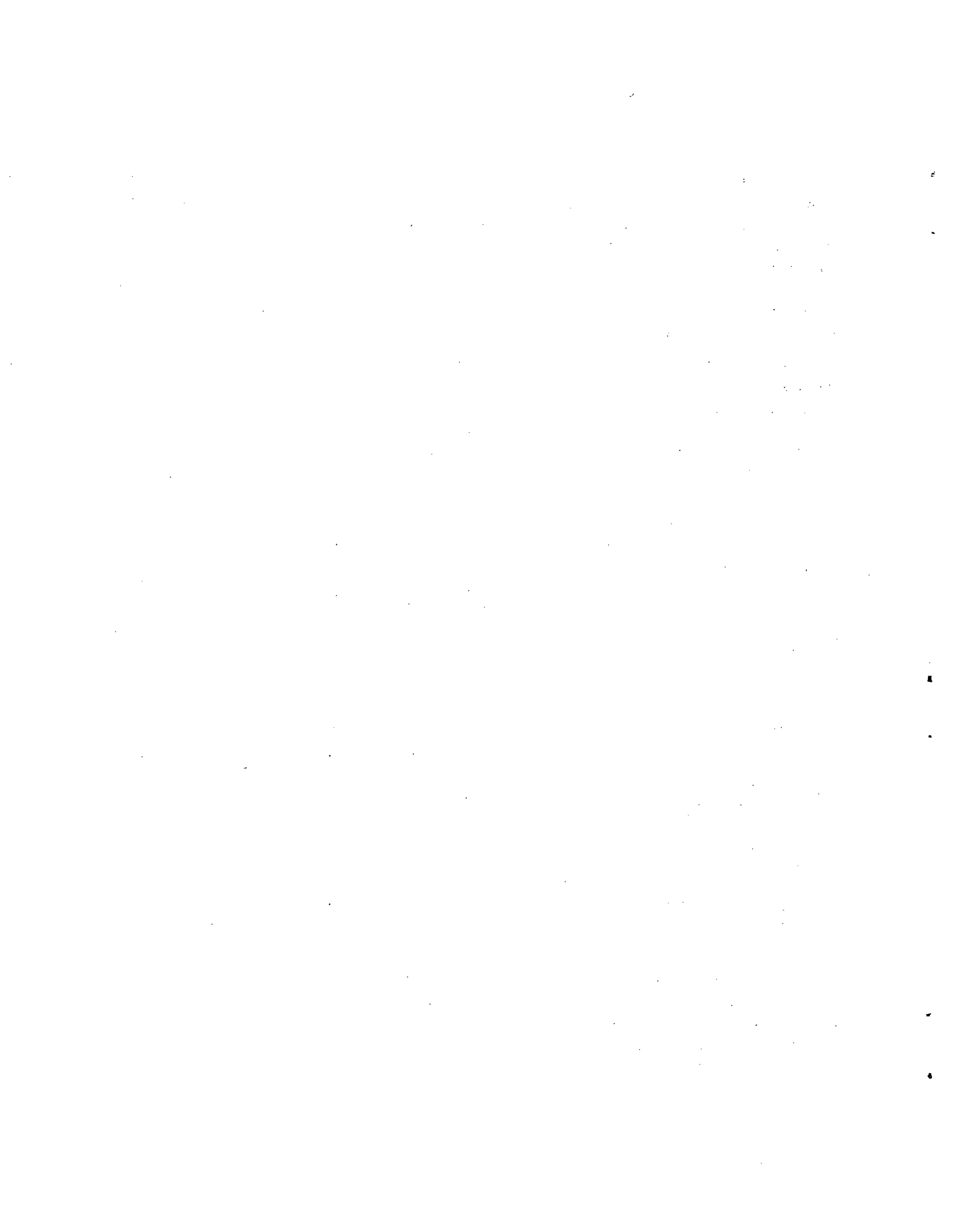
This report represents a major portion of the work performed at Sandia National Laboratories, Livermore under the Sandia Hydrogen Program for the U.S. Nuclear Regulatory Commission. Computational methods are described which permit techniques previously used for modeling small-scale laboratory experiments to be extended to the simulation of experiments with much larger length scales. The specific configurations considered are the propagation of hydrogen-air burns in the FLAME facility at Sandia National Laboratories, Albuquerque. The largest length scales appearing in these experiments approach in size those which might occur in nuclear reactor accident scenarios.

These length scales exceed the thicknesses of the hydrogen flames by a large factor. Because of this, it was necessary to invent a new procedure to represent the flow variables on a finite-difference grid in which computer limitations require that the grid spacing exceed the physical flame thickness. The new method consists of imposing minimum values of turbulence intensity and turbulent length scale so as to artificially thicken the flame. This is done in such a way that the burn velocity obeys established dependencies on turbulence level, pressure, and unburned gas temperature.

The resulting model is applied to the simulation of one of the experiments performed with obstructions in the channel of the FLAME facility. By using *only* the initial flame velocity to adjust parameters in the model, a quite successful representation of the experimental flame trajectory and pressure histories is obtained. The calculation does display some inadequacies; it fails to reproduce a sudden acceleration midway in the experiment, and it exhibits a detonation near the end. Nonetheless, it provides a meaningful study of many features of the gas flow and flame propagation.

As one example of this, the computations point out the way in which the acceleration of the flame and its propagation in the choking regime are accompanied by large increases in the amplitude of pressure waves which reflect off the obstacles. This mechanism contributes to the positive feedback which drives the flame acceleration in two ways: (1) it leads to an increased combustion rate via compression and shock heating and (2) it produces increased turbulence through the generation of large flow velocities with high shear, thereby augmenting the thermal mixing. These increasing pressure and turbulence levels are also undoubtedly indicative of a buildup of sensitivity to detonation. This emphasizes the importance of a careful interpretation of experiments with regard to the degree of confinement of the gas, which has been well-established experimentally. The results are consistent with a reduction in flame acceleration in the presence of pressure relief due to venting. (It is noted, however, that there is a potential for increased production of turbulence in the presence of partial venting which remains to be investigated.)

In summary, this work contains two major contributions: (1) the development of the numerical model, and (2) the use of the computer calculations to provide insight into the processes accompanying flame acceleration in experiments in the FLAME facility. It defines the attributes and limitations of current computational capabilities in this research area, and suggests additional steps that could be taken to improve them.



I. INTRODUCTION

In this paper, we describe a computational model for simulating the propagation of premixed turbulent flames which extend over spatial length scales which are large compared to those which characterize the turbulent flame zone. In these situations, the geometric complexity is often such that it is impossible to provide accurate resolution of the flame front on a computational grid which encompasses the entire domain of interest. The specific configurations to which this work has been applied are experiments performed in the FLAME facility¹⁻³ at Sandia National Laboratories in Albuquerque, New Mexico (see Figure 1). The FLAME facility consists of a reinforced concrete channel 2.44 m high by 1.83 m wide by 30.5 m long (8 ft by 6 ft by 100 ft). The particular experiments considered here involve the ignition of a hydrogen-air mixture at one (closed) end and the propagation of the flame past periodically spaced obstacles toward the other (open) end (see Figure 2).

Turbulence generated ahead of the flame as the unburned gas flows past the obstacles results in an increase in the combustion rate. This, in turn, causes the flow velocity of the unburned gas to increase, with a concurrent increase in the turbulence level. Hence, there is a positive feedback mechanism which leads to acceleration of the flame as it propagates down the channel.

This mechanism for flame acceleration has been described previously for experiments on a smaller scale.⁴⁻⁶ Some work has also been done on large-scale experiments.⁷ The primary purpose of the FLAME facility is to provide relatively large-scale results for hydrogen-air burns. The ultimate goal of the research is to determine scaling laws which will permit assessment of potential hazards to nuclear reactors in case of hydrogen production in reactor accidents (see, e.g., Reference 8). The length scales existing in the FLAME facility are much larger than those typically occurring in the small-scale experiments described in References 4-6, but are somewhat smaller than some which might be encountered in a reactor containment.

The purposes of this paper are to describe our method for simulating flame acceleration in such large-scale configurations, to compare computational results with a limited set of experimental data, and to provide some analysis of the processes occurring in the experiments.

The computer modeling of reacting flows as complex as those existing in the present experiments is extremely difficult. There are, in principle, a large number of chemical reactions to be accounted for. In all but the simplest flow configurations, one must approximate the true chemical kinetics with a reduced model. Furthermore, as noted above, turbulence plays a crucial role in determining the rate of mixing of burned and unburned gas, and therefore has a great influence over the rate of combustion. A complete solution to the Navier-Stokes equations for turbulent flow is manifestly impossible in practical engineering calculations such as these. It is therefore necessary to provide a turbulence model which permits the computation of turbulence intensities and time scales. In this work, we have used the $k-\epsilon$ model.⁹⁻¹⁰ Given such a method for the determination of turbulence parameters, one must couple it to the combustion model in order to have a realistic determination of the rate at which the unburned gas is consumed. There have been various proposals for reasonable ways to do this. Most notable for our purposes are the Magnussen-Hjertager model¹¹ and the eddy breakup model.¹²⁻¹³

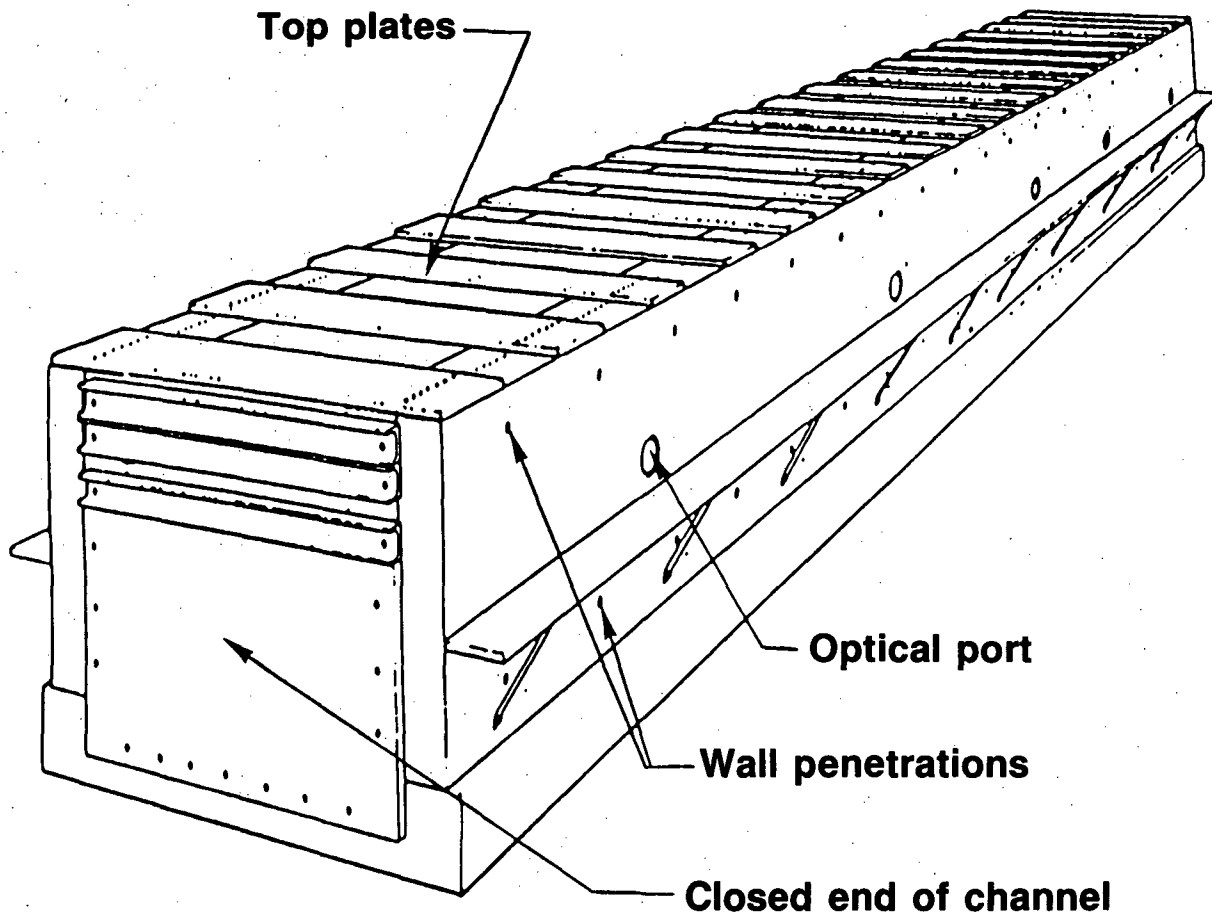


Figure 1. Sketch of the FLAME facility. (From Reference 3.) The vertical coordinate is assumed ignorable in the two-dimensional computer calculations. (Note: FLAME is an acronym for "FLame Acceleration Measurements and Experiments.")

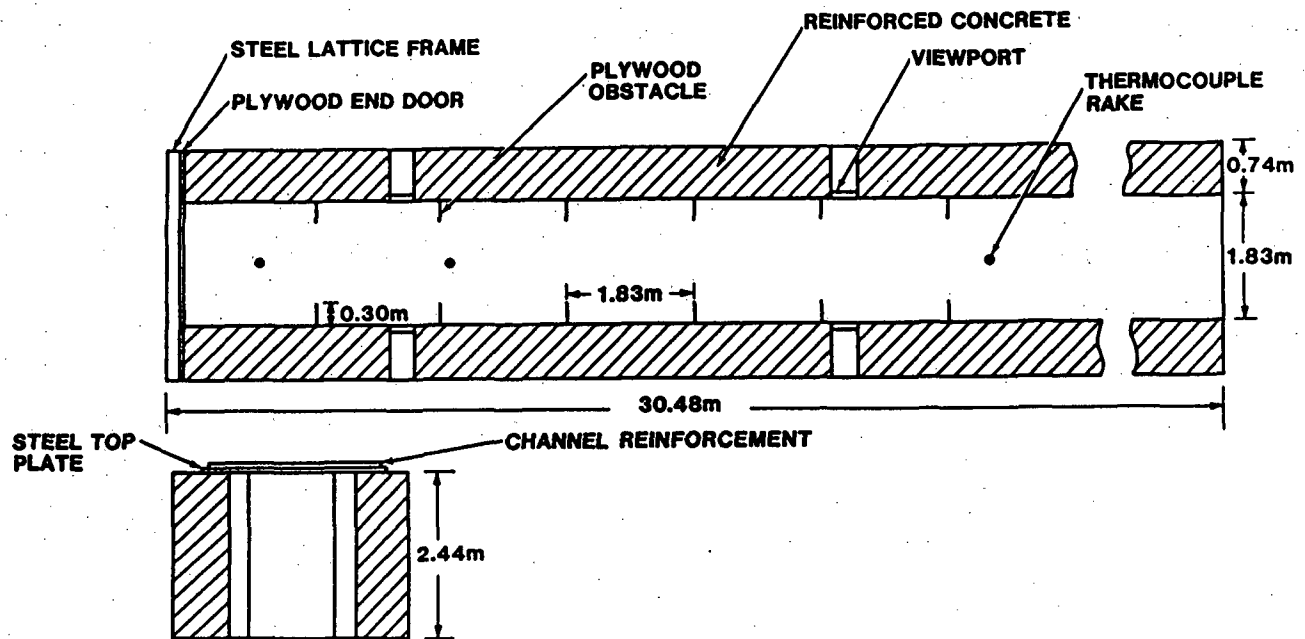


Figure 2. Schematic of the FLAME facility with obstacles installed. (From Reference 34.) The obstacles used in the experiments described in this work are shown to scale; the blockage ratio is $\frac{1}{3}$. The enclosed area in the top view is the two-dimensional domain of the computer calculations.

The Magnussen-Hjertager model is useful in situations where the flame propagation is determined by the rate of thermal mixing. It has been previously employed in studies of flame acceleration in small-scale experiments.¹⁴ However, when it was used in conjunction with the $k-\epsilon$ model in attempted simulations of flame acceleration experiments, the results were unfavorable. Strong spatial oscillations of the flow variables and turbulence parameters appeared in the solution. Although the oscillations were of short wavelength, i.e., alternating on adjacent grid points, no temporally increasing numerical instability appeared. It appeared that the difficulty was introduced by trying to resolve phenomena on a length scale incompatible with the grid spacing. As noted above, this is anticipated when features in the flow configuration are large compared to the flame thickness. In such cases, in order to achieve a numerically viable description of the fluid, it is necessary to find some way to define the flame front on a numerical grid which extends over a large spatial domain. Although there has been some success in the application of adaptive gridding techniques to this problem,¹⁵⁻¹⁶ we know of no attempts to apply them to calculations where a turbulence model must be used to define combustion rates. The reason for this is that the resulting turbulent flame profile may not be particularly well-justified theoretically, so there is no point in devoting a great deal of computational effort to its definition. It is also true that the geometric complexity of the present experiments would make application of adaptive gridding very difficult.

For these reasons, we have developed a combustion model which combines some of the features of the Magnussen-Hjertager and eddy breakup models with some artificial definitions of turbulence parameters in the flame zone for flame propagation at low turbulence levels. This allows us to resolve the flame thickness over a number of grid points sufficient for good numerical behavior, and to specify the burn velocity as a realistic function of turbulence level, pressure, and temperature of the unburned gas. It is important to note that, while we thereby do not compute the burn velocity from first principles, we are able to achieve fairly good agreement with many aspects of the experiment with only minimal adjustment of a small number of parameters.

In the next section, we give a brief description of the Conchas-Spray computer code¹⁷ which we have used for the calculations. (The simulations described here have been performed in a two-dimensional domain, but the model itself is not restricted to two dimensions.) We also discuss some features of the version of the $k-\epsilon$ turbulence model that we have implemented into the computer code. In Section III, we derive the new features of our combustion model and discuss its capabilities when integrated into the code.

Results of the simulation of an actual experiment in the FLAME facility are presented in Section IV. The reason for the concentration of effort on only one experiment is that only three experiments have been performed within the particular configuration to which our model currently applies, and they do not cover a large range of hydrogen concentrations. Both the experiments and the computer calculations are expensive; this unfortunately limits the data base and the number of simulations permissible.

A particularly noteworthy result is that there is a period of time during which the computed flame velocities and pressures agree quite well with the experimental values. During that time period, the flow velocities are approximately sonic, and it appears likely that these velocities are determined primarily by a choking mechanism. The pressure signals are characterized by oscillations determined by the burnout of the individual chambers formed by the obstacles.

Some conclusions and recommendations are offered in the final section of the paper.

II. COMPUTER CODE AND TURBULENCE MODEL

Flow Variables and Chemistry

The Conchas-Spray code (modified to include the k - ϵ turbulence model) solves the following system of equations for the flow variables:

$$\frac{\partial \rho_i}{\partial t} + \nabla \cdot (\rho_i \mathbf{u}) = \nabla \cdot [D \nabla (\rho_i / \rho)] + \dot{\rho}_i^c \quad (1)$$

$$\frac{\partial (\rho \mathbf{u})}{\partial t} + \nabla \cdot (\rho \mathbf{u} \mathbf{u}) = -\nabla p + \nabla \cdot \sigma \quad (2)$$

$$\frac{\partial (\rho I)}{\partial t} + \nabla \cdot (\rho I \mathbf{u}) = -p \nabla \cdot \mathbf{u} + \nabla \cdot [k_T \nabla T + \rho D \sum_i h_i \nabla (\rho_i / \rho)] + \dot{Q}_c + \rho \epsilon \quad (3)$$

where ρ_i is species density, \mathbf{u} is velocity, I is specific internal energy, $\dot{\rho}_i^c$ and \dot{Q}_c are the rates of change of ρ_i and energy per unit volume due to chemical reactions, k is the turbulent kinetic energy, and ϵ is the rate of dissipation of k . The index i denotes the individual species. In this paper four species are considered: H_2 , O_2 , N_2 , and H_2O . In the interest of conciseness, the identification and method of evaluation of many of the rest of the terms in these equations will only be briefly outlined. For further details, see References 17-19. The total mass density ρ is obtained by summing the ρ_i over all species. The temperature T is computed from the energy I by assuming that the species enthalpies h_i are functions only of T . The pressure p is then obtained from the ideal gas law. Diffusion of mass and heat are accounted for by the terms involving the mean diffusion coefficient D and the thermal conductivity k_T . The stress tensor σ is given by

$$\sigma = -\frac{2}{3} \rho k \delta + \mu \left[\nabla \mathbf{u} + \nabla \mathbf{u}^T - \frac{2}{3} (\nabla \cdot \mathbf{u}) \delta \right] \quad (4)$$

where δ is the unit tensor, the superscript T denotes the transpose operator, and the viscosity is

$$\mu = \mu_L + \mu_T \quad (5)$$

where μ_L is laminar viscosity and μ_T is turbulent eddy viscosity. The eddy viscosity is obtained from the k - ϵ turbulence model, and will be discussed later. The laminar viscosity is obtained from Sutherland's formula with appropriate coefficients, but is actually negligible in our calculations.

The term ϵ in (3) is the rate of dissipation of turbulent kinetic energy per unit mass. (The dissipation term describes the conversion of turbulent kinetic energy into heat; hence it is an

additive term in the energy equation (3).) Equations (1)–(3) are in Favre-averaged form,^{9,13,18} assuming that the turbulence model can appropriately account for the Reynolds stresses via Equations (4) and (5), and that ϵ can be correctly computed. We are neglecting differential species diffusion by using an average value of diffusion coefficient D . This is not well-justified for a hydrogen-air mixture, but in view of the fact that we are using an artificial model to define the flame zone, this discrepancy does not detract from the results.

The thermal conductivity k_T and diffusion coefficient D are related to viscosity μ by

$$k_T = \frac{c_p \mu}{Pr} \quad (6)$$

$$D = \frac{\mu}{\rho Sc} \quad (7)$$

where c_p is the specific heat at constant pressure and Pr and Sc are turbulent Prandtl and Schmidt numbers. We have used $Pr = Sc = 0.52$. However, because of the aforementioned flame front modeling, our results are not sensitive to this choice.

The following quantities appearing in the equations remain to be determined: The chemical contribution to the species conservation equation $\dot{\rho}_i^c$, and the chemical heat release Q_c . These terms describe processes that are too complex to be evaluated in detail numerically for the present experimental configuration. Our model for them will be derived in Section III.

In this work, the chemistry is assumed to consist of the global one-step reaction



In this case, given the ρ_i 's and h_i 's, all the chemical rates $\dot{\rho}_i^c$ and Q_c are completely defined by specifying only one of the species production rates. (We choose to use $\dot{\rho}_{H_2}^c$ for this purpose.)

At this point, it is convenient to define one more variable for later use. Models which assume that combustion is limited by the rate of thermal mixing usually make use of a progress variable, or something related to such a quantity. Our progress variable is defined as

$$C = \frac{Y_p}{Y_p^\infty}$$

where Y_p is the mass fraction of the product species and Y_p^∞ is the mass fraction of product that would result if the locally extant mixture was allowed to react to completion. (Subscripts f and p will be used for fuel and product henceforth. In our case these correspond to H_2 and H_2O .) Then

$$Y_p^\infty = \frac{\rho_p + \frac{\nu_p m_p}{\nu_f m_f} \rho_f}{\rho}$$

where the ν_i are stoichiometric coefficients (both equal to 2 in our one-step H_2 -air reaction—see Equation (8)), and the m_i are the corresponding molecular weights. Hence,

$$C = \frac{\rho_p}{\rho_p + \frac{\nu_p m_p}{\nu_f m_f} \rho_f} = \frac{n_p}{n_p + \frac{\nu_p}{\nu_f} n_f} \quad (9)$$

where n_f and n_p are the number densities of the fuel and product species. The quantity C always satisfies $0 \leq C \leq 1$. (Note that the denominators in Equation (9) are the densities of product species instantaneously available under conditions of complete reaction of a lean mixture (at constant volume), and $C = 1$ when the fuel is completely consumed. This equation can be used for a fuel-rich mixture; if the subscript f is replaced by o (denoting the oxidizer), $C = 1$ when the oxidizer is consumed.)

The computer code used for our calculations is an adaptation of the Conchas-Spray code developed by Los Alamos National Laboratory. It provides a solution to Equations (1)–(3) in two dimensions; the present calculations are performed in rectangular coordinates. The numerical algorithm employed in the code is a finite-difference approximation derived from an integral formulation of the conservation laws. For details see References 17 and 20.

All the computations employ an Eulerian method on a grid with square cells (see Figure 3). The thickness of the obstacles is taken to be two grid spacings for numerical simplicity. (The experimental obstacles were constructed of 13 mm (1/2 inch) plywood, and were therefore considerably thinner. However, the difference has negligible effect on our results.) The z -axis lies in the midplane of the facility, which is assumed to be a symmetry plane. Hence, the grid on which the computations were carried out encompassed only half the area of the facility. Except where noted otherwise, the grid consists of 13 points in the (transverse) x -direction by 397 grid points in the (axial) z -direction. This encompasses sixteen and one-half chambers formed in the channel by the obstacles used in the experiments. This is a very coarse grid; it is not adequate to resolve recirculating flows behind the obstacles with precision. Furthermore, errors will be incurred in the computation of the shock waves which form when the gas flows past obstacles at supersonic speeds. We have investigated the numerical accuracy to the extent possible by refining the grid spacing by a factor of 2/3. The results (discussed in Section IV) show some differences; nonetheless, the coarse grid suffices for calculations which provide insight into the processes involved.

The k - ϵ Turbulence Model

The turbulence model which we have used is the k - ϵ model as described in References 9 and 10. Although Reference 9 specifically addresses the question of compressible flows, it should be noted that turbulence models for compressible flows are not well-developed. Hence, the choice of the standard k - ϵ model in this situation cannot be regarded as definitive.

The model consists of the following transport equations for the evaluation of turbulent kinetic energy k and dissipation rate ϵ .

$$\frac{\partial}{\partial t}(\rho k) + \nabla \cdot (\rho k \mathbf{u}) = \sigma : \nabla \mathbf{u} + \nabla \cdot (\mu \nabla k) - \rho \epsilon \quad (10)$$

$$\frac{\partial}{\partial t}(\rho \epsilon) + \nabla \cdot (\rho \epsilon \mathbf{u}) = C_{1\epsilon}(\sigma : \nabla \mathbf{u}) \frac{\epsilon}{k} + \nabla \cdot \left(\frac{\mu}{\sigma_\epsilon} \nabla \epsilon \right) - \frac{C_{2\epsilon} \rho \epsilon^2}{k} \quad (11)$$

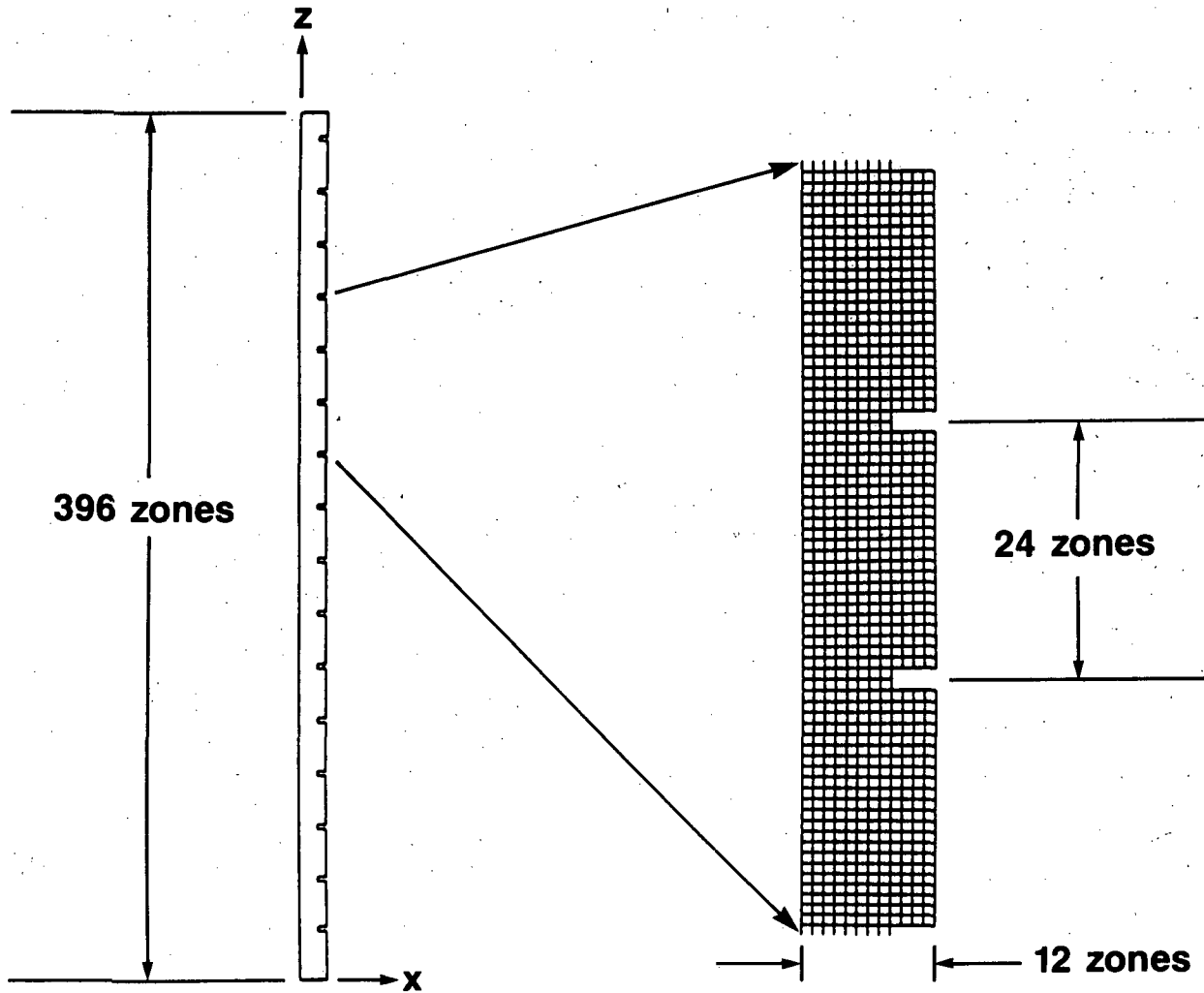


Figure 3. Problem domain and finite-difference grid used in most of the calculations. The full $16\frac{1}{2}$ chambers into which the facility is divided is shown on the left. The grid is too fine to be resolved on the scale used there. An expanded view of 3 chambers is given on the right.

The terms on the right sides of these equations represent (from left to right) the production, diffusion, and dissipation of the quantities k and ϵ . Strictly speaking, Favre averaging requires the inclusion of a term in (11) involving the correlation between velocity fluctuations and the pressure.^{9,13} Following a practice often used¹³, we omit this term to avoid undue complexity in a turbulence model which is still under development for compressible flows. The coefficients $C_{1\epsilon}$ and $C_{2\epsilon}$ are modeling constants, and σ_ϵ is a Schmidt number. These constants have been tuned¹⁰ for agreement with certain experiments, with optimum values $C_{1\epsilon} = 1.92$, $C_{2\epsilon} = 1.44$, and $\sigma_\epsilon = 1.3$. (The experiments used for tuning are much simpler than those addressed here. Furthermore, they involve incompressible flows. Hence, the use of these constants should not be regarded as definitive.)

The turbulent part of the viscosity (the eddy viscosity) is given by

$$\mu_T = C_\mu \rho \frac{k^2}{\epsilon} \quad (12)$$

The coefficient C_μ is set equal to the usual value of 0.09 (see, e.g., Reference 10).

Since k and ϵ are defined to be nonnegative, it is important that the numerical scheme preserve this property. The production and dissipation terms in the k and ϵ equations require special consideration in this regard. Since turbulent regimes are sometimes characterized by the fact that production approximately equals dissipation, care must be taken to ensure that numerical errors in either term do not result in negative k or ϵ . A special numerical scheme was devised to alleviate such difficulties. It is given in Appendix A.

In the Conchas-Spray code, the boundary conditions on tangential velocity are obtained by implementing the law of the wall for turbulent boundary layers.^{17,21,22} To this end, the tangential velocity at walls is not zero, but is allowed to vary to account for fluid momentum in the wall grid cells, which are in the boundary layer. We have essentially retained the numerical boundary condition as in the original code except that we restrict the velocity in a cell at a wall to be less in magnitude than the tangential velocity in the adjacent cell one grid point in from the wall. This prevents occasional nonphysical profiles from occurring.

The boundary conditions on k and ϵ are likewise obtained from consideration of the law-of-the-wall shear layer. The wall shear stress τ is obtained by assuming that the tangential velocities at grid points one cell away from the wall are in the law-of-the-wall boundary layer. This allows one to solve a simple equation for the shear stress.¹⁷ Assuming that the Reynolds stresses are nearly constant, it can be shown¹⁰ that the turbulent kinetic energy in the wall cell may be approximated by

$$k = \frac{u_*^2}{\sqrt{C_\mu}}$$

where u_* is the shear velocity

$$u_* = \sqrt{\tau/\rho}$$

This provides the boundary condition on k . The associated boundary condition on ϵ is

$$\epsilon = \frac{u_*^3}{\kappa y}$$

where y is the distance to the wall and $\kappa = 0.4$ is the von Kármán constant. This $1/y$ behavior of ϵ can give rise to some numerical inaccuracy, especially in the diffusive flux of ϵ . This can be alleviated by implementing a special differentiation formula near the wall. Details are given in Appendix B.

III. THE COMBUSTION MODEL

Properties of Turbulent Flames and Numerical Flames

As noted in the Introduction, simulation of combustion processes in large experiments places extreme demands on the capabilities of even the largest and fastest computers. In the present case, it is necessary to give up the idea of resolving the flame thickness on the computational grid. A possible exception arises in situations in which the turbulent length scale is very large and the turbulent flame thickness, defined as the thickness of a region where burned and unburned mixture both exist, extends over several grid points. But for satisfactory numerical behavior we must usually thicken the flame artificially. To illustrate this point, a plot of the laminar, turbulent, and computational flame profiles are given in Figure 4. Turbulence results in rapidly fluctuating wrinkles and spirals of interpenetrating burned and unburned gas, as shown in the upper sketch in the figure. The turbulent flame thickness δ_T is defined by the region where the composition is intermittent due to the fluctuations, and the average value of C is greater than zero, but less than unity. For good numerical behavior, the computational flame thickness δ_c must be equal to a few grid spacings. (The size of one grid interval is indicated by Δx . The scale in the figure is not necessarily accurate; the various lengths actually satisfy

$$\frac{\delta_c}{4} \approx \Delta x > \delta_T > \delta_L$$

Artificial flame thickening has been done previously by a method known as the β - transformation.^{23,24} This involves changing the length scales in the problem by artificially increasing the thermal diffusivity and diffusion coefficient and decreasing the combustion rate. We have retained this essential idea. However, the original β - transformation established the scaling through the use of the local temperature gradient in the problem. Numerical experimentation indicated that this did not work well with mixing-limited combustion models such as the Magnussen-Hjertager model. Hence, it was decided to achieve the flame thickening in a different way.

Given that the flame will be somewhat artificial, it is necessary to first determine what properties it should have. In particular, it is desirable that the burn velocity be realistic. The

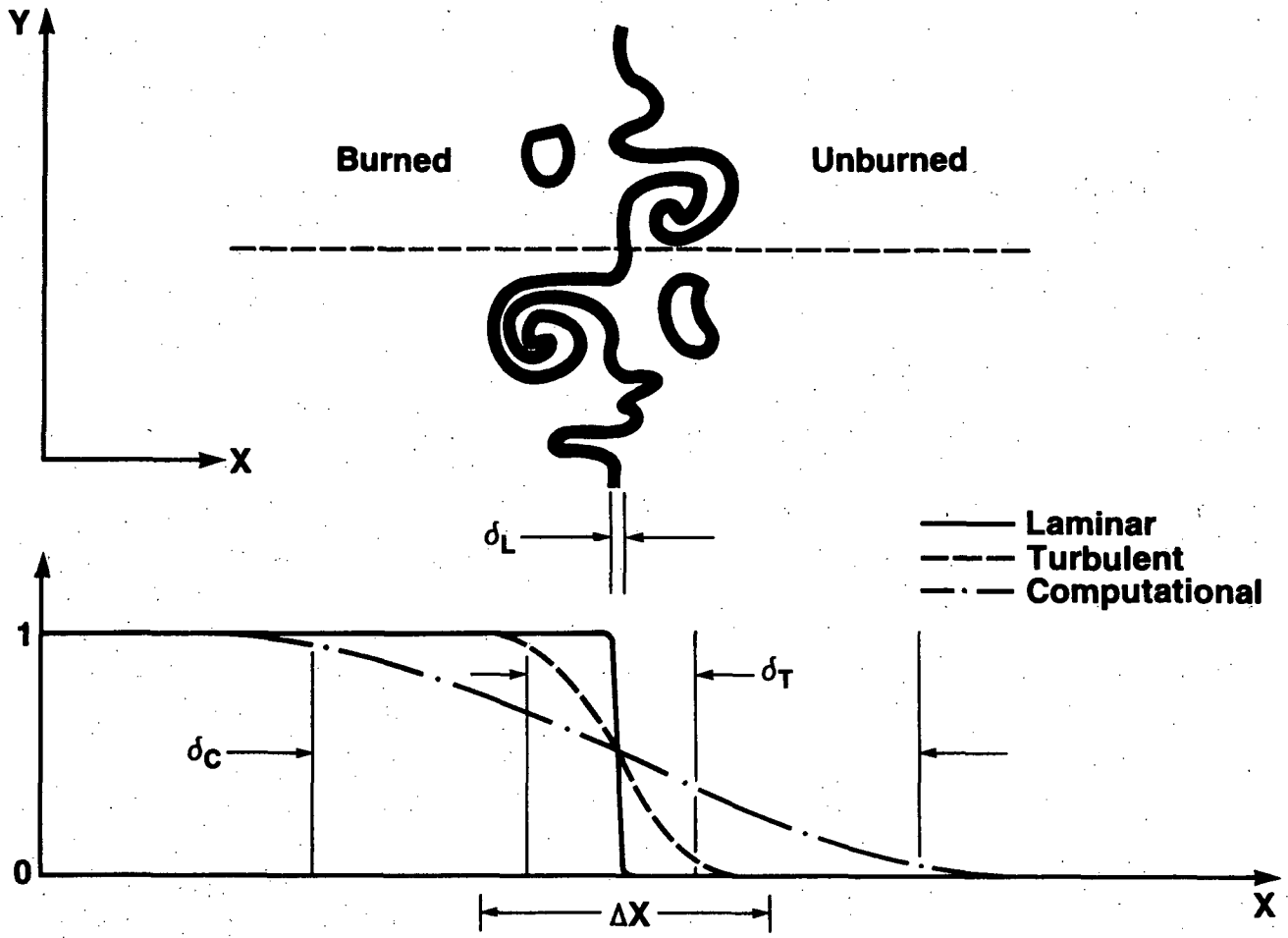


Figure 4. Schematic illustration of laminar flame thickness, turbulent flame thickness, and computational flame thickness. Above: A slice through a turbulent flame, plotted in (x,y) coordinates. The thickness of the dark lines is the laminar flame thickness δ_L . Below: A plot of the progress variable C (defined in Equation (9)), for y equal to the constant value defined by the dashed line in the upper figure.

following properties of turbulent flames have been extracted from a list given in Reference 13 (S_L and S_T refer to laminar and turbulent burn velocities, respectively):

1. $S_T > S_L$ (almost always)
2. S_T increases with $u' \equiv \sqrt{k}$. Often, the increase is linear, and

$$S_T = AS_L + Bu'$$

provides as good a correlation as anything else*.

3. Sometimes S_T is insensitive to the scale of approach flow turbulence.
4. In open flames, the variation of S_T with composition is much the same as for S_L .
5. In flames in ducts, S_T is larger than for open flames and is sometimes insensitive to approach flow turbulence and composition.

Our model represents an attempt to adhere to these properties, except for the latter clause in Number 5. It does not necessarily apply to our experimental configuration, as it was inferred from experiments on steady-state flames stabilized in small ducts.

To see how to embed the above properties 1 through 4 in a combustion model, we note that, for the case of mixing-limited combustion models such as Magnussen-Hjertager or eddy breakup, simple flat flames will be expected to have the following properties (see, for example, the discussion of laminar deflagrations in Section 5.1.2 of Reference 19):

The turbulent burn velocity will scale as

$$S_T \sim \sqrt{\chi/t_T} \quad (13)$$

where χ is the thermal diffusivity (assumed proportional to the diffusion coefficient—see Equations (6) and (7)) and t_T is the turbulent time scale. (This is commensurate with the assumption of burning limited by thermal mixing, where the rate of combustion is proportional to $1/t_T$).

The turbulent flame thickness will scale as

$$\delta \sim \sqrt{\chi t_T} \quad (14)$$

From the k - ϵ turbulence model,

$$\chi \cong C_\mu \sqrt{k} L / Pr$$

and

* Note that u' is defined here as the average turbulent velocity, and not as the instantaneous velocity fluctuation.

$$t_T = \frac{L}{\sqrt{k}} \quad (15)$$

where

$$L = k^{3/2}/\epsilon \quad (16)$$

is the integral length scale of turbulence. From (13) and (14), then

$$S_T \propto \sqrt{k} = u' \quad (17)$$

$$\delta \propto L \quad (18)$$

In other words, if the turbulence intensity \sqrt{k} and the length scale L are given for the gas, one can achieve a model which complies with the linear part of Property 2 and with Property 3.

Development of a Model With Appropriate Properties

In applying a mixing-limited combustion model to a computation such as this, it must be recognized that difficulties may occur when starting up a problem when the turbulence level is low. Initially, one expects the flame to be laminar, but in our experimental configuration this will be quickly superseded by a flame which exhibits some form of turbulence, e.g., a wrinkled laminar flame.^{13,19} Data from a variety of experiments in the FLAME facility suggest that the hydrogen-air flames studied in the facility achieve a relatively constant burn velocity which is greater than laminar and which persists until large-scale instabilities and/or obstacles cause the flame to accelerate.^{2,3,25}

The approach that we have developed is to endow the gas with minimum values of k and L , denoted k_m and L_m , which are used for the computation of thermal conductivity and diffusivity only. In that way, according to Equations (17) and (18), there will be minimum values of burn velocity and flame thickness. The minimum burn velocity provides a term like AS_L in property 2, although not in such a way that the equation there is exactly satisfied. The scheme which we employ is to use k_m and L_m in the formulas for k_T and D unless the true turbulence intensity k or length scale L predicted by the k - ϵ model exceeds those threshold values. Then we use k and/or L . It is crucial to note that only the true values k and L (or, equivalently, ϵ) are used in the viscosity. In particular, they are used in the transport equations (10) and (11) for k and ϵ themselves, and in (12) for μ_T , so that k_m and L_m affect the generation of turbulence only indirectly. (It may appear that this indirect effect is a very strong one, since the gas velocities appear in the turbulence production terms in (10) and (11). However, if k_m and L_m are chosen correctly, these gas velocities would be essentially the same as those occurring in a perfectly resolved flame.)

Now, how should k_m and L_m be determined? It would be desirable that k_m correspond to something physically realistic, because the point at which k exceeds k_m should represent some real point in parameter space at which the flame starts to propagate more rapidly.

We have extracted a reasonable choice from the work of Libby, Bray, and Moss (LBM).²⁶ In the limit of large turbulent Reynolds number $R_T \equiv \rho u' L / \mu$, they obtain a formula

$$S_T = S_L + 1.14\sqrt{k} \quad (19)$$

This formula is derived by making certain modeling assumptions regarding physical processes in flames. It is not intended to be universally valid, even in the limit $R_T \rightarrow \infty$. In fact, References 13 and 26 demonstrate clearly that no universal formula exists. But we choose to use this as a starting point. Given that we can extract an initial turbulent burn velocity S_{Ti} from experimental data, we obtain a provisional estimate for k_m by inverting (19):

$$k_m = \left(\frac{S_{Ti} - S_L}{1.14} \right)^2 \quad (20)$$

We emphasize that this is only an estimate. As discussed below, it is impossible to satisfy all the desired flame properties and still adhere to this value of k_m .

We now give our formula for the rate of consumption of fuel. (As noted in the discussion following Equation (8), for a one-step reaction, specification of the rate for only one species suffices to specify all chemical rates.) Except for a dependence on pressure and unburned gas temperature to be discussed later, the combustion rate is

$$\dot{\rho}_f = -A_c \rho f(T) C(1 - C) / t_T \quad (21)$$

where A_c is a dimensionless constant, and

$$f(T) = \begin{cases} 1 & T_a < T \\ \frac{T - T_o}{T_a - T_o} & T_o \leq T \leq T_a \\ 0 & T < T_o \end{cases}$$

where T_a is adiabatic flame temperature and T_o is the initial gas temperature. Note that the factor $C(1 - C)$ is similar to that appearing in approximations to the eddy breakup model (see Equation (4.72) of Reference 13) and to the minimum normalized mass fraction appearing in the Magnussen-Hjertager model¹¹. The function $f(T)$ serves a special numerical purpose. It does not really represent any physical process, except that it provides a qualitative increase in combustion rate with temperature up to the adiabatic flame temperature. It is inserted in Equation (21) so that the flame profile will be determined by thermal diffusion in such a way as to obey Equations (13) and (14), with the result that (17) and (18) are satisfied. Lacking the factor $f(T)$, Equation (21) results in flame zones that tend to diffuse too far ahead of and behind the flame, and which do not exhibit the functional behavior specified in (13) and (14). This spreading is predictable on the basis of comparison with solutions to the Kolmogoroff-Petrovsky-Piscounoff (KPP) equation²⁷⁻²⁹.

At this point we have three adjustable parameters: k_m , A_c and L_m . They are fixed by simultaneously specifying the following three flame properties: The initial turbulent burn velocity S_{Ti} , the derivative $S_T' \equiv dS_T/d\sqrt{k}$ for adiabatic flames, and an appropriate numerical flame thickness. Our initial choice for $dS_T/d\sqrt{k}$ is 1.14, in accordance with (19). A variation on this value will be discussed in Section IV. (The actual values of k_m , A_c , and L_m are determined by adjusting them in a series of one-dimensional flat flame calculations.) In most of our calculations, we have attempted to maintain a 10-90% thickness of 4 grid points. As noted above, our model does not precisely satisfy Equation (19). It does, however, provide values for the initial burn velocity and slope of the S_T vs \sqrt{k} curve which are physically well-justified. (See Figure 5.)

Dependence on Pressure and Pre flame Temperature

Finally, we describe the way in which the combustion model is augmented to include a dependence on pressure and the temperature of the unburned gas through which the flame is propagating. As the flame travels down the obstructed channel of the FLAME facility, the unburned gas in front of it is compressed due to the overall drag forces which build up. This compression results in an increase in pressure and temperature. Since the laminar burn velocity of a hydrogen-air mixture depends on the pressure and temperature of the unburned gas, the turbulent burn velocity will also exhibit such a dependence. In the spirit of property 4 which is desired for the combustion model, we simply choose to impose the same functional dependence of S_T on p and unburned gas temperature T_u as is expected for the laminar burn velocity S_L . Warnatz³⁰ has shown that in certain regimes S_L varies according to

$$S_L \propto p^m T_u^n$$

Consideration of Equations (13) and (14) indicates that, all else remaining constant, S_T will exhibit the same behavior if the burn rate, thermal diffusivity, and diffusion coefficient are multiplied by a factor

$$h(p, T_u) = \left(\frac{p}{p_o}\right)^m \left(\frac{T_u}{T_o}\right)^n \quad (22)$$

where p_o is the initial pressure and T_u is the unburned gas temperature. We have used the values $m = 0.2, n = 1.64$ as being representative of Warnatz' results; this choice is by no means clear-cut, however.³⁰

We have employed T_u , the *unburned* gas temperature, to alter the burn rate and diffusivities. But ρ , χ , and D vary *through* the flame. How do we know what T_u is at points inside the flame? This is determined by extrapolating back to an unburned mixture at the same pressure. (It is assumed that the pressure does not vary significantly through the flame.) We write

$$\int_{T_u}^T c_p(T) dT = \frac{\Delta H}{m_p} Y_p \quad (23)$$

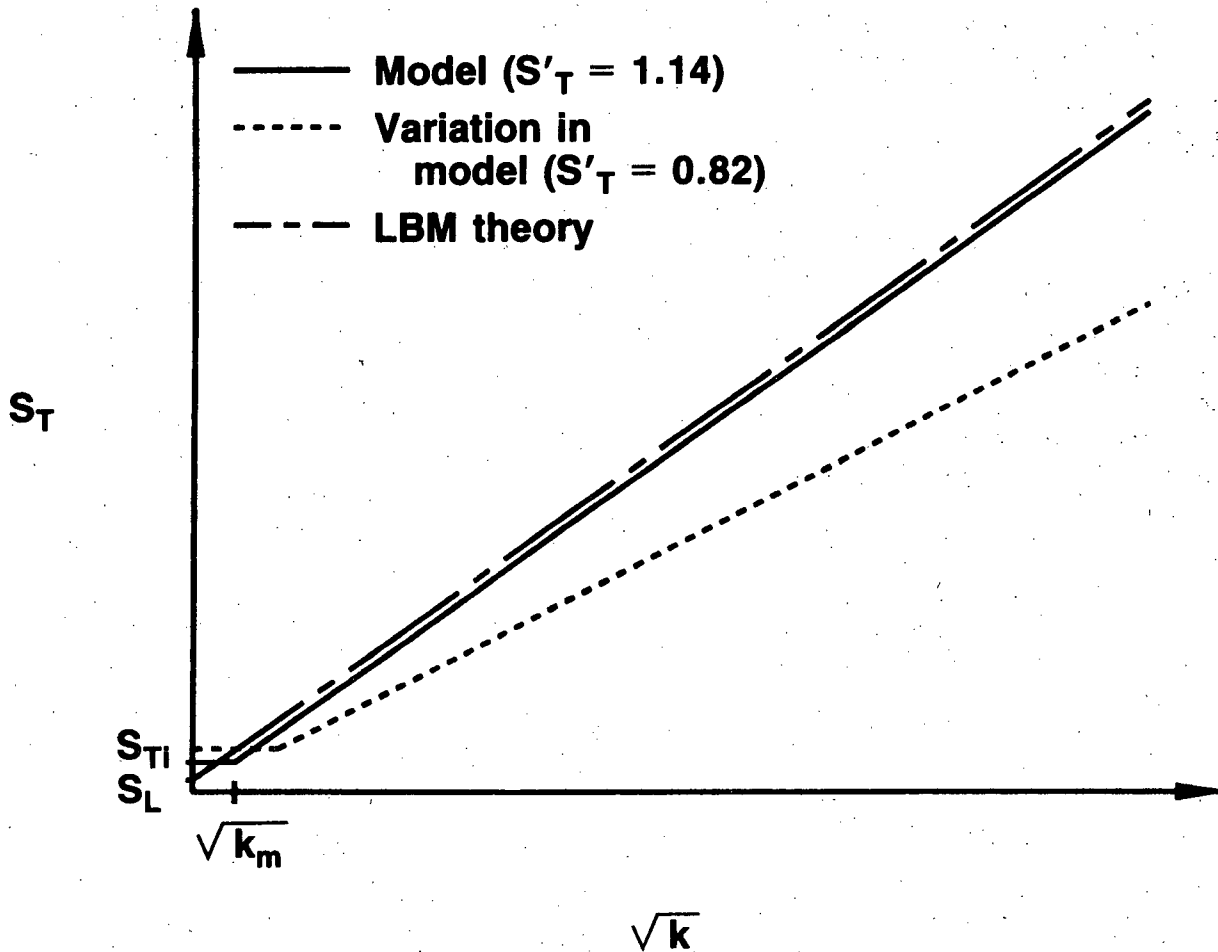


Figure 5. Turbulent burn velocity vs turbulence intensity for the Libby-Bray-Moss model²⁶ (chain-dashed line with slope 1.14) and for the present model (solid line). The difference between the two at low turbulence intensity results from the choice of numerical mechanism available in the present case, and not from any suggestion that the physical situation is better represented. The dashed line represents a variation in the model in which the combustion rate is reduced (see discussion in Section IV). The scales in the figure represent a realistic range of values encountered in the calculations; typical values of \sqrt{k} in the choking regime are about 30 times $\sqrt{k_m}$.

where $c_p(T)$ is the specific heat of the mixture and ΔH is the molar heat of reaction (57.8 Kcal/mole for H_2O). We have obtained a linear fit to the specific heat from data available in the CHEMKIN³¹ code. This approximation has the form

$$c_p = c_{p0} + c'_p(T - T_u) \quad (24)$$

When (24) is substituted into Equation (23), there results a quadratic equation for T_u ; the solution is substituted into Equation (22) to obtain the function $h(p, T_u)$.

Summary of the Model

This completes the description of the combustion model. The implementation of the material presented in the previous section requires a redefinition of the thermal conductivity and diffusion coefficient and an alteration of the formula for combustion rate given in equation (21). For convenience, the appropriate formulas are collected in the following:

$$k_T = \frac{c_p \mu'}{Pr} \quad (6')$$

$$D = \frac{\mu'}{\rho S_c} \quad (7')$$

$$\dot{\rho}_f = -A_c \rho f(T) h(p, T_u) C(1 - C)/t'_T \quad (21')$$

where

$$\mu' = \mu_L + \mu'_T \quad (5')$$

$$\mu'_T = C \mu \rho \sqrt{k_e L_e} \quad (12')$$

$$t'_T = L_e / \sqrt{k_e} \quad (15')$$

and k_e and L_e are effective values of k and L , defined as

$$k_e = \max\{k, k_m\} \quad (25)$$

$$L_e = \max\{L, L_m\} \quad (26)$$

The model has been tested by running one-dimensional calculations of adiabatic flames at constant pressure. For this purpose, the k - ϵ model was turned off so that k_m and L_m would

determine the flame properties. In such calculations the flame achieves a self-similar profile propagating at an approximately constant velocity. As indicated in the foregoing discussions, the desired behavior of the flame velocity and the computational flame thickness δ_c vary according to

$$S_T \propto \sqrt{k_e} p^m T_u^n \quad (27)$$

$$\delta_c \propto L \quad (28)$$

Furthermore, S_T and δ_c should be independent of the grid size. Table I gives some results obtained by varying the parameters around a representative baseline set. (Anticipating the simulations to be discussed in Section IV, the baseline calculation corresponds to a 14.5% hydrogen-air burn at atmospheric pressure and 300°K with k_m , L_m , and A_c chosen appropriately for one of the calculations.) The agreement between the computational values and the desired values is quite good, except possibly for the pressure and temperature dependences. The reason for the discrepancy in the case of the temperature variation is that there is some inaccuracy in the determination of T_u via Equations (23) and (24). Since there is some arbitrariness in the choices for m and n which are used in Equation (22), these discrepancies will be accepted for the remainder of this paper. For the most part, the model achieves its goals for the simple flat (one-dimensional) flame. In particular, it may be noted that the first three lines in the table verify that the slope $dS_T/d\sqrt{k}$ is approximately 1.14, as required by Equation (19).

In summary, the characteristics of the model are as follows: It is designed to provide for the consumption of fuel at a rate consistent with certain assumptions as to the phenomenological behavior of turbulent flame propagation. It permits the computation of the behavior of a compressible fluid ahead of and behind the flame front; it thereby accounts for the interaction of turbulence with the flame insofar as the assumptions relating the turbulent time scale to the combustion rate are correct. It does not permit a computation of burn velocity from a knowledge of only the state of the gas and the turbulent flow structure; it requires prior assumptions as to what the burn velocity would be in a given situation.

It should also be noted that, in the form presented here, the fluid model will exhibit a non-physical heat conduction and particle diffusion everywhere because of the universal application of the (artificially high) threshold values of k and L in Equation (12'). For the present application, errors due to this effect are negligible. To see this, consider the energy conservation equation (3). We wish to show that the artificial heat conduction is negligible on the time scales typical of changes in the specific energy. Suppose that the typical time scale t_t is the time for the initial flame to propagate the width of the channel:

$$t_t = \frac{w}{v_{fo}}$$

where w is channel width and v_{fo} is the initial flame speed. If w is used as the thermal diffusion length scale, the ratio of the diffusion time t_χ to t_t is

Table I.

Results of tests of the combustion model. The quantity Δx is the grid spacing. The burn velocity and flame thickness resulting from the model are S_T and δ_c ; the values of these quantities expected on the basis of simple theory are denoted S_T^e and δ_c^e . The constant A_c (see Equation (21)) is equal to 30.8. The exponents m and n (see Equation (22)) are equal to 0.2 and 1.64.

k_m (J/kg)	L_m (cm)	p (atm)	T_u (°K)	Δx (cm)	S_T^e (m/s)	S_T (m/s)	δ_c^e (cm)	δ_c (cm)	Comments
4.7	68	1	300	7.62	-	2.5	-	16	Baseline Case
19.0	68	1	300	7.62	5.0	4.9	16	16	$k_m = 4k_m^{base}$
1.2	68	1	300	7.62	1.25	1.24	16	16	$k_m = \frac{1}{4}k_m^{base}$
4.7	136	1	300	7.62	2.5	2.4	32	34	$L_m = 2L_m^{base}$
4.7	68	7.6	300	7.62	3.7	4.4	16	25	$(p/p^{base})^m = 1.5$
4.7	68	1	458	7.62	5.0	4.4	16	19	$(T/T^{base})^n = 2$
4.7	68	1	300	3.81	2.5	2.4	16	16	$\Delta x = \frac{1}{2}\Delta x^{base}$
4.7	68	1	300	15.24	2.5	2.6	16	18	$\Delta x = 2\Delta x^{base}$

$$\frac{t_X}{t_t} = \frac{w^2}{\chi t_t}$$

$$\approx \frac{v_{fo} w Pr}{C_\mu \sqrt{k_m} L_m}$$

For typical values $v_{fo} = 16$ m/s, $w = 1.83$ m, $Pr = 0.52$, $C_\mu = 0.09$, $k_m = 4.7$ J/kg, $L_m = 0.68$ m, this ratio is 115. Hence, the diffusion time is long compared to the time during which other processes are occurring, and the artificial diffusion is negligible (except in the flame, of course). As time elapses and the flame accelerates, t_t decreases and the relative error incurred becomes smaller. Inspection of the dispersion relation for acoustic waves shows that the attenuation of such waves is similarly negligible over a propagation distance of a channel width. The attenuation of acoustic waves that propagate the entire length of the FLAME Facility might not be negligible, but they would not be expected to contribute significantly to the results of the present study.

The effects of this nonphysical diffusion could probably be eliminated entirely if necessary. All that would be required is to remove the thresholds on k and L away from the flame. This would require some care, as it would be necessary to ensure that the resulting decrease in diffusivities was kept far enough away from the flame zone that the flame propagation velocity was not affected.

Finally, we note that no attempt has been made in this work to account for the effects of flame stretch and flame curvature in detail. (A general discussion is given in, e.g., Reference 19.) It is impossible to compute such effects in this case, since the flame is artificially thickened, but one might attempt to model them (see, e.g., the model for flame quenching in Reference 32).

IV. COMPARISON OF COMPUTATIONAL RESULTS WITH EXPERIMENT

Experimental Considerations

A total of 9 experiments in which obstacles were present have been performed in the FLAME facility. Table II gives a brief description of these tests and their results.^{33,34} In Tests F-21 through F-23, the facility was unvented; in F-24 through F-29, one-half of the top plates were removed, resulting in 50% venting. In the present report, we are considering only the unvented experiments. In experiment F-21, failure of the mixing fans resulted in uncertain hydrogen concentrations. Hence, only experiments F-22 and F-23 are available to us for comparison with the type of computations with which we are concerned.

The only difference in the experimental arrangement in F-22 and F-23 is that the initial hydrogen concentrations were 15% and 14.5%, respectively. In experiment F-23, the mixture appeared to detonate; in F-24 it did not. Since turbulent flows and conditions leading to detonation are random in nature, the 0.5% difference in concentrations in these two experiments

Table II.

Summary of FLAME tests with obstacles. (From Reference 34.) A total of 16 pairs of obstacles with a blockage ratio of 1/3 were used in the experiments. (See Figures 1 and 2.)

Test Number	Top Venting Area, %	Hydrogen Mole Fraction, %	Peak Overpressure, atm	Peak Equivalent Planar flame Speed m/s
F-21	0	10-15 ^a	6.5	580
F-22	0	15.0	31.0	700
F-23	0	14.5	12.0	540
F-24	50	15.5	<i>b</i>	46
F-25	50	19.7	16.5	890
F-26	50	28.5	19.7	1860
F-27	50	13.1	.09?	15?
F-28	50	14.9	.09?	33.4
F-29	50	18.5	.22?	130

a - mixing fans did not operate.

b - signal in noise level.

? - analysis not complete.

is not necessarily significant. In other words, it is not necessarily true that a 15% concentration would always lead to a deflagration-to-detonation transition (DDT), while a 14.5% concentration would not. Our computations are not capable of the spatial and temporal resolution or the detailed physics and chemistry required to provide a true simulation of DDT. Nonetheless, it will be seen that we observe a "numerical" transition. Hence, we will concentrate on a comparison with experiment F-23, with a brief observation on detonation with a view to experiment F-22.

In the FLAME facility, flame arrival times are measured by detecting temperature increases at 5 thermocouple "rakes" positioned vertically on the channel midplane. (See Figure 2.) In the present set of experiments, each rake has thermocouples at 7 vertical locations. From this arrival time data, it is possible to construct rough vertical profiles of the flame as it propagates down the channel.³³ The arrival time data for experiments F-22 and F-23 and the corresponding flame front profiles are given in Figures 6-9. The flame velocity obtained from the slope of the line connecting the last two data points in Figure 6 is only 700 m/s. This is below the Chapman-Jouguet (CJ) detonation velocity of 1520 m/s, but it is believed that the discrepancy is due to the poor resolution available from the thermocouple data. Presence of a detonation was inferred from visual observation. Note also the rapid propagation of the flat profiles which begins sometime between 300 ms and 320 ms in Figure 7. This is indicative of a detonation.

In addition to the thermocouples, there are pressure transducers located at various sites on the side walls. Data from these transducers will be compared with the computational results below.

Comparison of Flame Trajectories and Pressure Histories

The first calculation carried out to simulate Experiment F-23 was made with the coefficients in the combustion model selected precisely as described in Section III. (It will be referred to as the baseline calculation.) Parameters pertinent to the test configuration and the computation are collected in Table III. Ignition in these computations is accomplished by forcing a controlled burn over a small region at the closed end of the channel. This ignition process ends at a time of 50 ms. Some care must be taken in implementing ignition in these simulations; a discussion of this point is given later in this section. The initial computational burn velocity S_{Ti} was chosen as 2.5 m/s so that the initial computational flame speed would correspond to the experimental value of 20 m/s. It is to be emphasized that, for this calculation, this is the *only* parameter adjusted to agree with experiment. Note that the flame speed expected for an adiabatic flat flame with a constant burn velocity in an unobstructed tube would be

$$v_T = rS_{Ti}$$

where r is the volume expansion ratio. For a 14.5% hydrogen-air mixture, r is 4.45. Hence, according to the above formula, v_T would be 11 m/s. The reason that the experimental flame speed is greater than this is that the flame is not flat, but is stretched out, primarily by the obstacles. As an additional point of reference, it may be noted (see Table III) that the laminar burn velocity at this concentration is 0.9 m/s. The existence of a wrinkled laminar flame or a weakly turbulent flame with burn velocity equal to, say, 2.5 times the laminar burn velocity is consistent with other experimental results and theoretical considerations^{13,19}.

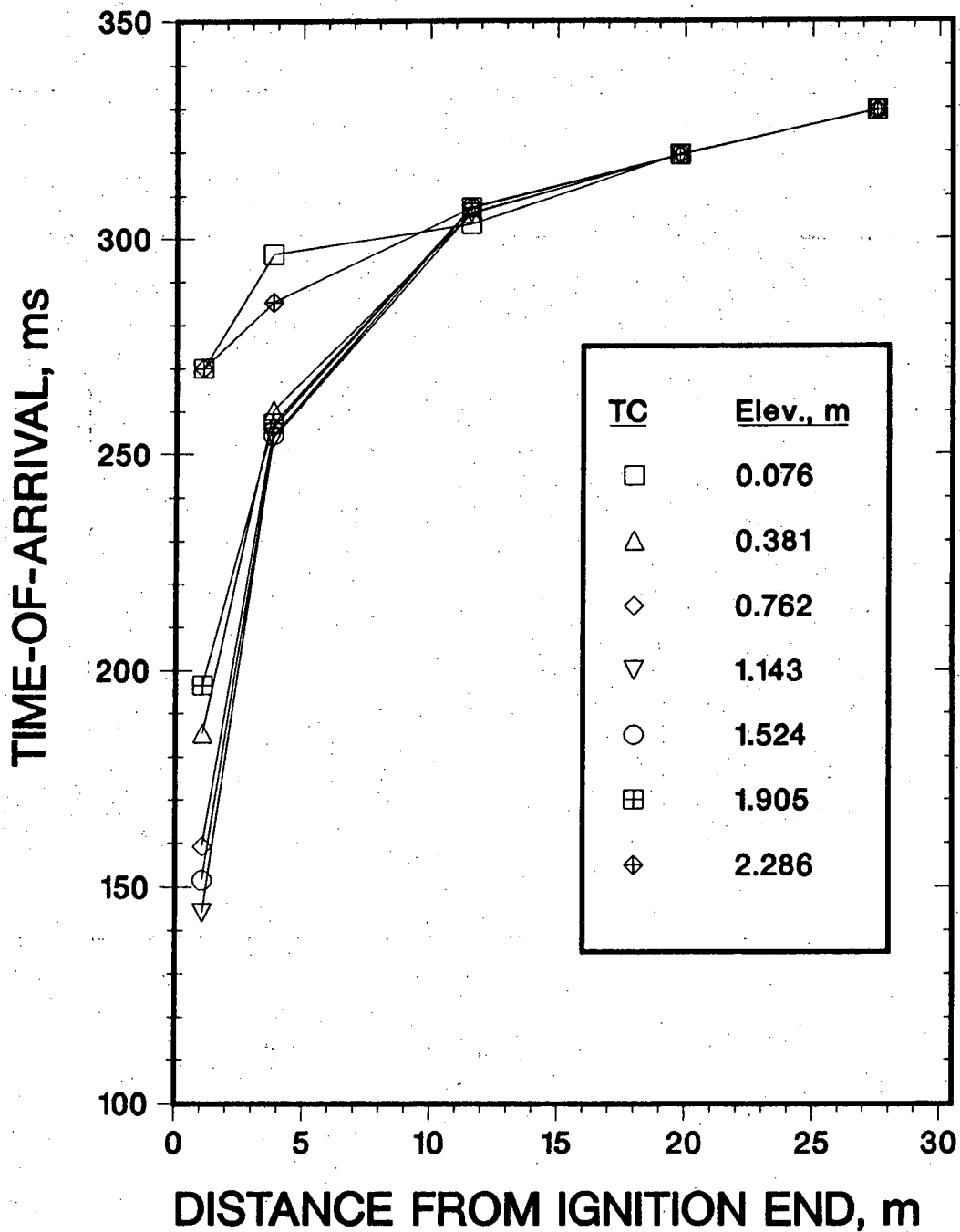


Figure 6. Flame arrival time data for Experiment F-22. (This and the following 3 figures were provided by Reference 34.) The elevations of the thermocouples are given in the key. The distances of the thermocouple rakes from the closed end of the channel are: 1.0 m, 3.8 m, 11.6 m, 19.8 m, and 37.8 m (see the locations of the sets of data points).

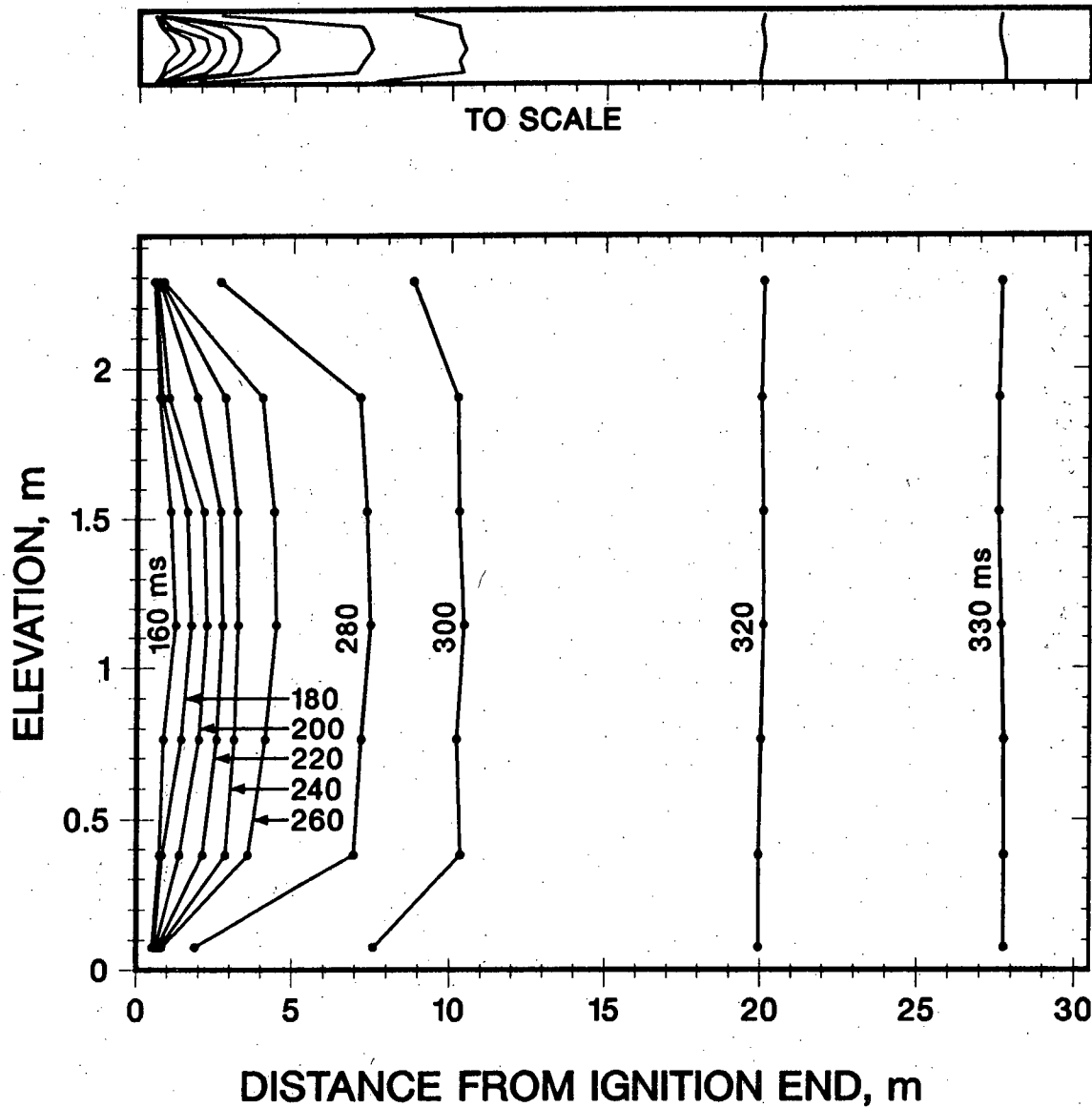


Figure 7. Flame front profiles for Experiment F-22. A side view of the facility is shown (the section is through the midplane, where the thermocouple rakes are located). The upper figure is to scale. The lower figure is expanded in the vertical direction, showing the times in milliseconds to which the contours correspond. The data points indicate the vertical positions of the thermocouples (but not their axial locations—these profiles are obtained by interpolation).

NUREG/CR-4855
SAND87-8203
R3

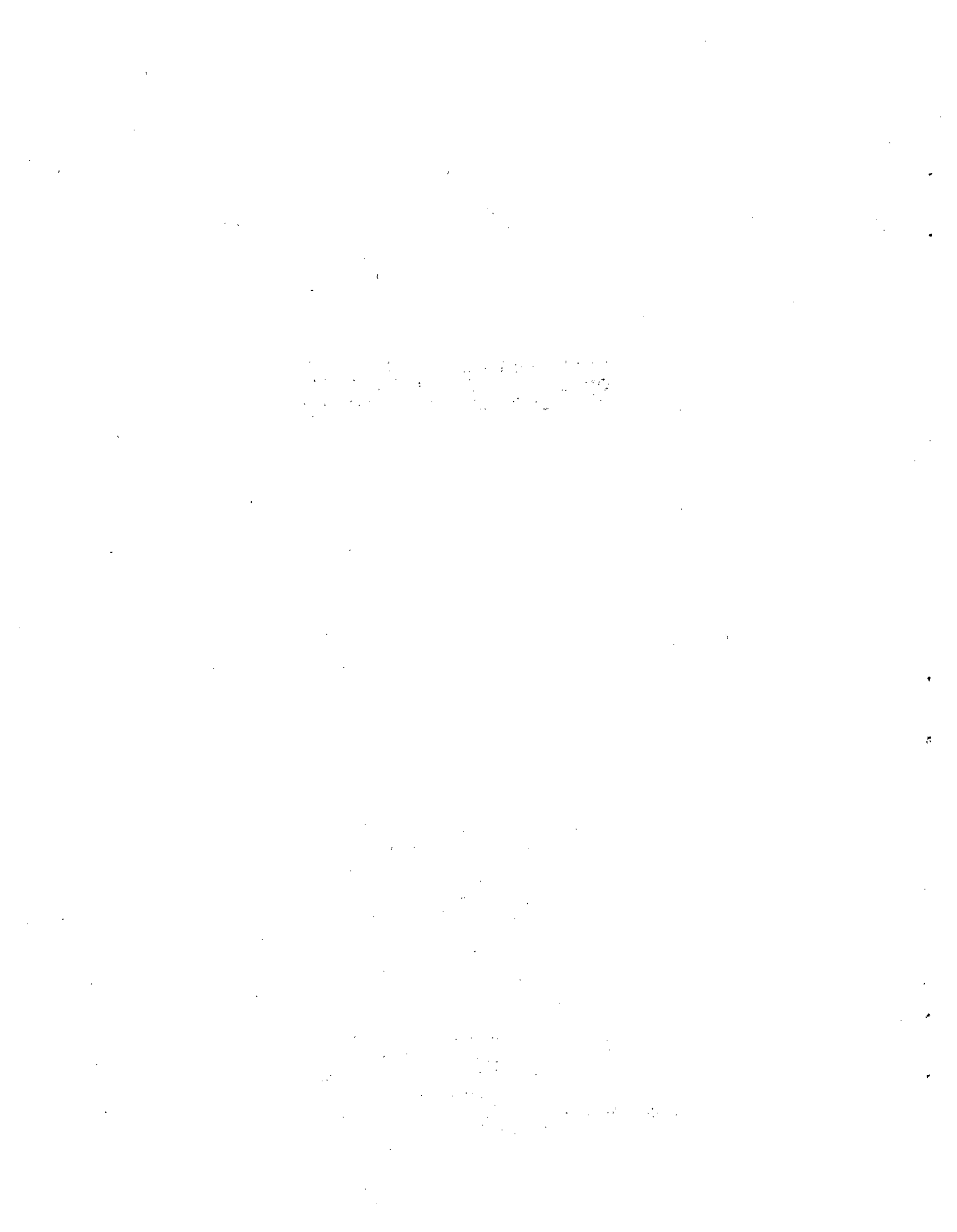
**DEVELOPMENT AND APPLICATION OF
A COMPUTER MODEL FOR LARGE-SCALE
FLAME ACCELERATION EXPERIMENTS**

K. D. Marx

July 1987

Sandia National Laboratories
Livermore, CA 94550
Operated by
Sandia Corporation
for the
U. S. Department of Energy

Prepared for
Division of Reactor Accident Analysis
Office of Nuclear Regulatory Research
U. S. Nuclear Regulatory Commission
Washington, DC 20555
Under Memorandum of Understanding DOE 40-550-75
NRC FIN No. A1246



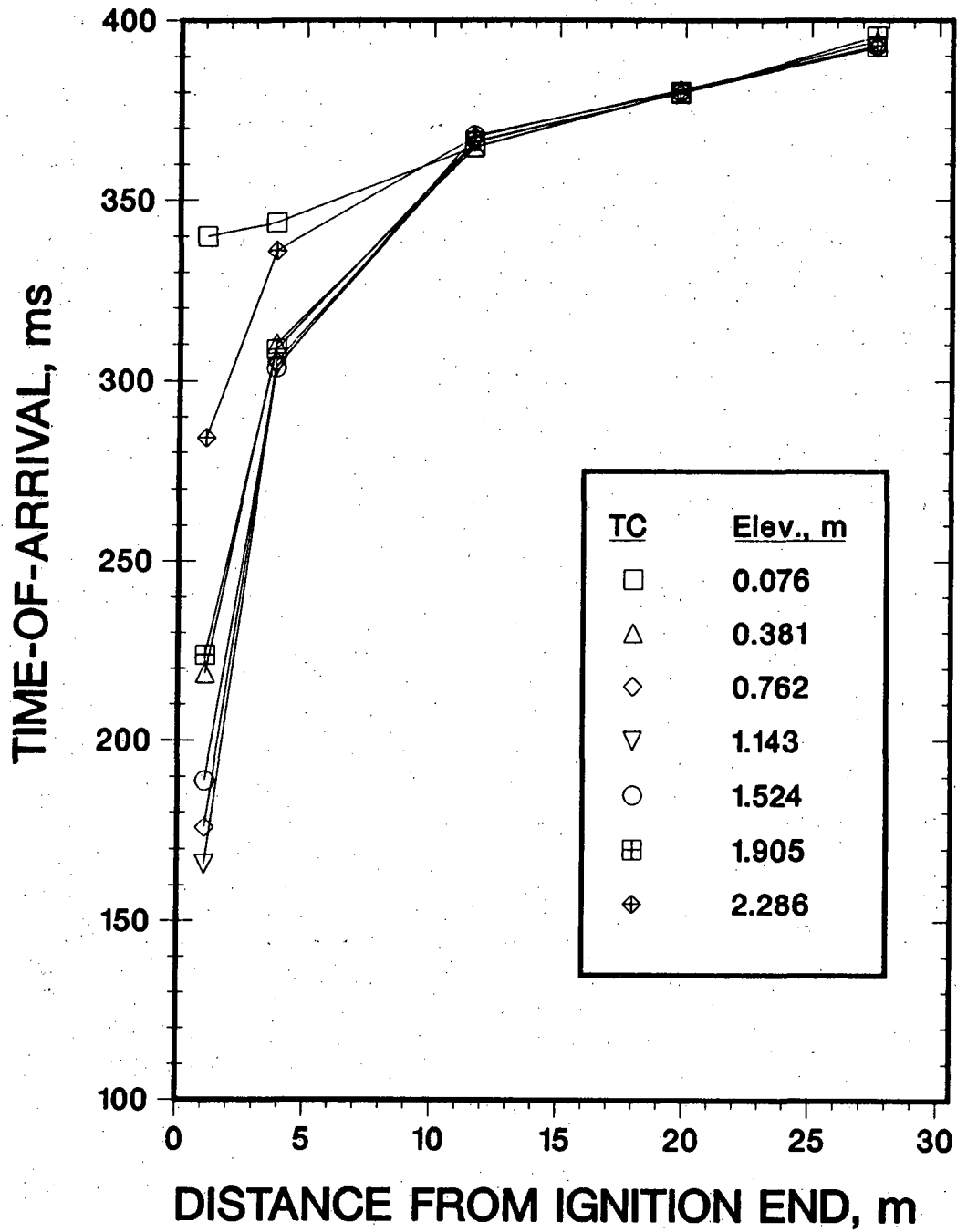


Figure 8. Flame arrival times for Experiment F-23. (See Figure Caption 6 for explanation.)

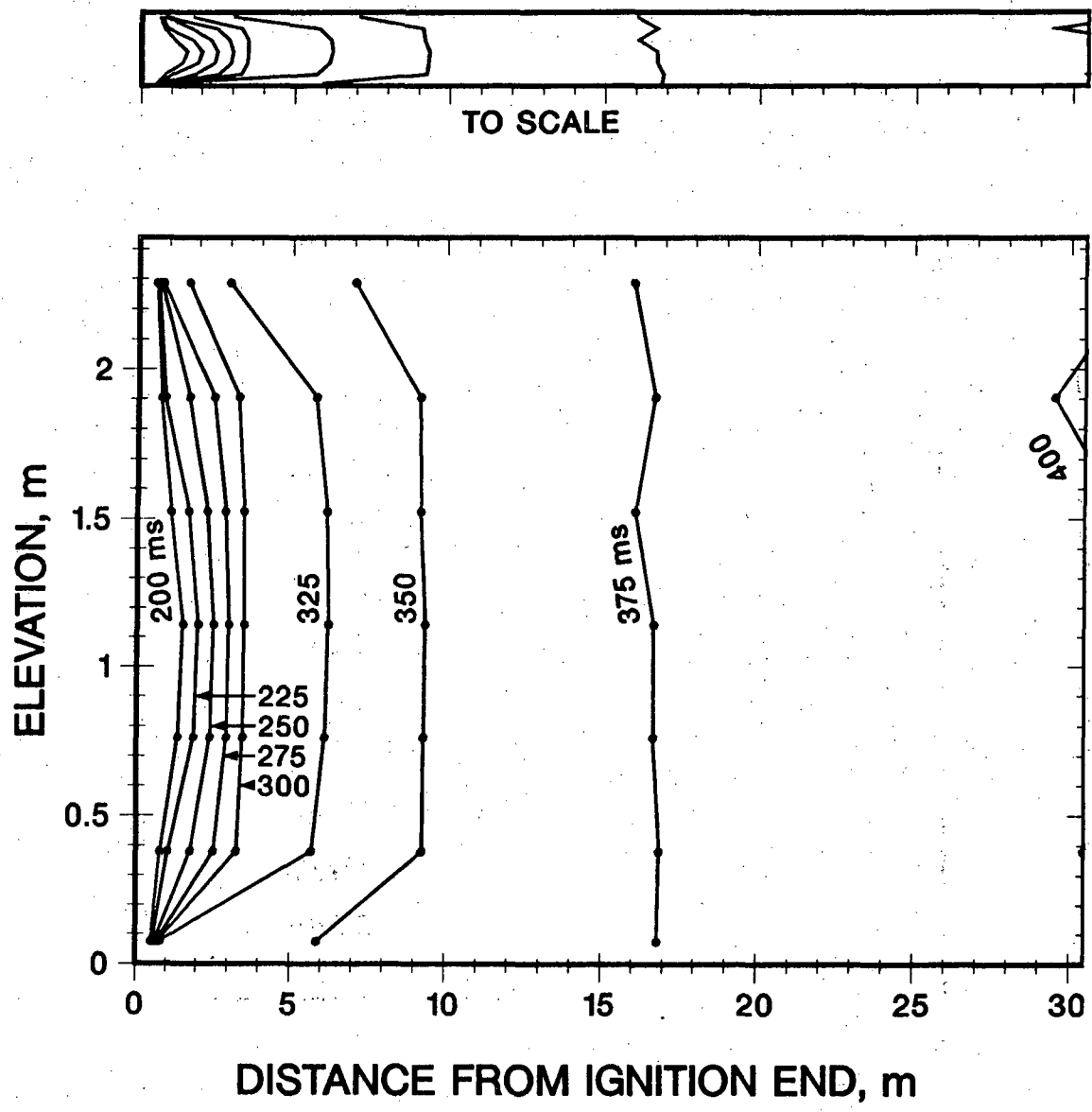


Figure 9. Flame front profiles for Experiment F-23. (See Figure Caption 7 for explanation.) No detonation occurred in this case, although in general the flame propagation rates appear to be only slightly slower than for F-22.

Table III.

Summary of parameters pertinent to Experiment F-23 and the numerical simulation.

Hydrogen mole fraction	0.145
Initial density	1.014 kg/m ³
Initial temperature T_i	300°K
Initial pressure	1 atm
Initial sound speed	374 m/s
Adiabatic flame temperature	1438 °K
Volume expansion ratio r for adiabatic flame	4.45
Laminar burn velocity S_L	0.9 m/s
Isobaric sound speed	758 m/s
Isochoric temperature	1757 °K
Isochoric pressure	5.43 atm
Isochoric sound speed	834 m/s
Chapman-Jouguet detonation velocity	1500 m/s
Chapman-Jouguet pressure	11 atm
Initial experimental flame speed	20 m/s
Combustion rate coefficient A_c	30.8
Threshold turbulent kinetic energy k_m	4.74 J/kg
Threshold turbulent length scale L_m	0.68 m
Pressure exponent m	0.2
Temperature exponent n	1.64
Prandtl number Pr	0.52
Schmidt number Sc	0.52
Initial turbulent burn velocity S_{T_i}	2.5 m/s
Initial computational flame speed	20 m/s

It is interesting to note that the burn velocity of 2.5 m/s for a hydrogen concentration of 14.5% is between 1/2 to 2/3 of the value computed independently from an analysis of experiments without obstacles²⁵. Since non-planarity of the flame was ignored in obtaining the latter results, this lower value is reasonably consistent.

A comparison of the computed and experimental flame trajectories of one calculation with the corresponding experimental data taken from Experiment F-23 (14.5% hydrogen) is given in Figure 10. Considering the size of the experiment and the complexity of the computational problem, the agreement is quite good. To some degree, the discrepancies in the computed flame trajectory must be viewed in light of the fact that the flame velocity is *extremely* sensitive to the burn velocity. (Because of the geometrical factors and the feedback loop involving gas flow velocities, turbulence intensities, and combustion rates, the dependence is nonlinear.) This sensitivity notwithstanding, the computation underestimates the rapid acceleration of the burn rate in the region from 200 to 275 milliseconds. The reasons for this are not known. Precise comparisons with experiment are not possible, as no measurements of turbulence levels are available and it is not possible to instrument the experiments sufficiently to make detailed spatial plots of such flow parameters as flame position, pressure, and temperature.

At a time of about 300 ms into the calculation, however, the computation is accelerating rapidly. Eventually, the computational flame trajectory essentially parallels that of the experiment while the flame traverses through axial positions from about 17 m through 22 m.

Figures 11-14 give a comparison of the computed and experimental pressures at the locations indicated in Figure 10. Data from two pressure transducers at axial positions 18.6 m, 21.5 m, and 25.6 m are shown. Table IV gives complete information on the locations of all transducers pertinent to this paper. The computed pressures are taken from the finite-difference zone next to the channel wall. (Note: All of our calculations terminated when their flames reached the end of the channel. That is why the computed pressure histories end abruptly at 320 ms in Figures 11-14.)

The agreement between computation and experiment at 14.6 m is rather poor, as seen in Figure 11. This simply illustrates the point that the computed combustion rate is significantly slower than that occurring in the experiment at that location. (Compare the flame speeds, i.e., the slopes of the trajectories in Figure 10.) It is important to realize that the agreement with the experimental pressures in this figure could easily be improved by adjusting the parameters k_m , L_m , and A_c until the flame speed in the region around $z = 14.6$ m approximately coincided with the experimental flame speed, but then the agreement would not be as good elsewhere (see below).

A significant improvement is apparent in Figure 12. The computed pressures agree reasonably well with those measured experimentally. The reason for this is that the structure of the pressure history is characterized by the timing of the burnout of the gas in the successive chambers. The fact that the flame velocities approximately agree means that the chambers are burning out at about the correct rate. It should be noted that the flame velocity of about 540 m/s is greater than the sound velocity in the unburned gas, but less than that in the burned gas. This is to be expected if the flow rates are reduced due to choking⁶. Note also that the experimental pressure signals from different transducers at the same axial location are somewhat different.

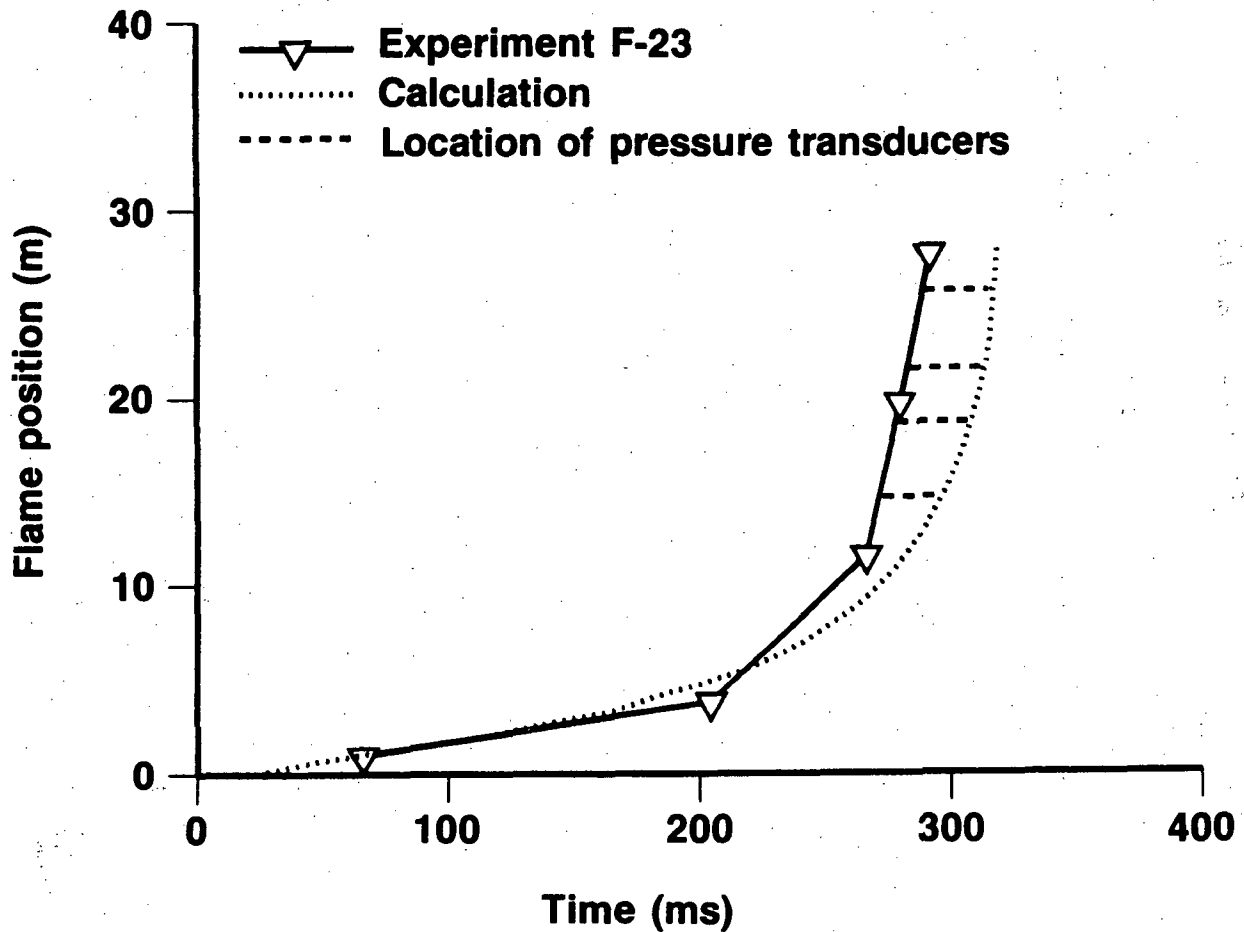


Figure 10. Comparison of computed and experimental flame trajectories for Experiment F-23. The experimental data has been shifted 100 ms to the left (relative to Figures 5-9) to facilitate comparison. (In view of the lack of a detailed simulation of ignition, the relative origins of the computational and experimental time scales is somewhat arbitrary.) The calculation used the baseline parameters as indicated in the text and the first line of Table I. The horizontal dotted lines show the location of the pressure transducers (at approximately 14.6 m, 18.6 m, 21.5 m, and 25.6 m down the channel) which provided the data discussed in this paper. (The complete array of experimental pressure data is not restricted to these locations.)

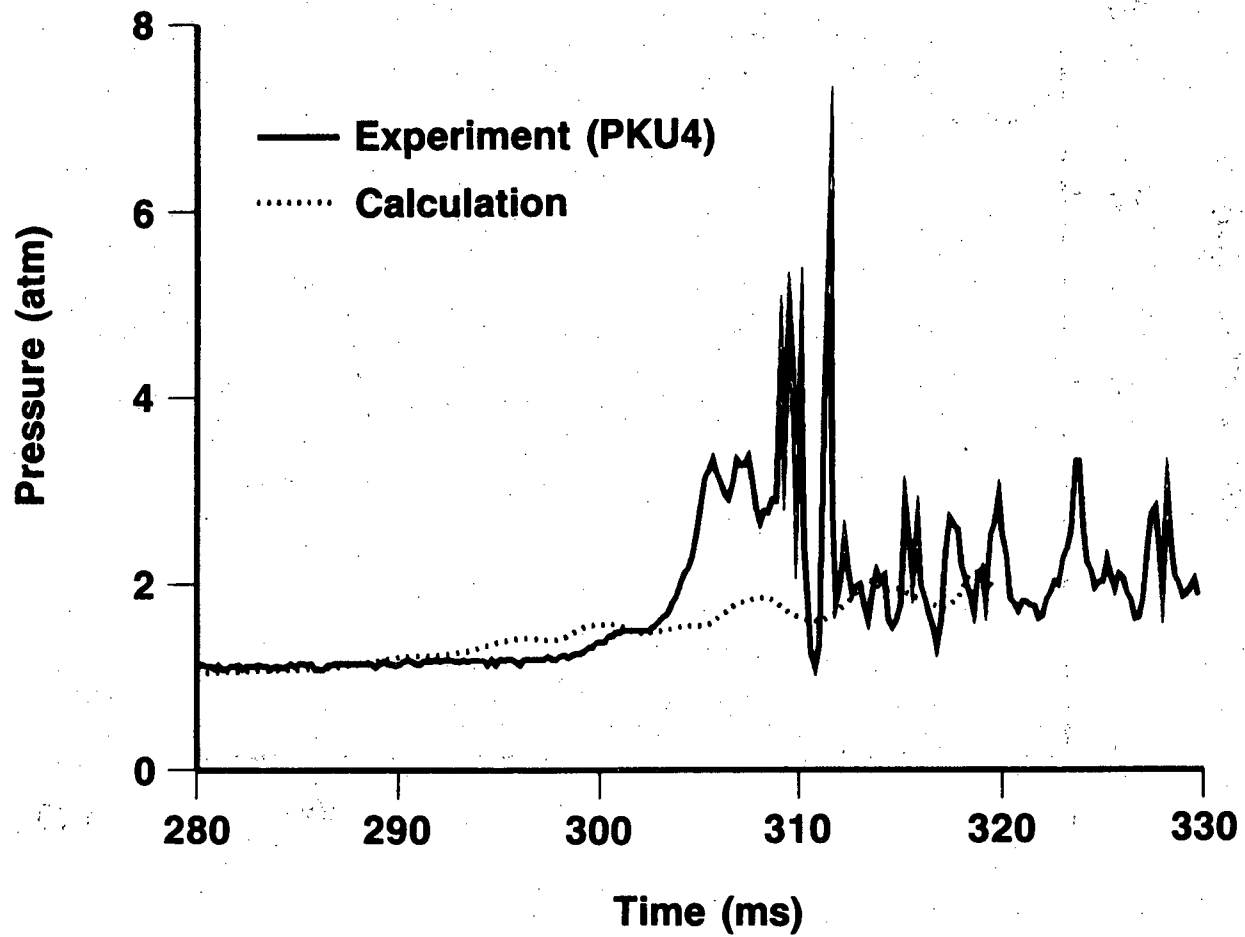


Figure 11. Pressure histories at 14.6 m from the baseline calculation and from transducer PKU4 in the experiment. (See Figure 10 and Table IV for a precise description of transducer location.) In this and all other pressure-time histories, the experimental signal has been shifted in time so that the times at which the flame passes the pressure transducer agrees with that obtained from the computation.

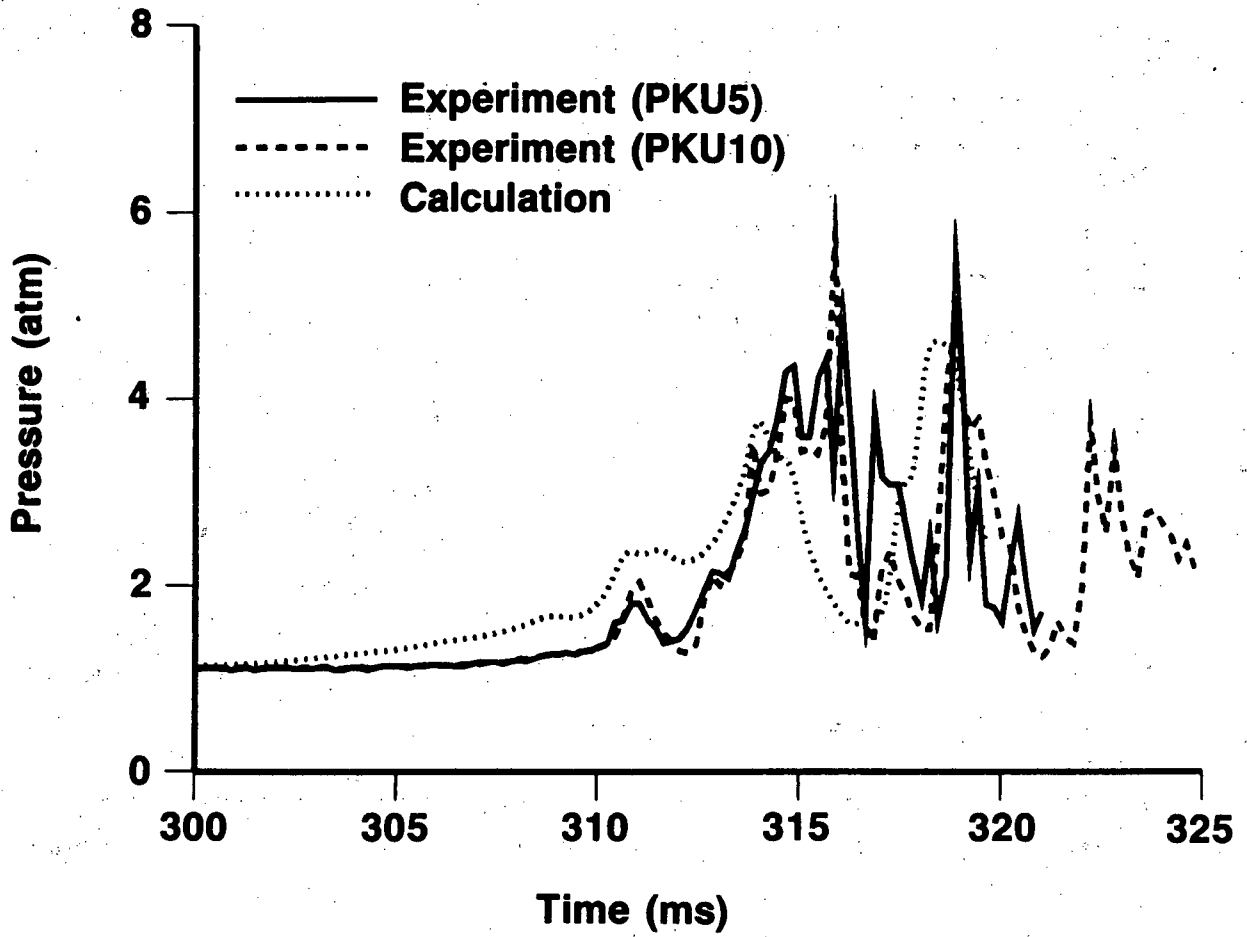


Figure 12. Pressure histories at 18.6 m.

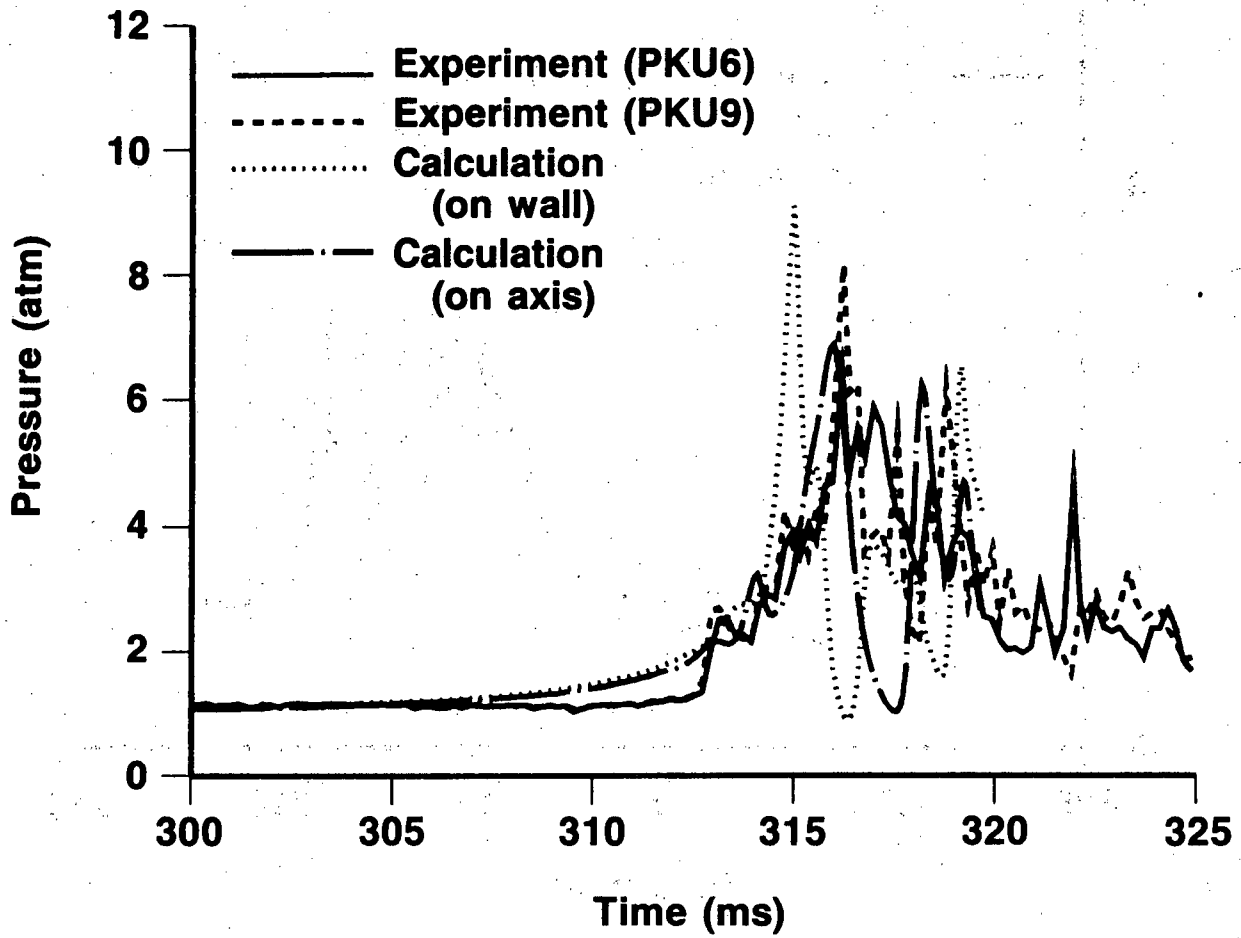


Figure 13. Pressure histories at 21.5 m. In this and the following figure, pressures computed on the axis of the facility are included for comparison (see text).

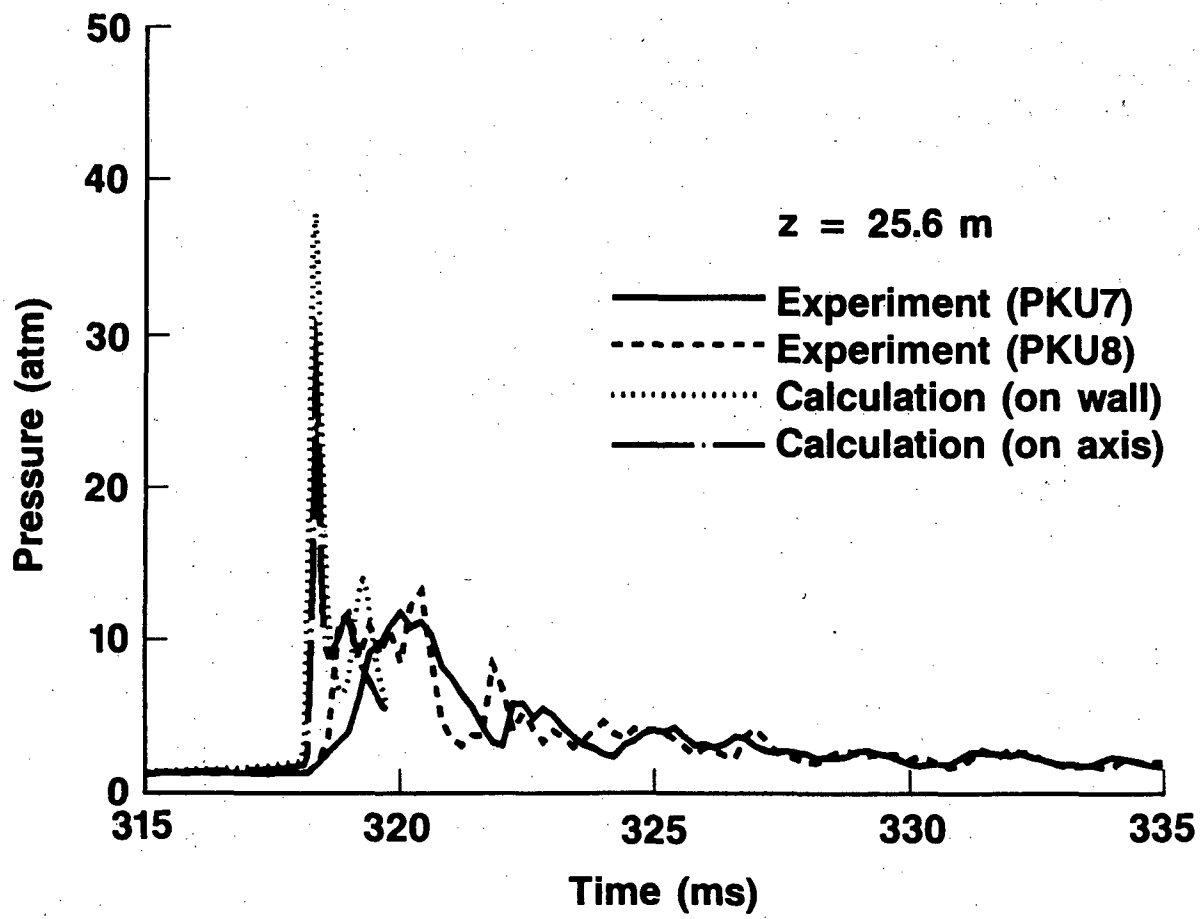


Figure 14. Pressure histories at 25.6 m.

Table IV.

Location of pressure transducers in Experiment F-23. (From Reference 34.) The coordinates x , y , and z correspond to spanwise, vertical, and axial directions. (Positive and negative values of x indicate transducers mounted on opposite sides of the channel.) All distances are in meters.

Transducer	x	y	z
PKU4	-0.914	0.30	14.6
PKU5	-0.914	0.31	18.6
PKU6	0.914	2.12	21.5
PKU7	0.914	0.29	25.5
PKU8	-0.914	2.12	25.6
PKU9	-0.914	2.11	21.4
PKU10	0.914	0.21	18.7

This illustrates the complexity of the problem; these signals may differ because of different proximity to the floor or ceiling, or simply because of random fluctuations in the combustion and pressure waves.

It may be noted that the computed pressure signals do not show as much high-frequency structure as the experimental data. This is undoubtedly due to some numerical dissipation exhibited by the computational algorithm. This will be discussed below with regard to a computation performed on a finer grid.

The order of magnitude of the pressure pulses which occur when the flow is choked, or nearly so, can be estimated as follows: The peak burn rate in the corners in front of the obstacles is very high. Hence, it is reasonable to suppose that the burn there is essentially isochoric. As noted in Table III, the isochoric pressure for 14.5% H_2 at 300° K is 5.4 atm (65 psi). This is seen to be roughly verified both experimentally and computationally in Figures 12 and 13. There is naturally some spreading due to dispersion, especially at locations far from the flame, and this reduces the amplitude of the pressure signals.

The agreement between computational and experimental pressures is not as good at the 21.5 m station (see Figure 13). The reason for this is that the numerical flame is burning more rapidly than was the case in the experiment; in fact, at this point the numerical flame is very close to a transition to detonation. It is interesting to note that for the case shown in Figure 13, the pressure computed on the axis of the facility agrees more closely with experiment than that computed in the zone next to the wall, where the experimental pressure is measured. The reason for this is believed to be that the computed combustion rate at the wall is too high, and that this is causing the transition to detonation.

Figure 14 shows the pressures at 25.6 m down the channel. Detonation has occurred in the computation. As noted above, no detonation was observed in the experiment, but the peak pressure of 13 atm (12 atm overpressure, as indicated in Table II) exceeds the Chapman-Jouguet pressure of 11 atm. The peak computed pressure of 48 atm far exceeds the CJ pressure as well. This may be due in part to numerical overshoot, but it is also true that in the computation, symmetric waves are reflecting off the side walls. Since the pressure in a reflected wave adds in phase and multiple reflected waves can occur, there is a strong mechanism leading to the computation of pressures higher than CJ. It should be noted that such collisions of strong waves would probably not be observed very often experimentally, since the symmetry imposed in the computation would not occur. The effect is enhanced because the calculation is carried out in two dimensions.

Further Discussion of the Computational Results

All of the behavior described above can be seen from a different perspective in Figures 15-18, which show the computed pressures, temperatures, turbulent kinetic energy, and rate of consumption of hydrogen in a series of three-dimensional plots over 7 of the chambers at 5 different times. These plots illustrate the progress of the flame as it propagates down the channel from an axial position of about 16.5 m to 22 m. The flame position is defined by the temperature plots in Figure 16. Note that burning continues for several chambers behind the flame front. Note also in Figure 17 that the flow ahead of the flame has generated turbulence,

primarily because of the strong shear in the flow behind the obstacles. Recall that the threshold turbulent kinetic energy k_m is 4.74 J/kg. The turbulence levels shown in Figure 17 (peaks of about 10 kJ/kg) far exceed the threshold level. This provides justification for introducing the threshold as a startup mechanism to simply provide a minimum burn velocity.

Because of the choking effect, the flame does not actually accelerate rapidly in the region shown in these figures until DDT occurs. However, the pressures are still rising rapidly in the choked regime. It is important to note the mechanism leading to this pressure rise. As the pressure wave propagates down the channel, it hits the obstacles. Reflection of these shocks off the front faces of the obstacles results in a large increase in pressure and some shock heating (see Figures 15 and 16). In accordance with Equation (27), this increases the burn rate (see Figure 18), which feeds back into an increase in the overall pressure level of the wave.

There is a further mechanism contributing to this feedback in the computation. When the gas burns in the corners in front of the obstacles, the increase in pressure there forces the gas out past the corner of the obstacle and into the central flow. (See the flow pattern in Figure 19.) The resulting shear stresses contribute to a strong increase in the production of turbulence. This, in turn, results in a further increase in the burn rate.

The computation exhibits the deflagration to detonation transition at about 315 ms, when the flame has reached an axial position of 22 m. Note that a sharp pressure ridge has formed all the way across the channel in the uppermost plot in Figure 15; i.e., the pressure spike is not restricted to the region just in front of an obstacle.

As noted above, detonation was *not* observed experimentally at the concentration of 14.5% H_2 used in this calculation, but was observed at 15% H_2 . It is likely that the actual concentrations at which DDT is or is not experimentally observed would fluctuate from experiment to experiment, so the computational prediction of a transition at 14.5% H_2 for the particular modeling parameters used is not regarded as being very conclusive. The fact is that we do not claim to be able to simulate the detailed physical processes which occur in DDT. But it is reasonable to assume that the computed trends in pressure, temperature, and turbulence levels are indicative of real processes, and that what is being calculated is the evolution of a system that is progressing toward a tendency to detonate. (Note that it was assumed in Section III that the pressure was constant through the flame when determining the dependence of the combustion rate on temperature. This is not true for a detonation; however, the propagation velocity for a detonation is determined by the conservation laws and driving forces, and not the combustion rate, so this discrepancy is irrelevant for the numerical detonation, regardless of its validity on other grounds.)

Results of Variations in the Computational Parameters

In order to assess the accuracy of the calculation, a second calculation was performed on a refined grid. The baseline computation required about $3\frac{1}{2}$ hours of computer time on a Cray-1S computer. Because of the expense of these calculations, it was not possible to reduce the grid size enough to make a thorough study of convergence. What was done was to decrease the spacing by a factor of 2/3. (The grid for the complete domain was changed from 13 x 397 to 19 x 595.)

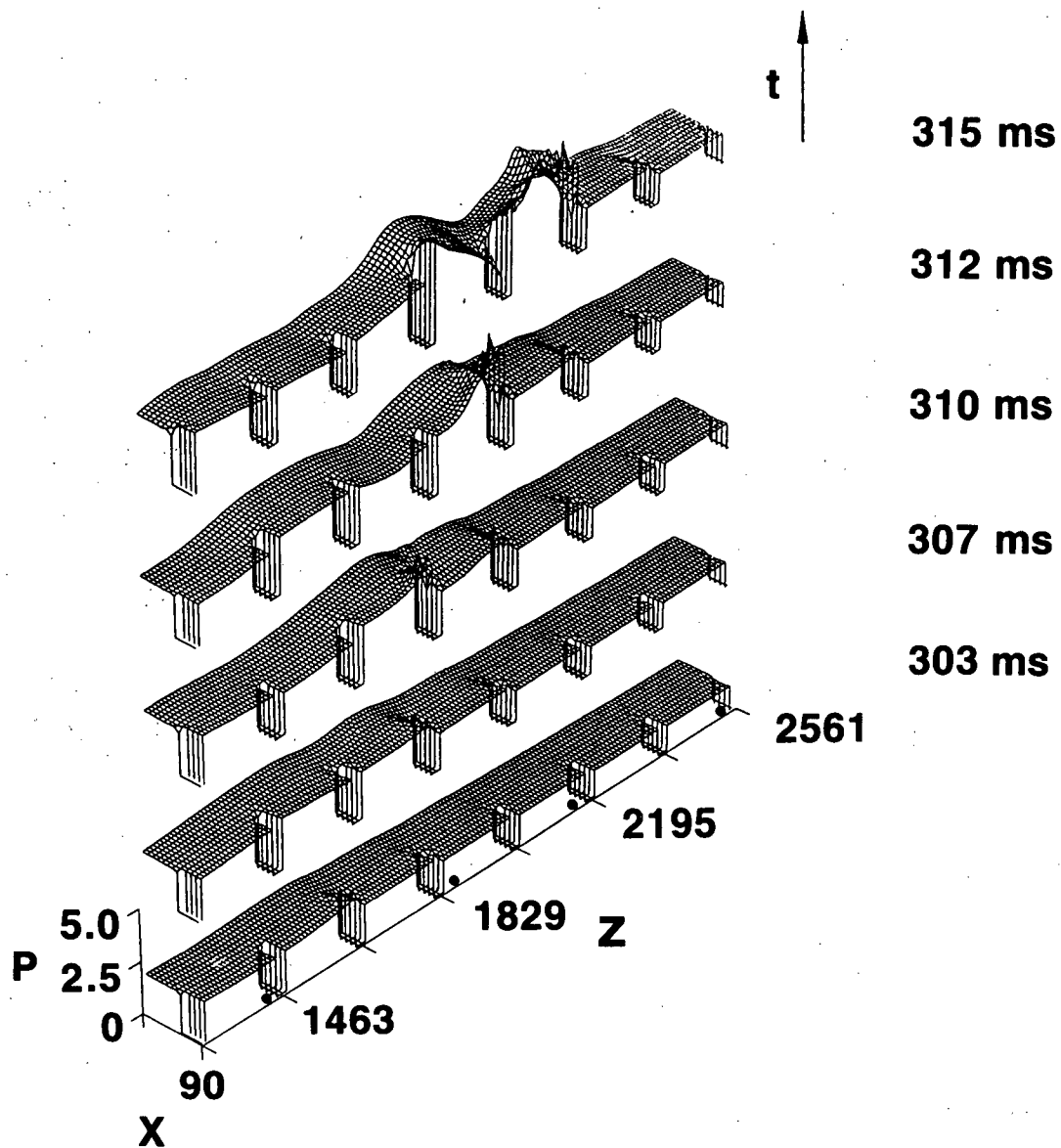


Figure 15. Three-dimensional plots of pressure from the baseline calculation shown in Figures 10–14. Only the region between the 7th through the 14th obstacles along the FLAME facility channel are shown. Coordinates are indicated in centimeters, and absolute pressure is given in atmospheres. The configuration has a symmetry plane at $x = 0$. The times corresponding to each plot appear on the right side of the figure. The axial positions of the pressure transducers which provided the pressures shown in Figures 11–14 are indicated by bullets (\bullet). (Note: In all three-dimensional plots, the values of the dependent variables (pressure, temperature, turbulent kinetic energy, and rate of combustion of hydrogen) have been set equal to zero in the region occupied by the obstacles. This is done simply to make the obstacles easily identifiable; the variables are actually undefined there.)

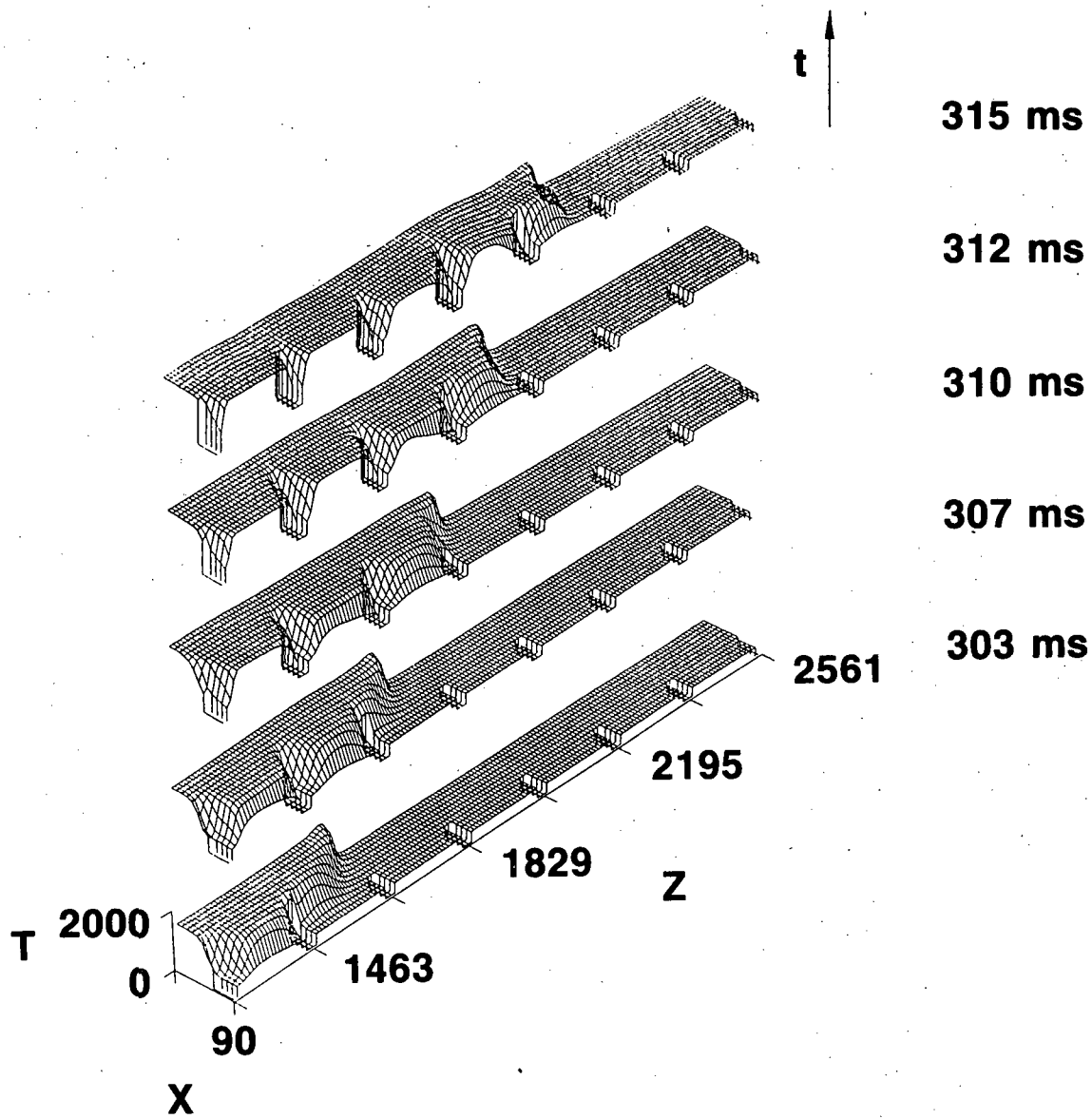


Figure 16. Three-dimensional plots of temperature (in degrees Kelvin) from the baseline calculation.

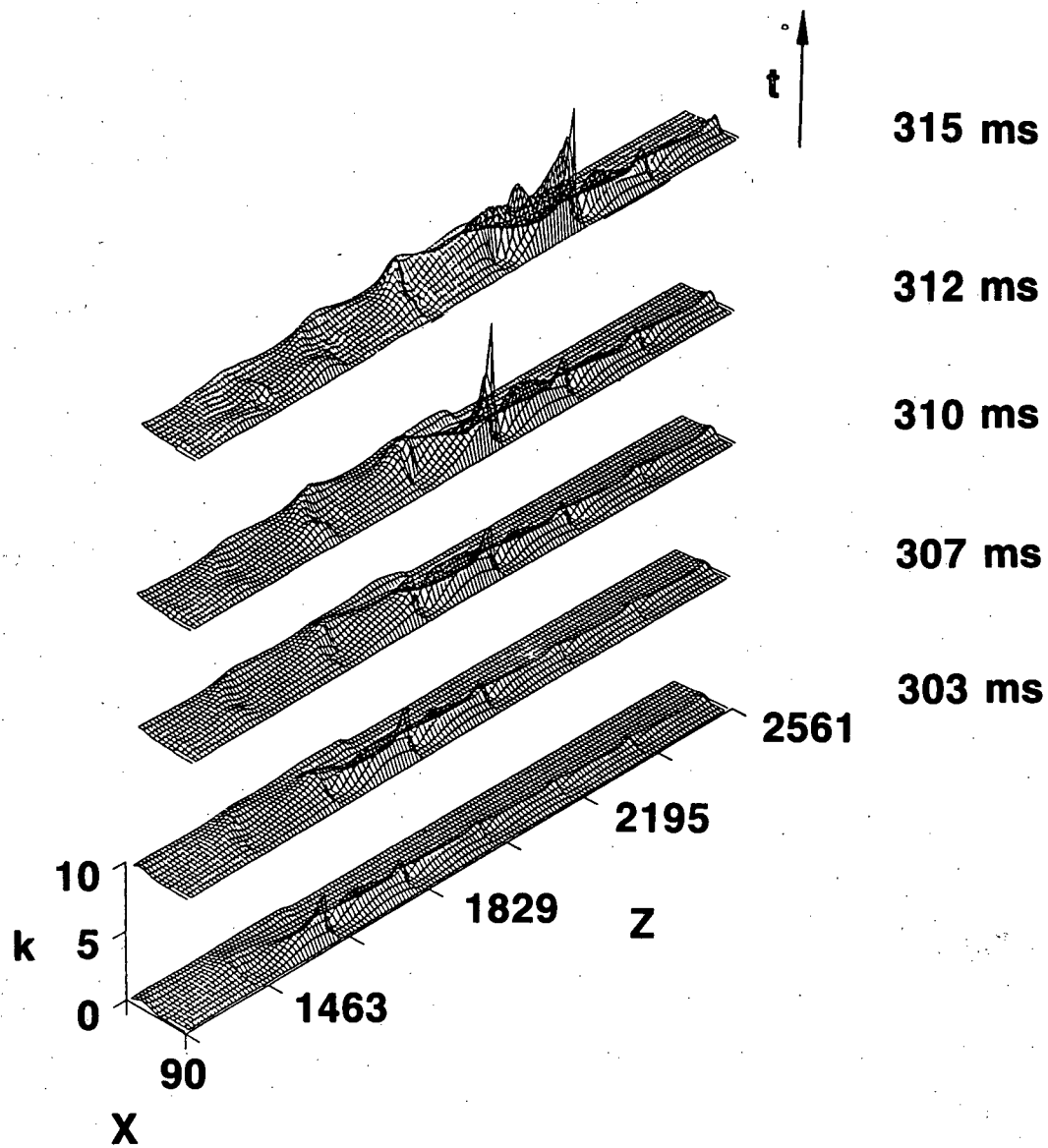


Figure 17. Three-dimensional plots of turbulent kinetic energy (in kJ/kg) from the baseline calculation.

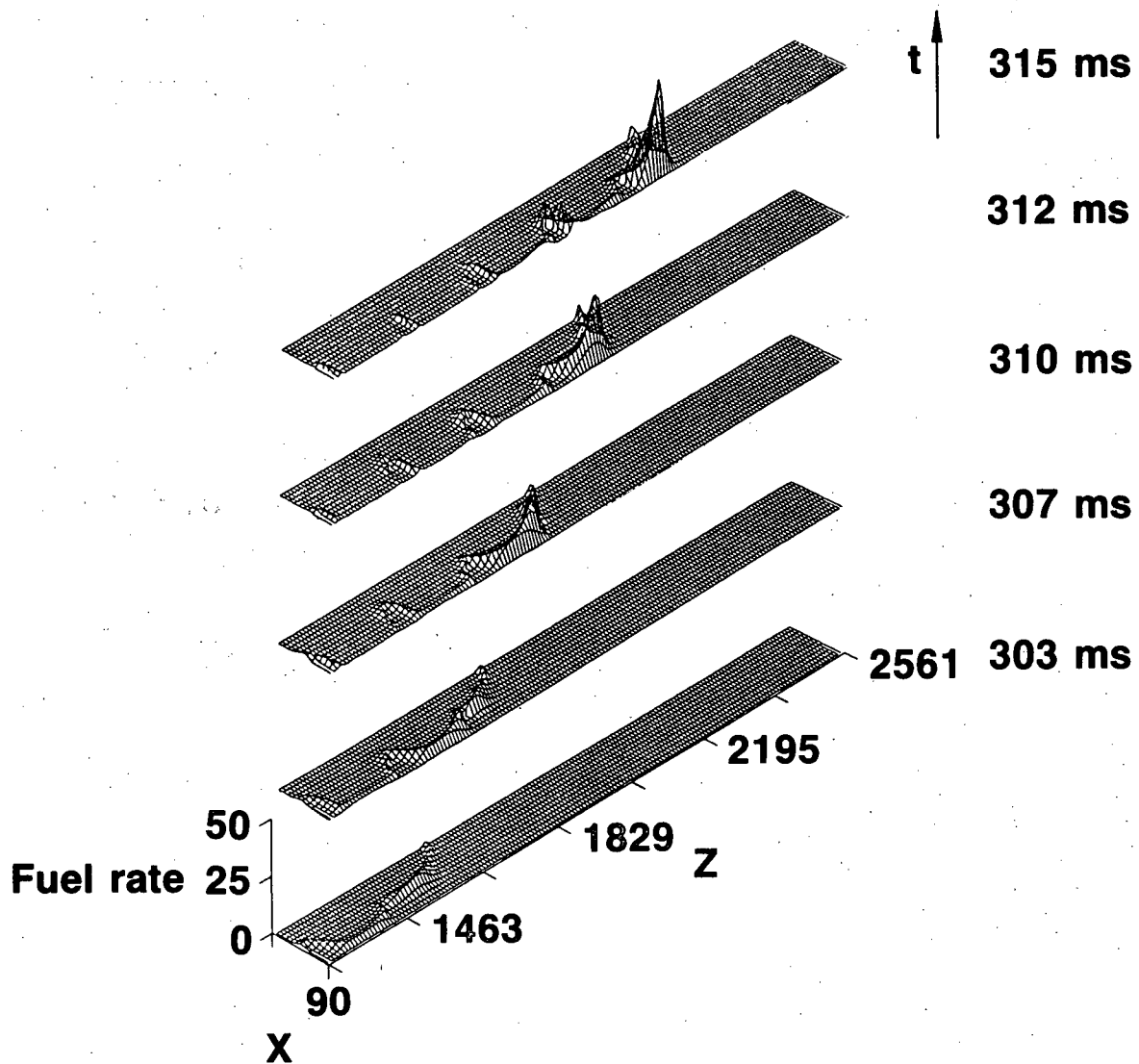


Figure 18. Three-dimensional plots of the hydrogen combustion rate (in kg/(m³-s)) from the baseline calculation.

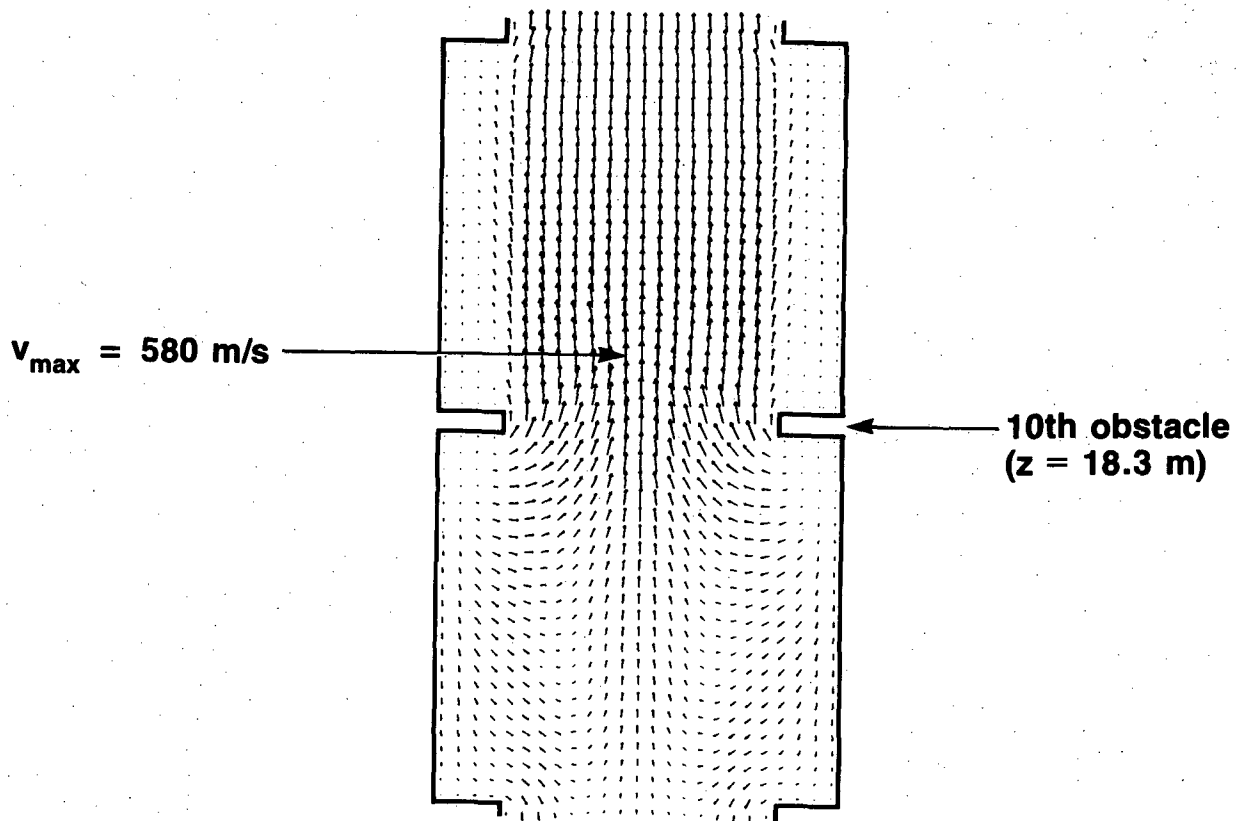


Figure 19. Computed flow pattern between the 9th and 11th obstacles at $t = 310$ ms. The calculation is actually restricted to the domain $x \geq 0$, with a symmetry boundary condition at $x = 0$. However, in this figure the velocity vectors are reflected across the midplane to show the full width of the channel for clarity.

Some of the results are presented in Figures 20-22. The flame trajectory (see Figure 20) is seen to be quite similar to that obtained from the previous calculation, although the flame accelerates faster on the finer grid and detonates sooner. These differences are the result of relatively small errors in the numerical solution on the coarse grid compared to the fine grid. Because of the feedback mechanisms described above, any errors in the flow variables or turbulence parameters become amplified.

To illustrate this sensitivity, an additional simulation was carried out (on the coarse grid) in which the only difference from the baseline calculation was that the rate of combustion during ignition was increased by 31%. The results are given by the dashed line in Figure 20. It is seen that, even though ignition ends before the flame has propagated very far, the gas flow has been given a boost sufficient to generate a higher initial turbulence level and cause considerably greater acceleration of the flame. This example shows how susceptible the progress of such experiments can be to initial conditions. If the burn in the first chamber proceeds differently from shot to shot because of, e.g., different manifestations of fluid instabilities, the end results may vary significantly. For example, if the concentration is marginally detonable, the startup of the burn may determine whether detonation actually occurs.

The pressure histories in Figure 21 and the three-dimensional pressure plot in Figure 22 display the behavior suggested earlier; when numerical dissipation is diminished by lowering the grid size, the shocks and acoustic waves are resolved better and exhibit more structure.

Two more calculations were made to determine the sensitivity of the results to the parameters used in the combustion model. In the first, the values of A_c , k_m , and L_m were adjusted so that the slope $dS_T/d\sqrt{k}$ was reduced to 0.82. (See Figure 5.) The initial burn velocity S_{Ti} and the flame thickness δ_c were changed to 3.6 m/s and 17 cm, respectively. The new values of A_c , k_m , and L_m were 18, 15.6 J/kg and 52 cm. For this run, the pressure and temperature exponents m and n were held at 0.2 and 1.64, as before.

For the second calculation, these same new values of A_c , k_m , and L_m were used, but the temperature exponent n was raised to 2.0. The pressure exponent m remained at 0.2. Both these calculations were made on the 13 x 397 grid.

The results are compared with those from the original computation in Figures 23-25. Qualitatively, the effects on the flame trajectories are entirely predictable. The flame does not burn as rapidly as before with either of the new sets of parameters, but a more rapid burn is obtained for the higher value of n . In both cases, a numerical detonation occurs.

As seen in the sample pressure histories in Figures 24 and 25, the pressure levels are lower with the new parameters, also as expected.

V. CONCLUDING REMARKS

This paper has presented a method for simulating large-scale premixed turbulent flames. The emphasis here has been on developing a way to model the burn rate so that the gas flow driven by the expansion of the burned gases can be computed. A crucial aspect of the application of the model to the computation of the behavior of accelerating flames is that the resulting turbulence intensity and compression of the gas feeds back into the combustion rate.

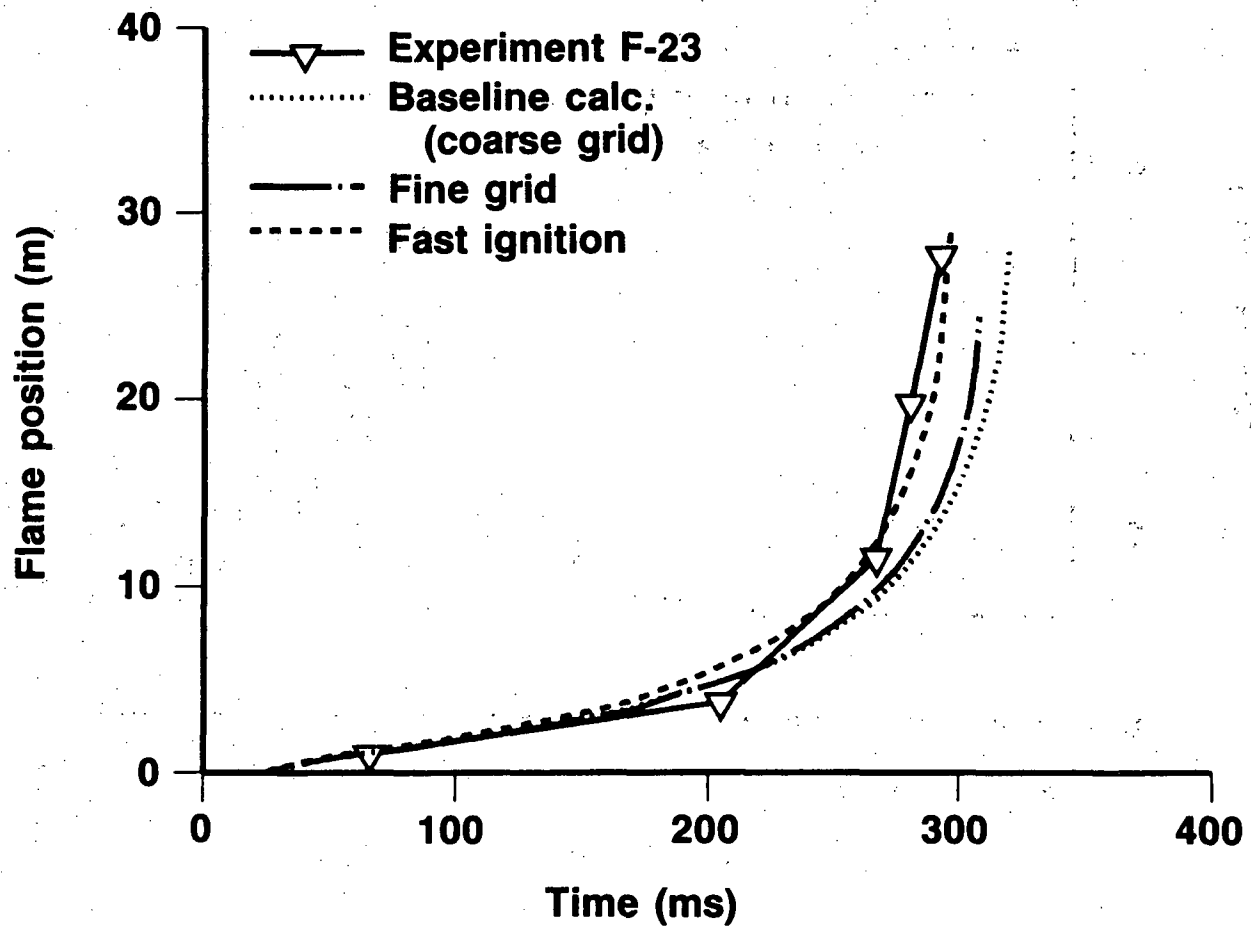


Figure 20. Comparison of experimental flame trajectories with those obtained from the baseline calculation, from a similar calculation on a refined finite-difference grid, and from a calculation in which the ignition strength was increased by 31% (see text).

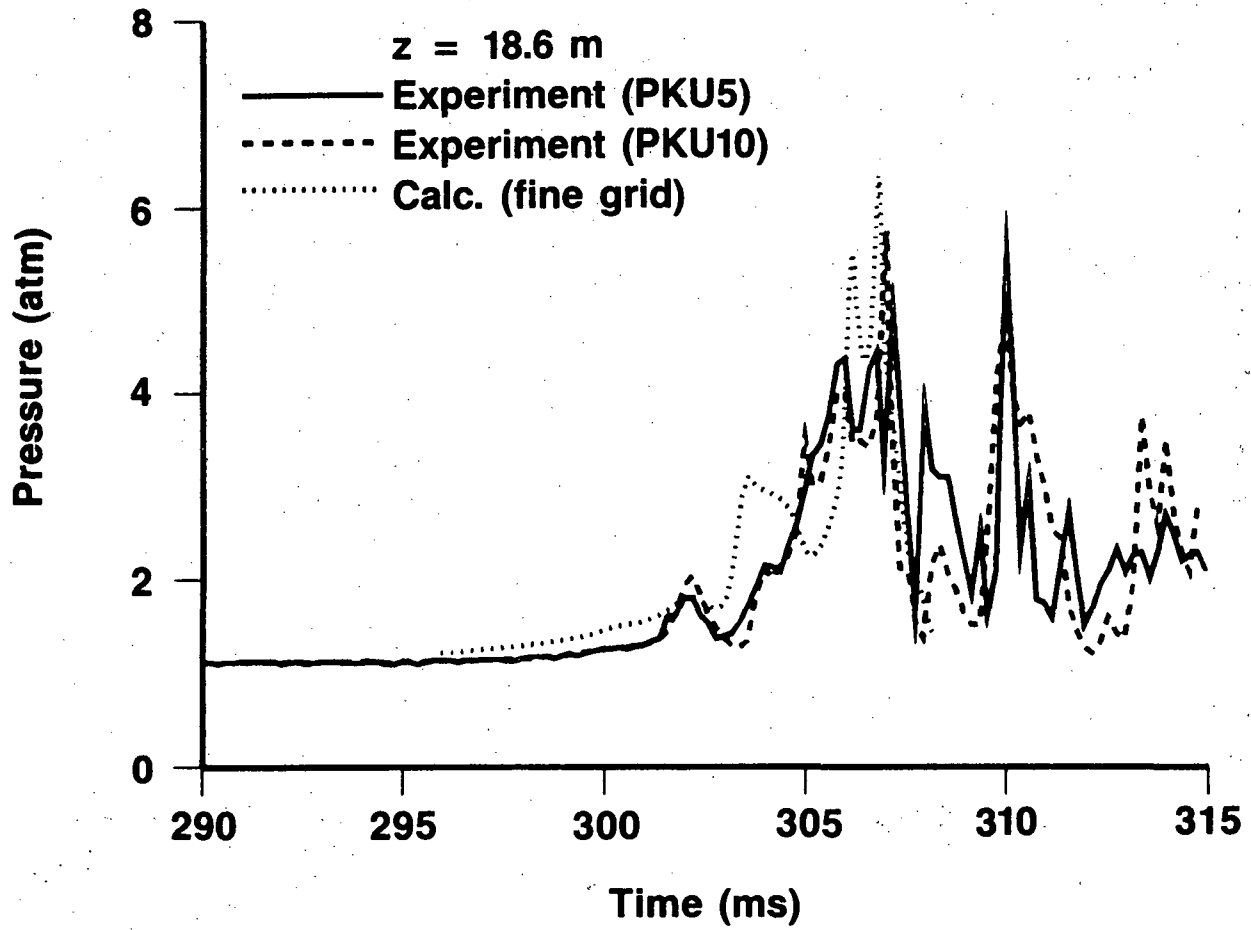


Figure 21. Pressure histories at 18.6 m: From the experiment and from the calculation on the refined grid.

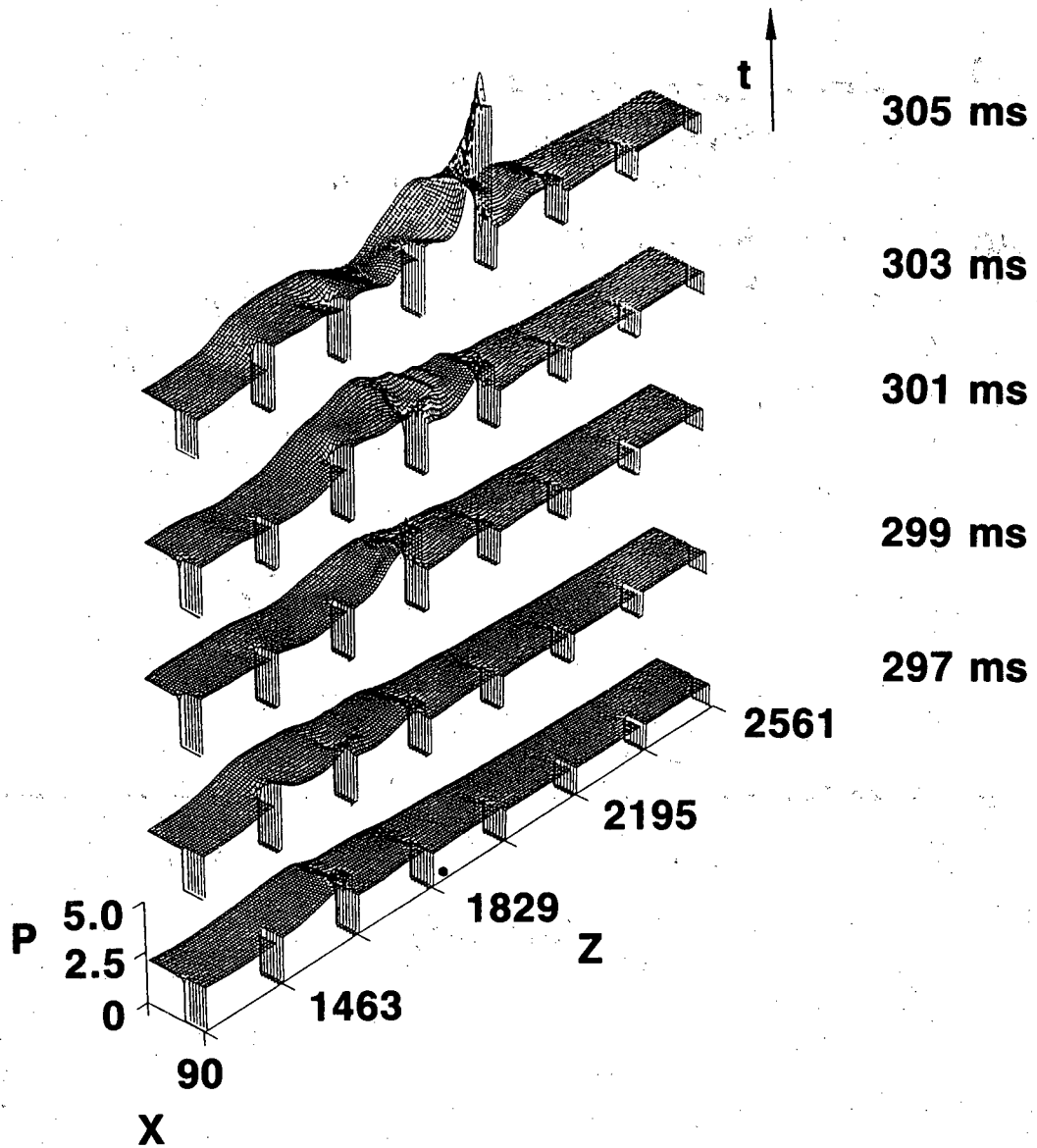


Figure 22. Three-dimensional plots of pressure from the calculation on the fine grid. The bullet indicates the location of the pressure transducer corresponding to the results shown in Figure 21.

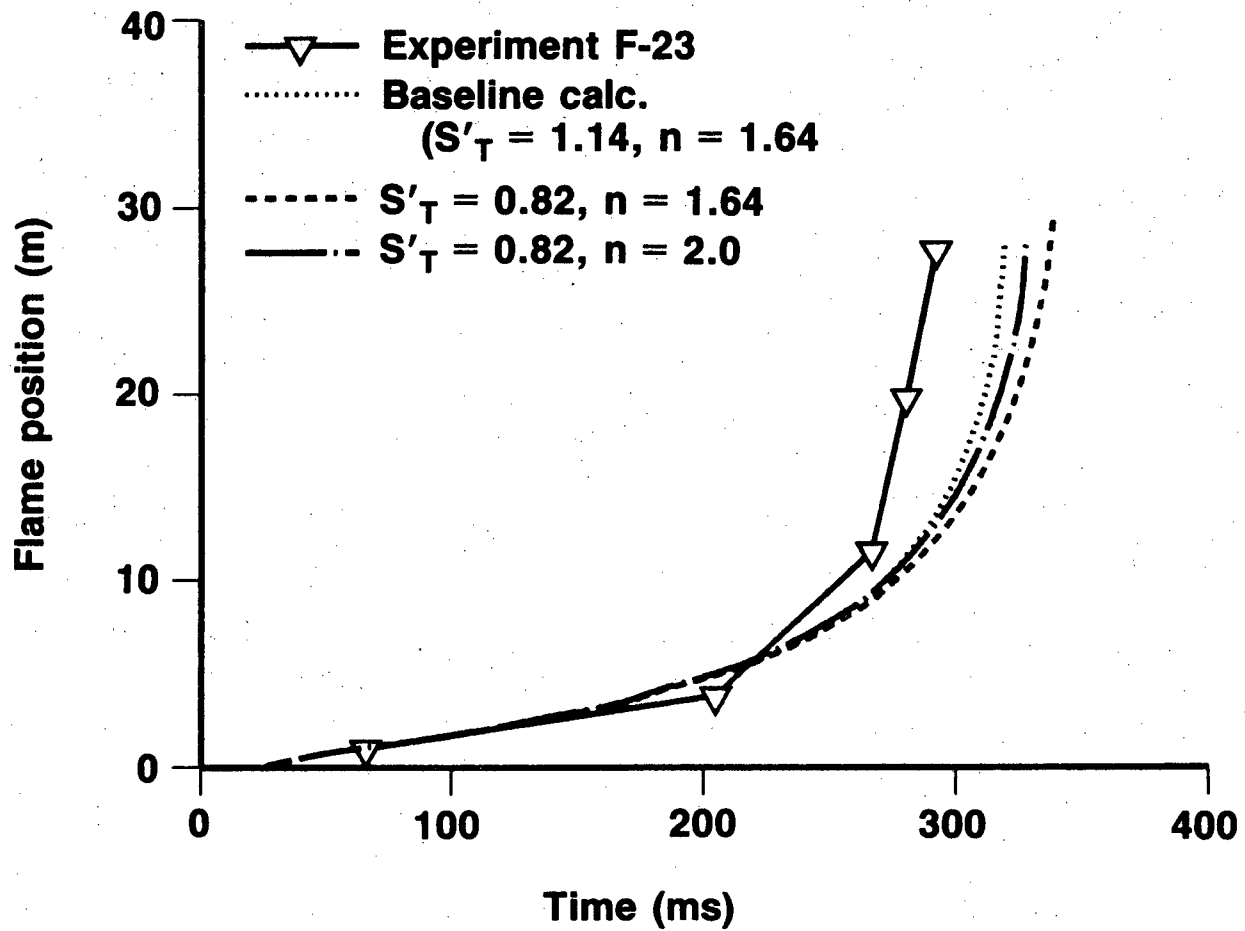


Figure 23. Comparison of the flame trajectory obtained from the baseline calculation and from the calculations in which the combustion model was altered (see text).

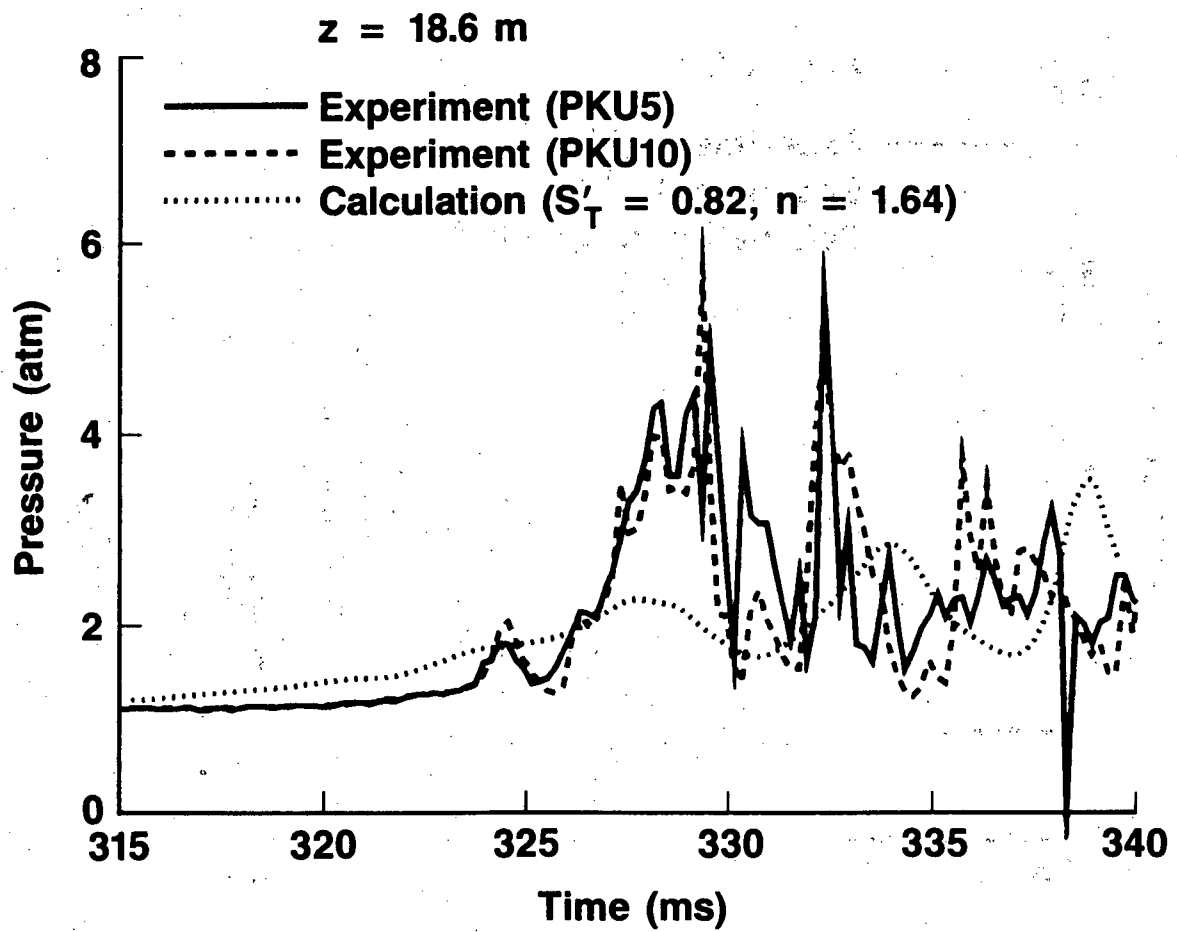


Figure 24. Pressure histories at 18.6 m: From the experiment and from the calculation with reduced combustion rate.

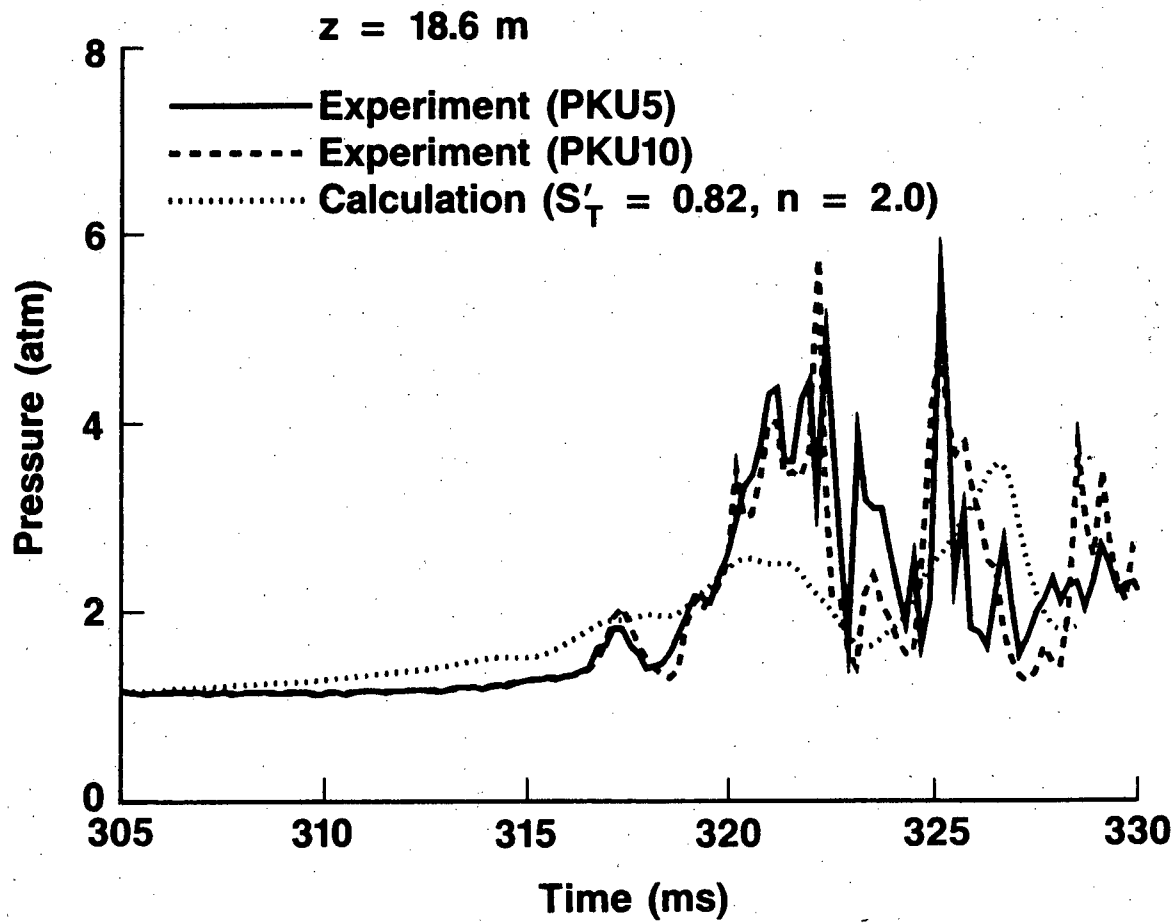


Figure 25. Pressure histories at 18.6 m: From the experiment and from the calculation with reduced combustion rate, but with temperature exponent $n = 2$.

A second important aspect, pertinent to the simulation of large-scale flames, is that the flame thickness is artificially increased and controlled for satisfactory numerical behavior.

The development of the model has been guided by the desire to use as much general experimental information as possible to determine parameters in the model, while minimizing the amount of knob-twisting to tune to specific experiments. The application to the simulation of experiments in the FLAME facility has been quite successful. The simulated flame trajectories and pressures provide reasonably accurate reproductions of experimental behavior. Some of the computed pressure histories exhibit amplitudes and low frequencies which agree quantitatively with experimental data to within about 25%. It has been shown that computation of pressures which match experiment follows from a good reproduction of the rate of burnout of the individual chambers formed by the obstacles. These rates, in turn, depend on the accuracy of the burn velocities. We have been able to obtain adequate burn velocities by requiring the numerical flames to behave in a way consistent with known properties of turbulent flames and applying flame speed data from the weakly turbulent regime of the experiments.

The resulting combustion model should be of interest to those confronted with the type of simulation addressed here; viz., one in which the size of the computational domain greatly exceeds the flame thickness. In order to apply the method, the following are required: (1) Some experimental and/or theoretical information on turbulent flame speeds and their dependence on the state of the gas, and (2) A computer code which solves the equations of reacting flow (for a one-step reaction), computes the state of turbulence in the gas, and provides for flexibility in the specification of the burn rate and diffusion coefficients. Once a numerical flame with the desired properties has been developed, it can be used for the prediction of flame behavior in a variety of situations.

These computations are not intended to describe deflagration-to-detonation transitions. However, they do graphically demonstrate the way in which feedback mechanisms produce a combustion wave which propagates down the FLAME channel with increasing gas velocities and pressure levels. This suggests that there is a potential for the eventual development of the ability to numerically simulate the evolution of the state of the gas as it approaches a sensitivity to detonation. Given a suitable experimental data base, this might provide a means for predicting DDT.

The combustion model should still be regarded as being under development. In particular, there are two features specific to flame acceleration which need improvement. The first is that a mechanism should be provided that will simulate the sudden burst of acceleration observed in the experiments (the sharp knee in the experimental curve in Figures 10, 20, and 23). The second is the tendency of the numerical flame to exhibit a transition to detonation in the absence of corresponding experimental behavior. As noted earlier, however, this latter problem may not be particularly severe, in view of the demonstrated detonability of mixtures at concentrations close to that studied here.

One way to inhibit numerical DDT would be to include a mechanism for flame quench due to turbulent flame stretch, which is a plausible physical process. Simulating the rapid acceleration while still inhibiting detonation appears less straightforward. It may be that a more accurate treatment of thermal mixing due to turbulence is required, perhaps in concert with compressional heating, but this is merely speculation.

Future work should address these questions. In particular, a joint experimental and computational study of the effects of varying hydrogen concentration would be of interest. Also of interest to the reactor safety community would be the inclusion of gas venting in the simulations. It should be emphasized that the mechanism for the extremely rapid acceleration of the flame fronts which appears in the present work arises to a large extent from the fact that the channel is enclosed except for the opening at one end. Pressure relief due to venting can reduce flame speeds dramatically^{3,5}. However, in some cases, venting may enhance the combustion rate, presumably by introducing additional turbulence³.

Another direction that future research could take would be to break the computational problem with its large spatial domain up into smaller pieces. Two or three chambers could be considered with appropriately chosen inlet and outlet boundary conditions. This would permit grid refinement to ascertain the convergence properties of the solution. It would also allow better resolution of the turbulent flame fronts, recirculation regions and shock and acoustic waves.

APPENDIX A. INTEGRATION OF PRODUCTION-DISSIPATION TERMS

The following numerical scheme is used to ensure that numerical errors in the production and dissipation terms do not result in nonnegative k or ϵ . First, the production and dissipation terms are split off from the rest of the two equations. This means that in each cell, these terms are allowed to advance k and ϵ within one computational time step according to

$$\frac{d}{dt}(\rho k) = P - \rho\epsilon \quad (A-1)$$

$$\frac{d}{dt}(\rho\epsilon) = C_{1\epsilon}P\frac{\epsilon}{k} - C_{2\epsilon}\rho\frac{\epsilon^2}{k} \quad (A-2)$$

where

$$P = \sigma:\nabla\mathbf{u}$$

(Mesh subscripts are dropped for simplicity. Ordinary derivatives are indicated, since the quantities are decoupled from those in other computational cells. The convection and diffusion terms in Equations (10) and (11) are added separately.)

In the strong turbulence regime we have

$$\mu_T \gg \mu_L$$

This is essentially always true in our calculations. Then

$$\mu \cong C_{\mu}\rho\frac{k^2}{\epsilon}$$

Define

$$Q \equiv \rho k$$

$$E \equiv \rho\epsilon$$

Then

$$\mu = C_{\mu}\frac{Q^2}{E}$$

and

$$P = C_\mu f_p(\mathbf{u}, k, \epsilon) \frac{Q^2}{E}$$

where

$$f_p(\mathbf{u}, k, \epsilon) \equiv \frac{\sigma: \nabla \mathbf{u}}{\mu}$$

The rationale behind separating out the term $f_p(\mathbf{u}, k, \epsilon)$ is that it will be held constant while equations (A-1) and (A-2) are integrated over one time step. This is justifiable in that f_p is not a strong function of k and ϵ . (In incompressible flow, it has no k or ϵ dependence at all.)

Equations (A-1) and (A-2) can now be written

$$\frac{dQ}{dt} = \frac{P'Q^2}{E} - E \quad (\text{A-3})$$

$$\frac{dE}{dt} = C_{1\epsilon} P'Q - C_{2\epsilon} \frac{E^2}{Q} \quad (\text{A-4})$$

where

$$P' = C_\mu f_p(\mathbf{u}, k, \epsilon)$$

From (A-3) and (A-4) we obtain

$$\begin{aligned} \frac{d}{dt} \left(\frac{Q}{E} \right) &= \frac{1}{E} \frac{dQ}{dt} - \frac{Q}{E^2} \frac{dE}{dt} \\ &= - \left(C_{1\epsilon} - 1 \right) P' \frac{Q^2}{E^2} + \left(C_{2\epsilon} - 1 \right) \end{aligned}$$

Let $\xi = Q/E$. Then

$$\frac{d\xi}{dt} = - \left(C_{1\epsilon} - 1 \right) P' \xi^2 + \left(C_{2\epsilon} - 1 \right)$$

and we use the following implicit scheme to integrate ξ :

$$\xi^{n+1} = \frac{\xi^n + (C_{2\epsilon} - 1)\Delta t}{1 + (C_{1\epsilon} - 1)P'\xi^n\Delta t} \quad (\text{A-5})$$

where superscripts n and $n + 1$ denote old and new time levels and Δt is the time step. Since $C_{1\epsilon}, C_{2\epsilon} > 1$, positive ξ^n insures positive ξ^{n+1} .

From Equation (A-3),

$$\frac{dQ}{dt} = P'\xi Q - \frac{Q}{\xi}$$

and the scheme

$$Q^{n+1} = \frac{(1 + P'\Delta t\xi^{n+1})Q^n}{1 + \frac{\Delta t}{\xi^n}} \quad (\text{A-6})$$

is consistent and results in nonnegative Q^{n+1} . Applying first (A-5), then (A-6), and using

$$E^{n+1} = \frac{Q^{n+1}}{\xi^{n+1}}$$

permits evaluation of

$$k^{n+1} = Q^{n+1}/\rho$$

$$\epsilon^{n+1} = E^{n+1}/\rho$$

and these quantities are positive as long as k^n and ϵ^n are positive.

APPENDIX B. DIFFERENCE FORMULA FOR ϵ AT WALLS

A function which varies as $1/y$ cannot be differentiated accurately by the usual second-order central difference formulas. Since ϵ has this behavior near walls, a special differentiation formula was derived for this purpose, as described below. A formula which is exact for $1/y$ is

$$\left. \frac{\partial \epsilon}{\partial y} \right|_i \cong \frac{3}{4} \left(\frac{\epsilon_{i+\frac{1}{2}} - \epsilon_{i-\frac{1}{2}}}{\Delta y} \right)$$

where i is a grid index. (In Conchas-Spray, ϵ is a cell-centered quantity, so $\partial \epsilon / \partial y$ is centered on the cell faces.) We have found that such an alteration at only the first grid point in from the wall yields a more accurate solution; however, it is an inconsistent formula for the derivative and should not be carried into the interior of the fluid. The discontinuity in transferring from this formula to the second-order approximation

$$\left. \frac{\partial \epsilon}{\partial y} \right|_i \cong \frac{\epsilon_{i+\frac{1}{2}} - \epsilon_{i-\frac{1}{2}}}{\Delta y}$$

obviously leads to some inaccuracy, but it appears to be less severe than carrying the second-order approximation all the way to the wall.

Note added in proof: In the most recent version of the Kiva code (a descendant of Conchas-Spray¹⁷), Los Alamos researchers are solving the ϵ -equation by advecting the length scale L rather than ϵ . This alleviates the aforementioned difficulties with ϵ at wall boundaries.

REFERENCES

1. Fisk, J. W., Sherman, M. P., Tieszen, S. R. and Benedick, W. B. "Experimental Facilities to Study Hydrogen Combustion and Detonation." Designing for Hydrogen in Nuclear Power Plants, Niyogi, K. K. and Bernstein, M. D., Eds. pp. 25-30. A.S.M.E., New York, Y.Y. (1984)
2. Sherman, M. P., "Hydrogen Flame Acceleration and Detonation." Twelfth Water Reactor Safety Research Information Meeting, Oct. 1984. pp. 338-356, NUREG/CP-0058 Vol. 3, U. S. Nuclear Regulatory Commission (1985).
3. Sherman, M. P., Tieszen, S. R., Benedick, W. B., Berman M., and Carcassi, M. "The FLAME Facility-The Effect of Transverse Venting on Flame Acceleration and Transition to Detonation," in "Dynamics of Explosions," Progress in Aeronautics and Astronautics, vol. 106, J. R. Bowen, et al, eds., pp. 66-89 (1986).
4. Lee, J.H.S., Knystautas, R. and Freiman, A., "High Speed Turbulent Deflagrations and Transition to Detonation in H₂-Air Mixtures." Combustion and Flame 56, 227 (1984).
5. Chan, C., Moen, I. O., and Lee, J. H. S., "Influence of Confinement on Flame Acceleration Due to Repeated Obstacles." Combustion and Flame 49, 27-39 (1983).
6. Lee, J. H., Knystautas, R., and Chan, C. K., "Turbulent Flame Propagation in Obstacle-Filled Tubes," Proc. Twentieth Symposium (International) on Combustion, The Combustion Institute, Pittsburgh (1984).
7. Moen, I. O., Donato, M., Knystautas, R., and Lee, J. H., "Flame Acceleration Due to Turbulence Produced by Obstacles," Combustion and Flame 39, 21-32 (1980).
8. Henrie, J. O. and Postma, A. K. "Analysis of the Three Mile Island (TMI-2) Hydrogen Burn," in "Thermal-Hydraulics of Nuclear Reactors," Volume II, Amer. Nucl. Soc. LaGrange Park, Ill., U.S.A.S.M.E. 1157-1170 (1983).
9. Jones, W. P., "Models for Turbulent Flows with Variable Density and Combustion," in "Prediction Methods for Turbulent Flows," W. Kollmann, ed., McGraw-Hill, New York (1980).
10. Rodi, W., "Turbulence Models and Their Application in Hydraulics," International Association for Hydraulic Research, Rotterdamseweg 185-P.O. Box 177, 2600 MH Delft, The Netherlands (1980).
11. Magnussen, B. and Hjertager, B., "On Mathematical Modeling of Turbulent Combustion with Special Emphasis on Soot Formation and Combustion," Proc. Sixteenth Symposium (International) on Combustion, The Combustion Institute, Pittsburgh, pp. 719-729 (1976).
12. Spalding, D. B., "Mixing and Chemical Reaction in Steady Confined Turbulent Flames," Proc. Thirteenth Symposium (International) on Combustion, The Combustion Institute, Pittsburgh, pp. 649-657 (1971).
13. Bray, K. C. N., "Turbulent Flows with Premixed Reactants," Chapter 4 of "Turbulent Reacting Flows," P. A. Libby and F. A. Williams, Eds., Springer-Verlag, Berlin (1980)
14. Marx, K. D., Lee, J. H. S., and Cummings, J. C., "Modeling of Flame Acceleration in Tubes with Obstacles," Proceedings of the 11th World Congress of the International Association for Mathematics and Computers in Simulation, Oslo, Norway, August 5-9, 1985.

15. Thompson, J. F., (Ed.), "Numerical Grid Generation," North-Holland, Amsterdam (1982).
16. Smooke, M. D. and Kosykowski, M. L., "Two-Dimensional Fully Adaptive Solutions of Solid-Solid Alloying Reactions," J. Comp. Phys. 62, 1 (1986).
17. Cloutman, L. D., Dukowicz, J. K., Ramshaw, J. D. and Amsden, A. A., "Conchas-Spray: A Computer Code for Reactive Flows with Fuel Spray," Los Alamos National Laboratory Report LA-9294-MS, May, 1982.
18. Libby, P. A. and Williams, F.A. in "Turbulent Reacting Flows," loc. cit., Chapter 1.
19. Williams, F. A., "Combustion Theory," 2nd Edition, Addison-Wesley, Reading, MA (1985).
20. Harlow, F. H. and Amsden, A. A., "A Numerical Fluid Dynamics Calculation Method for All Flow Speeds," J. Comp. Phys. 8, 197 (1971).
21. Tennekes, H., and Lumley, J. L., "A first Course in Turbulence," MIT Press, Massachusetts Institute of Technology, Cambridge, MA (1972).
22. Hinze, J. O., "Turbulence," McGraw-Hill, New York (1975).
23. Butler, T. D., and O'Rourke, P. J., in Proc. Sixteenth Symposium (International) on Combustion, The Combustion Institute, Pittsburgh, pp. 1503-1516 (1976).
24. O'Rourke, P. J. and Bracco, F. V., "Two Scaling Transformations for the Numerical Computation of Multidimensional Unsteady Laminar Flames," J. Comp. Phys. 33, 185 (1978).
25. Marx, K. D., unpublished work on FLAME experiments without obstacles.
26. Libby, P. A., Bray, K. N. C., and Moss, J. B., "Effects of Finite Reaction Rate and Molecular Transport in Premixed Turbulent Combustion," Combustion and Flame 34, 285 (1979).
27. A. N. Kolmogoroff, I. G. Petrovsky, and N. S. Piscounoff, "Etudes de l'équations de la diffusion avec croissance de la quantité de matière et son application a un problème biologique," Bull. Univ. Moscou. Ser. Internat., Sec. A, 1 No. 6, 1 (1937).
28. Clavin, P., and Liñan, A., "Theory of Gaseous Combustion," NATO Advanced Study Institute Series B, Physics 116, Plenum Press, pp. 291-338 (1984).
29. Kerstein, A. R., "Pair-Exchange Model of Premixed Flame Propagation," to appear in Proc. 21st Symposium (International) on Combustion, Munich, Federal Republic of Germany, August 3-8, (1986).
30. Warnatz, J., "Concentration-, Pressure-, and Temperature-Dependence of the Flame Velocity in Hydrogen-Oxygen-Nitrogen Mixtures," Comb. Sci. Tech. 26, 203 (1981).
31. Kee, R. J., Miller, J. A., and Jefferson, T. H., "CHEMKIN: A General-Purpose, Problem-Independent, Transportable, Fortran Chemical Kinetics Code Package," Sandia Laboratories Report SAND80-8003, Sandia National Laboratories, Livermore, CA (1980).
32. Hjertager, B., "Numerical Simulation of Turbulent Flame and Pressure Development in Gas Explosions," in "Fuel-Air Explosions," University of Waterloo Press, p. 407 (1981).
33. Sherman, M. P., Tieszen, S. R., and Benedick, W. B., "The Effect of Obstacles on Flame Acceleration and Transition to Detonation in a Large Channel," to appear in Proc. 21st

Symposium (International) on Combustion, Munich, Federal Republic of Germany, August 3-8, 1986.

34. Sherman, M. P., Tieszen, S. R., and Benedick, W. B., private communication (1986).

UNLIMITED RELEASE:

U. S. Government Printing Office
Receiving Branch (Attn: NRC Stock)
8610 Cherry Lane
Laurel, MD 20707
(250 Copies for R3)

U. S. Nuclear Regulatory Commission (12)
Division of Accident Evaluation
Office of Nuclear Regulatory Research
Washington, DC 20555

Attn: B. W. Morris T. Lee
 P. Worthington J. Mitchell
 B. Burson R. Meyer
 W. S. Farmer J. Telford
 M. Fleishman R. W. Wright
 M. Silberberg C. W. Nilsen

U. S. Nuclear Regulatory Commission (8)
Office of Nuclear Reactor Regulation
Washington, DC 20555

Attn: V. Benaroya K. I. Parczewski
 W. R. Butler Z. Rosztoczy
 J. T. Larkins T. M. Su
 R. Palla C. G. Tinkler

U. S. Department of Energy
R. W. Barber
Office of Nuclear Safety Coordination
Washington, DC 20545

U. S. Department of Energy (2)
Albuquerque Operations Office
Attn: J. R. Roeder, Director
 Transportation Safeguards
 J. A. Morley, Director
 Energy Research Technology
 For: C. B. Quinn
 R. N. Holton

P.O. Box 5400
Albuquerque, NM 87185

D. M. Austin
Office of Energy Research
U. S. Dept. of Energy
ER-7, MS G-226 Germantown
Washington DC 20545

Mr. J. Coleman
Office of Energy Research
U.S. Dept. of Energy
MS G-226 Germantown
Washington, DC 20545

Marvin Gunn, Jr., Manager
Energy Conversion Technology Proj.
Div. of Energy Conversion and
Utilization Technologies C-12
U. S. Department of Energy
1000 Independence Avenue
Washington, D.C. 20585

Ramesh Jain
Buildings and Community Systems
U. S. Department of Energy
1000 Independence Avenue
Washington, D.C. 20585

Dr. A. H. Laufer
Fundamental Interactions Branch
Division of Chemical Sciences
Office of Basic Energy Sciences
U. S. Department of Energy
Washington, D. C. 20545

Dr. Danny C. Lim
Industrial Programs
U. S. Department of Energy
1000 Independence Avenue
Washington, D.C. 20585

Dr. O. Manley
Division of Engineering
and Geosciences
Office of Basic Energy Sciences
Department of Energy
Washington, D.C. 20545

Dr. R. S. Marianelli
Division of Chemical Sciences
U. S. Department of Energy
Washington, D.C. 20585

K. D. Smith, Program Coordinator
Energy Technology Division
DOE Albuquerque Operations Office
Albuquerque, NM 87115

Donald K. Stevens, (Acting)
Associate Director
Basic Energy Sciences
U. S. Department of Energy
Washington, D. C. 20545

Dr. F. Dee Stevenson
Office of Energy Research
U. S. Dept. of Energy
R-142, MS G-226 Germantown
Washington DC 20545

Argonne National Laboratory (2)
Attn: Dae Cho
R. Anderson
9700 South Cass Avenue
Argonne, IL 60439

Brookhaven National Laboratory (2)
T. Ginsberg
G. Greene
Upton, NY 11973

Los Alamos National Laboratory (7)
Attn: F. J. Edeskuty
R. Gido
J. Carson Mark
G. Schott
M. Stevenson
J. Travis
K. D. Williamson, Jr.
P.O. Box 1663
Los Alamos, NM 87545

A. A. Amsden
T-3, MS-B216
Los Alamos National Laboratory
Los Alamos, NM 87545

T. D. Butler
T-3, MS-B216
Los Alamos National Laboratory
Los Alamos, NM 87544

J. K. Dukowicz
T-3, MS-B216
Los Alamos National Laboratory
Los Alamos, NM 87545

J. Ramshaw
T-3, MS-B216
Los Alamos National Laboratory
Los Alamos, NM 87545

Dr. Elaine Oran
Naval Research Laboratory
Code 4040
Washington, D.C. 20375

Oak Ridge National Laboratory (2)
Attn: A. P. Malinauskas
T. Kress
NRC Programs
P.O. Box X, Bldg. 4500S
Oak Ridge, TN 37831

Prof. Philip J. Smith
Brigham Young University
Department of Chemical Engineering
350 C.B.
Provo, UT 84602

Prof. A. Chorin
Mathematics Department
University of California
Berkeley, CA 94720

Prof. John W. Daily
University of California, Berkeley
Department of Mechanical Engineering
Berkeley, CA 94720

Prof. A. K. Oppenheim
Dept. of Mechanical Engineering
University of California
Berkeley, CA 94720

Robert F. Sawyer
Mechanical Engineering
University of California, Berkeley
Berkeley, CA 94720

Prof. W. A. Sirignano
Office of the Dean
School of Engineering
University of California, Irvine
Irvine, CA 92717

Prof. W. G. Kollmann
Mechanical Engineering
University of California
Davis, CA 95616

Prof. C. K. Law
Dept. of Mechanical Engineering
University of California
Davis, CA 95616

University of California @ Los Angeles
Nuclear Energy Laboratory (2)
Attn: Prof. I. Catton
Prof. D. Okrent
405 Hilgard Avenue
Los Angeles, CA 90024

Prof. P. Libby
Dept. of Applied Mechanics and
Engineering Science
University of California at
San Diego
La Jolla, CA 92093

Professor S. S. Penner
Energy Center - B-010
University of California, San Diego
La Jolla, CA 92093

Prof. T. G. Theofanous
Chemical and Nuclear Engineering Dept.
University of California
Santa Barbara, CA 93106

Josette Bellan
Jet Propulsion Laboratory
California Institute Tech.
4800 Oak Grove Drive
Pasadena, CA 91109

Prof. P. E. Dimotakis
Graduate Aeronautical Lab 301-46
California Inst. of Technology
Pasadena, CA 91125

A. Leonard
Graduate Aeronautical Lab 301-46
California Inst. of Technology
Pasadena, CA 91125

Prof. K. N. C. Bray
University of Cambridge
Silver St.
Cambridge, CB3 9EW
England

Prof. Norman Chigier
Carnegie-Mellon University
Mechanical Engineering Department
Pittsburgh, PA 15213

Prof. Melvyn C. Branch
University of Colorado
Mechanical Engineering
Boulder, CO 80309

Universita Degli Studi Di Pisa
Attn: M. Carcassi
Dipartimento Di Costruzioni
Meccaniche E. Nucleari
Facolta Di Ingegneria
Via Diotisalvi 2
56100 Pisa
ITALY

Dr. V. P. Roan
College of Engineering
University of Florida
Gainesville, FL 32611

Universität Heidelberg
Attn: Juergen Warnatz
Heidelberg
FEDERAL REPUBLIC OF GERMANY

Professor R. Strehlow
Dept of Aeronautics
University of Illinois
Urbana-Champaign, IL 61801

Imperial College of Science and
Technology
Attn: Dr. A. D. Gosman
Dept. of Mechanical Engineering
Exhibition Road
London SW7 2BX
UNITED KINGDOM

Prof. James H. Whitelaw
Fluids Section
Dept of Mechanical Engineering
Imperial College of Science and Technology
Exhibition Road
London SW7 2BX
Great Britain

Dr. A. C. McIntosh
Fuel and Energy Dept.
Leeds University
Leeds LS2 9JT
ENGLAND

McGill University
Attn: Prof. John H. S. Lee
315 Querbes
Outremont, Quebec H2V 3W1
CANADA

Simon Engineering Laboratory
Attn: Prof. W. B. Hall
University of Manchester
M139PL
UNITED KINGDOM

Judson R. Baron
Dept. of Aeronautics & Astronautics
Massachusetts Inst. Technology
Room 33-217
Cambridge, MA 02139

Massachusetts Institute of Technology
Attn: N. C. Rasmussen
Nuclear Engineering Department
Cambridge, MA 02139

Claus Borgnakki
Dept. of Mechanical Engineering
University of Michigan
550 East University
Ann Arbor, MI 48109

Dr. G. M. Faeth
University of Michigan
Ann Arbor, MI 48109-2140

University of Michigan
Attn: Prof. M. Sichel
Department of Aerospace Engineering
Ann Arbor, MI 47109

University of Michigan
Nuclear Engineering Department
Ann Arbor, MI 48104

Northwestern University
Attn: Prof. S. G. Bankoff
Chemical Engineering Department
Evanston, IL 60201

Prof. Bernard J. Matkowsky
Dept. of Engineering Sciences
and Applied Mathematics
Northwestern University
Evanston, IL 60201

Prof. Frediano V. Bracco
Princeton University
Department of Mechanical and
Aerospace Engineering
The Engineering Quadrangle
Princeton University
Princeton, NJ 08544

Prof. Forman A. Williams
Dept. of Mechanical and
Aerospace Engineering
Princeton University
Princeton, NJ 08544

Prof. Colin R. Ferguson
Purdue University
Dept. of Mechanical Engineering
North Grant Street
West Lafayette, IN 47907

Rensselaer Polytechnic Institute
Attn: Dr. J. E. Shepherd
Troy, NY 12180-3590

Prof. C. T. Bowman
Stanford University
Mechanical Engineering, Bldg. 520
Stanford, CA 94305

Prof. William Reynolds
Mechanical Engineering Bldg.
Stanford University
Stanford, CA 94305

Institute für Kernenergetik und
Energiesysteme (2)
Attn: M. Buerger
H. Unger
University of Stuttgart
Stuttgart
FEDERAL REPUBLIC OF GERMANY

Prof. R. W. Bilger
Mechanical Engineering
University of Sydney
New South Wales, 2006
Australia

Technische Universität München
Attn: Dr. H. Karwat
8046 Garching
FEDERAL REPUBLIC OF GERMANY

Texas A & M University
Nuclear Engineering Dept.
College Station, TX 77843

Prof. J. R. Bowen, Dean
College of Engineering
University of Washington
Seattle, WA 98185

Prof. David T. Pratt
University of Washington
Mechanical Engineering FU-10
Seattle, WA 98195

University of Wisconsin
Attn: Prof. M. L. Corradini
Nuclear Engineering Department
1500 Johnson Drive
Madison, WI 53706

Prof. Mitchell D. Smooke
Dept. of Mechanical Engineering
Yale University
New Haven, CT 06520

AERE Harwell (2)
Attn: J. R. Matthews, TPD
Didcot
Oxfordshire OX11 0RA
UNITED KINGDOM

Atomic Energy Ltd. (2)
Attn: D. Liu
D. Wren
Whiteshell Nuclear Research
Establishment
Pinawa, Manitoba
CANADA

Atomic Energy Canada Ltd.
Attn: P. Fehrenbach
Chalk River, Ontario K0J 1J0
CANADA

Ms. Kathryn L. Barnes
British Gas pic
Research & Development Division
Midlands Research Station
Wharf Lane, Solihull
West Midlands B91 2JW

Battelle Columbus Laboratory (2)
Attn: R. Denning
M. Leonard
505 Kind Avenue
Columbus, OH 43201

Battelle Institut E. V. (3)
Attn: Dr. Werner Geiger
Dr. Guenter Langer
Dr. Manfred Schildknecht
Am Roemerhof 35
6000 Frankfurt am Main 90
FEDERAL REPUBLIC OF GERMANY

Battelle Pacific Northwest Laboratory (2)
Attn: M. Freshley
G. R. Bloom
P.O. Box 999
Richland, WA 99352

Belgonucleaire S. A.
Attn: H. Bairiot
Rue de Champ de Mars 25
B-1050 Brussels
BELGIUM

CEC
Director of Research
Science & Education
Attn: B. Tolley
Rue De La Loi 200
1049 Brussels
BELGIUM

Dr. Pierre Joulain
Chimie Phsique deLa
Combustion ERA160 au CNRS
Domaine du Deffend
Mignaloux Beauvoir
86800 St. Julien l'Ars
France

Dr. Paul Clavin
Dept. de Combustion
Centre St. Jerome
Marseille Cedex 13 13397
France

Paul Thibault
Combustion Dynamics Ltd.
Box 175
Ralston, Alberta
Canada T0J 2N0

Dr. Rudy Maly
Daimler Benz AG
Abteilung E6T/E
Postfach 202
D-7000 Stuttgart
West Germany

Duke Power Company (2)
Attn: F. G. Hudson
A. L. Sudduth
P.O. Box 33189
Charlotte, NC 28242

John H. Pohl
Energy & Environmental Research Corp.
18 Mason
Irvine, CA 92718

EG&G Idaho (3)
Willow Creek Building, W-3
Attn: D. Croucher
R. Hobbins
Sever Sadik
P.O. Box 1625
Idaho Falls, ID 83415

Electric Power Research Institute (4)
Attn: J. Haugh
W. Loewenstein
B. R. Sehgal
R. Vogel
3412 Hillview Avenue
Palo Alto, CA 94303

ENEA Nuclear Energ Alt Disp (2)
Attn: P. L. Ficara
G. Petrangeli
Via V. Brancati
00144 Roma
ITALY

ENSMA
Prof. Numa Manson
Rue Guillaume VII
86034 Poitiers
FRANCE

Dr. Thomas S. Bustard
Energetics, Incorporated
9210 Route 108
Columbia, MD 21045

Factory Mutual Research Corporation
Attn: R. Zalosh
P.O. Box 688
Norwood, MA 02062

Fauske & Associates
Attn: R. Henry
16W070 West 83rd Street
Burr Ridge, IL 60521

James A. Kezerle
Gas Research Institute
8600 West Bryn Mawr Ave
Chicago, IL 60631

General Electric Corporation
Attn: K. W. Holtzclaw
175 Curtner Avenue
Mail Code N 1C157
San Jose, CA 95125

General Electric Corporation
Attn: M. I. Temme, Manager
Probabilistic Risk Assessment
Advanced Reactor Systems Dept.
P.O. Box 3508
Sunnyvale, CA 94088

Charles A. Amann
G. M. Research Laboratories
Twelve Mile and Mound Roads
P. O. Box 9055
Warren, MI 48090-9055

Dr. Roger B. Krieger
G. M. Research Laboratories
Twelve Mile and Mound Roads
P. O. Box 9055
Warren, MI 48090-9055

Gesellschaft für Reaktorsicherheit (GRS)
Postfach 101650
Glockengasse 2
5000 Koeln 1
FEDERAL REPUBLIC OF GERMANY

Gesellschaft für Reaktorsicherheit (2)
Attn: Dr. E. F. Hicken
Dr. H. L. Jahn
8046 Garching
Forschungsgelände
FEDERAL REPUBLIC OF GERMANY

Institute of Nuclear Power Operation
Attn: Henry Piper
1100 Circle 75 Parkway, Suite 1500
Atlanta, GA 30339

International Technology Corporation
Attn: Mario H. Fontana
575 Oak Ridge Turnpike
Oak Ridge, TN 37830

Japan Atomic Energy Research Institute
Attn: Dr. K. Soda, Manager
Chemical Engineering Safety Laboratory
Dept. of Nuclear Fuel Safety
Tokai-mura, Naku-gun Ibaraki-ken
319-11
JAPAN

Japan Atomic Energy Research Institute
Attn: Dr. T. Fujishiro, Manager
Dept. of Fuel Safety Research
Tokai-mura, Naka-gun, Ibaraki-ken
319-11
JAPAN

Japan Atomic Energy Research Institute
Attn: Dr. Kazuo Sato, Director
Dept. of Reactor Safety Research
Tokai-mura, Naka-gun Ibaraki-ken
319-11
JAPAN

Kraftwerk Union
Attn: Dr. M. Peehs
Hammerbacherstrasse 12 & 14
Postfach 3220
D-8520 Erlangen 2
FEDERAL REPUBLIC OF GERMANY

Lehrgebiet für Mechanik der
RWTH Aachen
Attn: Prof. Dr. Ing. N. Peters
Templergraben 55
D5100 Aachen
FEDERAL REPUBLIC OF GERMANY

Dr. Ingar O. Moen
Head/Shock and Blast Group
Defence Research Establishment
Suffield
Ralston, Alberta
Canada TOJ 2N0

Mississippi Power & Light
Attn: S. H. Hobbs
P.O. Box 1640
Jackson, MS 39205

National Nuclear Corp. Ltd.
Attn: R. May
Cambridge Road
Whetstone, Leicester, LE8 3LH
UNITED KINGDOM

Netherlands Energy Research Foundation
Attn: K. J. Brinkmann
P.O. Box 1
1755ZG Petten NH
NETHERLANDS

NUS Corporation
Attn: R. Sherry
4 Research Place
Rockville, MD 20850

Dr. Arthur A. Boni
Physical Sciences Inc.
P. O. Box 3100
Andover, MA 01810

Power Authority State of NY
10 Columbus Circle
New York, NY 10019

Power Reactor Nuclear Fuel
Development Corp. (PNC)
Attn: Dr. Watanabe
FBR Project
9-13, 1 Chome, Akasaka
Minato-Ku, Tokyo
JAPAN

Projekt Schneller Brueter (3)
Attn: Dr. Kessler
Dr. Heusener
Dr. M. Reimann
Kernforschungszentrum Karlsruhe
Postfach 3640
7500 Karlsruhe
FEDERAL REPUBLIC OF GERMANY

Pak-Yan Liang
Rockwell Int'l, Rocketdyne Div.
6633 Canoga Ave., FB47
Canoga Park, CA 91303

C. H. Priddin
Mgr. Combustion Methods
Rolls-Royce plc
P. O. Box 31
Derby DE28BJ
Great Britain

Shell Research Ltd.
Paul H. Taylor
Thornton Research Centre
P.O. Box 1
Chester CH1 3SH
ENGLAND

Jana Backovsky
SRI International
33 Ravenswood Avenue
Menlo Park, CA 94025

Stratton & Associates, Inc.
2 Acoma Lane
Los Alamos, NM 87544
Attn: W. Stratton

Statens Karnkraftinspektion
Attn: L. Hammar
P.O. Box 27106
S-10252 Stockholm
SWEDEN

Studsvik Energiteknik AB
Attn: K. Johansson
S-611 82 Nykoping
SWEDEN

Swedish State Power Board
Attn: Wiktor Frid
S-162 Fach 87 Vallingby
SWEDEN

UKAEA Safety & Reliability Directorate (2)
Attn: J. H. Gittus
M. R. Hayns
Wigshaw Lane, Culcheth
Warrington WA3 4NE
Cheshire
UNITED KINGDOM

UKAEA, Culham Laboratory
Attn: F. Briscoe
Abingdon
Oxfordshire OX14 3DB
UNITED KINGDOM

UKAEA AEE Winfrith (6)
Attn: M. Bird, S. Board
T. Butland, D. Fletcher
R. Potter, A. Wickett
Dorchester
Dorset DT2 8DH
UNITED KINGDOM

Westinghouse Corporation (3)
Attn: N. Liparulo
J. Olhoeft
V. Srinivas
P.O. Box 355
Pittsburgh, PA 15230

L. Cloutman, LLNL, L-035

C. K. Westbrook, LLNL, L-321

Gladys Shaw (15)
Sandia National Laboratories
P.O. Box 5800
Albuquerque, NM 87185

1131	W. B. Benedick	8350	J. S. Binkley
1510	J. W. Nunziato	Attn:	8351 J. Y. Chen
1512	J. C. Cummings		8351 R. P. Lucht
1513	M. R. Baer		8353 G. A. Fisk
1530	L. W. Davison		8354 R. E. Palmer
	Attn: 1534 J. R. Asay		8357 R. J. Carling
1636	F. G. Blottner	8360	W. J. McLean
6000	D. L. Hartley	8361	D. R. Hardesty
6400	A. W. Snyder	Attn:	8361 T. Fletcher
6412	A. L. Camp	8362	T. M. Dyer
6415	F. E. Haskin	Attn:	8362 T. T. Bramlette
6419	K. D. Bergeron	8363	B. R. Sanders
6420	J. V. Walker	Attn:	8363 W. T. Ashurst
6422	D. A. Powers		8363 P. K. Barr
6425	W. J. Camp		8363 H. A. Dwyer
6425	M. F. Young		8363 A. R. Kerstein
6427	M. Berman		8363 S. B. Margolis
6427	D. F. Beck	8363	K. D. Marx (7)
6427	J. T. Hitchcock	8400	R. C. Wayne
6427	B. W. Marshall, Jr.	8265	Publication Division/ Tech. Library Proc. Div. 3141
6427	L. S. Nelson	8024	P. W. Dean, Central Technical Files (3)
6427	M. P. Sherman	3141	Tech. Library Proc. Div. (3)
6427	S. E. Slezak	3151	W. L. Garner
6427	D. W. Stamps		
6427	S. R. Tieszen		
6427	C. C. Wong		
6440	D. A. Dahlgren		
8000	J. C. Crawford		
8100	E. E. Ives		
8200	R. J. Detry		
8240	C. W. Robinson		
	Attn: 8244 C. M. Hartwig		
	8245 R. J. Kee		
	8245 A. E. Lutz		
8244	D. R. Cheoweth		
8245	S. Paolucci		
8300	P. L. Mattern		
	Attn 8310 R. W. Rohde		
	8340 W. Bauer		

NRC FORM 335 (2-84) NRCM 1102, 3201, 3202 SEE INSTRUCTIONS ON THE REVERSE.		U.S. NUCLEAR REGULATORY COMMISSION		1. REPORT NUMBER (Assigned by TIDC, add Vol. No., if any) NUREG/CR -4855 SAND87-8203 R3	
2. TITLE AND SUBTITLE DEVELOPMENT AND APPLICATION OF A COMPUTER MODEL FOR LARGE-SCALE FLAME ACCELERATION EXPERIMENTS			3. LEAVE BLANK		
5. AUTHOR(S) K. D. Marx			4. DATE REPORT COMPLETED MONTH YEAR April 1987		
7. PERFORMING ORGANIZATION NAME AND MAILING ADDRESS (Include Zip Code) Sandia National Laboratories Livermore, CA 94550 Division 8363			6. DATE REPORT ISSUED MONTH YEAR July 1987		
10. SPONSORING ORGANIZATION NAME AND MAILING ADDRESS (Include Zip Code) Division of Reactor Systems Safety Office of Nuclear Regulatory Research U. S. Nuclear Regulatory Commission Washington, DC 20555			8. PROJECT/TASK/WORK UNIT NUMBER		
12. SUPPLEMENTARY NOTES			9. FIN OR GRANT NUMBER A1246		
13. ABSTRACT (200 words or less) A new computational model for large-scale premixed flames is developed and applied to the simulation of flame acceleration experiments. The primary objective is to circumvent the necessity for resolving turbulent flame fronts; this is imperative because of the relatively coarse computational grids which must be used in engineering calculations. The essence of the model is to artificially thicken the flame by increasing the appropriate diffusivities and decreasing the combustion rate, but to do this in such a way that the burn velocity varies with pressure, temperature, and turbulence intensity according to prespecified phenomenological characteristics. The model is particularly aimed at implementation in computer codes which simulate compressible flows. To this end, it is applied to the two-dimensional simulation of hydrogen-air flame acceleration experiments in which the flame speeds and gas flow velocities attain or exceed the speed of sound in the gas. It is shown that many of the features of the flame trajectories and pressure histories in the experiments are simulated quite well by the model. Using the comparison of experimental and computational results as a guide, some insight is developed into the processes which occur in such experiments.			11a. TYPE OF REPORT Technical		
14. DOCUMENT ANALYSIS -- a. KEYWORDS/DESCRIPTORS			b. PERIOD COVERED (Inclusive dates)		
b. IDENTIFIERS/OPEN-ENDED TERMS			15. AVAILABILITY STATEMENT		
			16. SECURITY CLASSIFICATION (This page) (This report)		
			17. NUMBER OF PAGES		
			18. PRICE		

